Investigating Karyopherin B1:

Small molecule interactions for

cancer therapy

Erin Strydom

Thesis Presented for the Degree of

DOCTOR OF PHILOSOPHY

In the Department of

Integrative Biomedical Sciences

Division of Medical Biochemistry

UNIVERSITY OF CAPE TOWN

May 2016

Declaration

I, Erin Strydom, hereby declare that the work on which this thesis is based, is my own unaided work, both in concept and execution, and that apart from the normal guidance from my supervisor, I have received no assistance (except where acknowledgements are stated). I grant the University of Cape Town free licence to reproduce the above thesis, in whole or in part, for the purpose of research.

Signature: Signed by candidate

Date: 25 MAY 2016

Dedication

To you who taught me, "It is only from tempered steel, a noble sword can be forged."

And so I found my strength.

Acknowledgments

As with all of these projects, it is the sum total of a many great minds, combined with the strength, unswayable willpower and support of family and friends that are responsible for what you hold here, the end result. To begin with I would like to say a special thank you to my supervisor A/Prof Virna Leaner. To our lab manager, Hajira Guzguy, thank you for your organisational skills and support. Robbie Samuels, our lab tech, you always had my solutions ready when I needed them and put up with monumental volumes of malodourous broth and you fearlessly fought off the interminable quantities of bacteria I produced, thank you.

A very big thanks to Prof. Pete Meissner who was not only a superb leader, but a comrade to us all. You were always there to help and provide excellent advice. You have my respect for your endless knowledge and all the great things you do.

Dr Nina Holderness-Parker, thank you for showing me there is a silver lining in everything; your pure joy each and every day was infectious. Cherise Dunn and Dr Nelusha Shunmoogam-Gouden, my special friends, thank you for the laughter and the tears but most of all for being there. Dr Kate Hadley, your knowledge and level head has saved me more than once. Dr Luke Esau, thank you for teaching me to think outside the box and just being Luke, you are my guardian angel.

Thank you my best friend Mateen Wagiet for being at my side throughout a very challenging final year and guiding me when I lost my way multiple times. You are such an incredible person and your strength alone has brought me through.

To Dr Brandon Weber, and the structural biology team thank you for all your help with the protein purification it was great to work with you and learn from your skills.

Thank you to the Stellenbosch team. Just when I thought all the doors where closed, you opened a window and let the light in- Prof Marina Ratenbauch, Dr Jacob Band thank you for your help the CD and protein analysis.

Thank you Dr Dave Wooly for all the help with ITC, troublesome and fickle we got there in the end.

To the phenomenal Dr Dirk Lang and Susan Cooper, thank you for all the work you did with me for FRET and confocal microscopy, you two are just incredible.

Finally I saved the best for last, to my family, you are the best, you supported me with unconditional love and you never wavered in your strength or your belief in me, even when I lost all hope in myself. When I lost my balance you were there to right me again. I love you beyond words or measure and I am mystified by your strength. Mum, Dad and my big brother Michael, you are my sunshine, my stars. Carl Sagan said, “We are all made of star stuff” but you are my universe, you are everything to me and I love you. I hope one day I can give back to you

just what you gave me. It is you who made this possible because you believed in me.

Table of Content

Figures and Tables Index

Abbreviations

ΔG	Gibbs free energy
ΔH	Enthalpy
ΔS	Entropy
Amp	Ampicillin
AML	Acute myeloid leukemia
ATP	Adenosine triphosphate
BamH1	Restriction enzyme
BCA	Bicinchonic acid
BCR-ABL	Fusion gene which creates the Philadelphia chromosome
BSA	Bovine serum albumin
bp	base pairs (DNA)
°C	Degrees Celsius
CD	Circular dichroism
CaSki	Cervical cancer cells containing HPV-16 gene as well as sequences related to HPV 18
CLL	Chronic lymphatic leukaemia
CO_2	Carbon dioxide
CRM1	Chromosome maintenance 1
DAP1	4',6'-diamidio-2'-phenylindole dihydrochloride
dATP	Deoxyadenosine triphosphate
DMEM	Dulbecco's modified Eagles Medium
DMSO	Dimethyl Sulphoxide
DNA	Deoxyribonucleic acid

DNTP	Deoxynucleoside triphosphate
DTT	Dithiothretiol
E6	Oncoprotein
E7	Oncoprotein
EcoR1	Restriction enzyme
FCS	Fetal calf serum
FG-Repeat	Phenylalanine and glycine repeat
FOXO	Forehead box protein 01
FRET	Fluorescence resonance energy transfer
FRFP	Far end fluorescent red protein
GFP	Green fluorescent protein
GST	Glutathione transferase
GTP	Guanidine triphosphate
HEAT Repeats	Huntington elongation factor 3 (EF3) Protein phosphatase 2A (PP2A) and yeast kinase (TOR1). Rod like helical structures involved in intracellular transport.
Her 1	Human epidermal growth factor 1
Her 2	Human epidermal growth factor 2
Her 3	Human epidermal growth factor 3
HeLa	Immortal cervical cancer cell line derived from the patient Henrietta Lacks in 1951
HPV	Human papillomavirus
His	Histadine purification tag
IC50	Half the maximum inhibitory concentration
IKB	Nuclear factor of Kappa light polypeptide gene enhancer in B-cells inhibitor
IL-2	Interleukin 2
INI-43	Inhibitor of nuclear transport number 43

IPTG	Isopropyl β-D-1-thiogalactopyranoside binds to lac repressor
ITC	Isothermal titration calorimetry
K_a	Association constant
K_d	Dissociation constant
kDa	Kilodalton
KpnB1	Importin B1/ Karyopherin B1, nuclear importer
KpnA2	Karyopherin A2, nuclear importer
Kan	Kanamycin
L1	Oncoprotein
LA	Luria agar
Lac	Lactose operon and is a regulatory mechanism in cloning
LB	Luria broth
Luc	Luciferase
Min	Minute
mL	Millilitres
mRNA	Messenger RNA
MTT	3’-(4’,5’-DDimethylthiazol-2’-yl)2’,5’-diphenyltetralolium
NE	Nuclear envelope
NFAT	Nuclear factor of activated T cells
NHL	Non-Hodgkin lymphoma
NLS	Nuclear localisation sequence
NMR	Nuclear magnetic resonance
Not 1	Restriction enzyme
NPC	Nuclear pore complex
Nups	Nuclearporins
OD	Optical density

p21	Protein 21
p27	Protein 27
p53	Protein 53
PARP-1	Poly (ADP-ribose) polymerase 1
PBS	Phosphate buffered saline
PCR	Polymerase chain reaction
pRB	Retinoblastoma protein
p/s	Penicillin and streptomycin
ranGTP	Ran GTPase
RanGEF	Ran GTPase exchange factor
RCC1	Regulator of chromosome condensation 1
RIPA	Radioimmunoprecipitaion assay buffer
rpm	Revolutions per minute
Sac 1	Restriction enzyme
Sac 11	Restriction enzyme
SD	Standard deviation
SDS-PAGE	Sodium dodecyl sulphate poly acrylamide gel electrophoresis
SINE	Selective inhibitor of nuclear import
siRNA	Small interfering ribonucleic acid
SREBP2	Sterol regulatory element binding protein 2
Taq	Taq polymerase
T4 Ligase	DNA ligation enzyme
µL	Microliter
µM	Micromole
VP1	Viral protein 1
XGAL	5’-bromo-4’chlolro3’-indolyl-β-D-galactopyranoide

Xma 1 Restriction enzyme

ABSTRACT

The advent of gene expression profiling studies has allowed for the identification of genes with potential as disease markers and therapeutic targets. Our laboratory identified the eukaryotic nuclear importer protein Karyopherin B1 (KpnB1), to be up-regulated in different cancer cell lines, including cervical and oesophageal as well as transformed cells. Inhibition of KpnB1 in these cells using small interfering RNA (siRNA) resulted in significant cancer cell death via apoptosis, suggesting KpnB1 is essential for cancer cell survival. Within our laboratory, we established that candidate small molecules targeted against KpnB1 identified using a rational drug design approach. The outcome of this research is for examine inhibitors of KpnB1 for potential as future anti-cancer agents using.

Based on the long-term goal of this research, this particular project was aimed at investigating a small molecule inhibitor identified in our laboratory, known as Inhibitor of Nuclear Import-43 (INI-43) for its potential to bind to the nuclear importer, KpnB1. Using conventional assays as well as cutting edged techniques including circular dichrosim (CD) and isothermal titration calorimeter (ITC), an examination of INI-43 and its interactions with KpnB1 was made.

In vitro analysis showed that INI-43 exhibits cytotoxic effects on cervical cancer cells with an IC_{50} of ≈10μM and induces apoptotic cell death. The NFAT dual luciferase assay measured nuclear import of KpnB1 associated proteins, showing that INI-43 inhibits nuclear import/activity of NFAT in a dose dependent manner.

Confocal microscopy of exogenous FRFP-KpnB1 as well as endogenous KpnB1 in the presence of INI-43 showed a change in the localisation of KpnB1 upon drug treatment. Both FRFP-KpnB1 and endogenous KpnB1 appear to be prevented from entering the nucleus, and is retained in the peri-nuclear space and the cytoplasm suggesting that INI-43 inhibits KpnB1 movement into the nucleus.

To investigate KpnB1-INI-43 interactions, purified KpnB1 was prepared and used in biophysical techniques. Purified KpnB1 protein was prepared using GST-tagged purification methods and the tagged protein confirmed by mass spectrometry. Purified GST-KpnB1 was used in drug binding studies including circular dichrosim (CD) isothermal titration calorimetry (ITC). CD showed a drug concentration dependant shift in the spectra at around 233nm, indicative of drug protein interaction possibly occurring in a region of KpnB1 containing aromatic amino acids. The purified GST-KpnB1 was used in ITC, which confirmed an interaction between KpnB1 and INI-43, a relatively weak interaction. In conclusion, our data shows that the small molecule, INI-43 kills cancer cells, likely by interfering with KpnB1 associated nuclear import pathways. We show that INI-43 interferes with the nuclear localisation of KpnB1 itself and biophysical assays provide evidence for possible KpnB1-INI-34 interactions. Small molecules such as INI-43 present as promising tools to studying the potential of KpnB1 as an anticancer target.

Chapter 1

Literature Review

1.1 Cancer: Global Statistics

Despite continuous technological advancements aimed at combating cancer, it remains one of the leading causes of death worldwide and thus a major contributor to the total global health burden. The GLOBOCAN statistics estimated that in 2012 a total of 14.1 million cancer cases occurred worldwide, and of these, 8.2 million cancer deaths were estimated to have occurred that same year (Ferlay et al. 2013; Ferlay et al. 2015). Cancer is primarily a genetic disease, and this being the case, the dominant form of cancer varies between genders and races and between different socioeconomic groups (Jemal et al. 2011). There is still much work to be done to gain control of the disease and the need for novel treatments with fewer side effects remains paramount.

In developing countries, medical care is often substandard and screening methods for cancer is poor or non-existent in rural areas. In many rural patients the disease is therefore able to progress unchecked (Hoffman et al. 2003; Fiander 2011). In sub-Saharan Africa, the focus region of this study, cervical cancer is the leading cause of cancer-related death in women (Adewole et al. 2013; Fiander 2011; Hoffman et al. 2003). Approximately 200 million women from the age of 15 years and older are at risk of suffering from this disease, and in sub-Saharan Africa more than 75 000 new cases are diagnosed with over 50 000 deaths occurring each year (Adewole et al. 2013). These figures may still

not be a true reflection of the devastation caused by this disease, as many women fail to report to a hospital or any clinical setting and accurate data collection in the region is consequently also limited (Adewole et al. 2013; Francis et al. 2010). The reason for this disease presenting in such high numbers of women is the presence of the human papilloma virus (HPV) (Hebner & Laimins 2006; zur Hausen 2002; Bonanni et al. 2015).

Inroads have been made in preventing HPV, and therefore cervical cancer, with the use of vaccinations such as Cervarix (GlaxoSmithKline) and Gaurdasil (Merk & Co) (Adewole et al. 2013; Botha & Dochez 2012; Ladner et al. 2012). Programs being run by the WHO that are currently active in the region aim to educate and vaccinate as many women as possible (Botha & Richter 2015). Despite the existence of the vaccine, there is still a growing need for requisite treatments for those women already suffering from cancer; among these would be women who have not been vaccinated and have the disease, such as older patients, women who missed the vaccination program and women who did not want to take part or were unable to do so (Adewole et al. 2013; Botha & Dochez 2012; Francis et al. 2010). There has also been discussion suggesting that having received the vaccine does not mean women are one hundred per cent protected from cervical cancer (Ault 2007; Villa et al. 2005). The vaccine does however prevent them from being susceptible to the more virulent strains of HPV that cause a majority of the cases of cervical cancer, if they have not yet been exposed to these strains of the virus (Ault 2007; Villa et al. 2005).

1.2 Cervical Cancer and Human Papilloma Virus (HPV)

As mentioned, most cases of invasive cervical cancer are a result of infection with various oncogenic strains of HPV (Hebner & Laimins 2006; Bonanni et al. 2015) There are over 100 different strains of HPV, most of which are naturally removed from the body by the immune system post infection (Adewole et al. 2013). Fifteen problematic strains of the virus exist, however, that are oncogenic in nature, and these persist post infection, causing the pathologies commonly diagnosed in cervical cancer. In Southern Africa, the HPV 16 and 18 strains are responsible for most of the recorded cases of cervical cancer (Adewole et al. 2013). The infection rate in all women in Southern Africa is estimated at 17.4% (Adewole et al. 2013; Mbulawa et al. 2015). The HPV variants 16 and 18 are reported to be responsible for ±70% of all invasive forms of cervical cancer cases recorded worldwide (Adewole et al. 2013; Mbulawa et al. 2015). The vaccines Cervarix and Gardasil both provide protection against HPV 16 and 18 strains. In addition, Gardisil is a quadrivalent vaccine that provides added benefit of protection against HPV 6 and 11 and also provides the recipient with protection against genital warts, thereby reducing the transmission of HPV (Adewole et al. 2013). Globally, there are significant regions where HPV is highly prevalent, one of these regions being sub-Saharan Africa (Fiander 2011). Research has shown that in such regions there is a distinct benefit in administering the vaccine to young males as well as to females (Giuliano 2007; Marty et al. 2013; Blomberg et al. 2015). Research in Europe has confirmed that vaccinating young males in addition to females provides promising results in reducing the global health

burden resulting from HPV and related cancers (Marty et al. 2013; Giuliano 2007; Bonanni et al. 2015). HPV infection, in particular is associated with the oncogenic HPV E6 and E7 proteins, and is known to have major impacts on the gene regulation via transcription. This leads to on-going cell survival and other hallmarks of the cancer phenotype.

1.3 The Upregulation of Karyopherin B1 in Cervical Cancer

Prior research has examined the association of the increased risk of developing cervical cancer, post HPV infection (Dyson, 1998). Reports have documented that 90% of all cervical cancers are associated with infection by high-risk HPV DNA. The basis for this observation is the fact that the HPV infection is associated with the presence of the HPV oncoproteins E6 and E7, which inhibit the normal functions of cell cycle proteins p53 and pRb (Dyson 1998). Typically, p53 and pRb routinely control cellular transcription during cell cycle; however, the presence of E6 and E7 leads to the development of a cancer phenotype via uncontrolled growth and replication (Dyson, 1998; van der Watt et al., 2009).

Gene expression studies in our laboratory using control and cervical cancer patient material identified numerous genes with altered expression in the cancer group (van der Watt et al. 2009). It was proposed that some of the proteins encoded by these genes may be necessary for cancer cell survival and thus be used as possible anti-cancer targets. One such target is the nuclear transporter Karyopherin B1 (KpnB1). Indeed, specifically relevant to this project are our previous studies which have shown that upregulation of KpnB1 is associated with cervical cancer (van der Watt et al. 2009; Ward et al. 2011).

Karyopherin proteins are implicated in assembly of the HPV virus in host cells, (Conway & Meyers 2009; Zhou et al. 1994). The viral proteins L1 and VP1 pentamerize into capsomeres, and interact with KpnB1 and its adapter protein Karyopherin A2 (KpnA2) via what is known as the classical import pathway (Stanley 2015). Briefly, this pathway involves the import of cargo molecules, in this case the viral proteins, into the nucleus using KpnB1 partnered to the adaptor protein KpnA2 via the nuclear pore complex. The viral molecules are subsequently shuttled into the nucleus of host cells, and once inside the host cell nucleus, the virus can fully assemble (Bird et al. 2008). Karyopherin proteins have been reported to enable the virus to enter the host cells, and in high-risk versions of the virus (HPV 16 and 9) the Karyopherins perform a greater role in promoting the long-term survival of cancer cells (Bird et al. 2008).

Our laboratory has previously performed gene expression analysis to identify genes that associate with cervical cancer as potential biomarker and therapeutic targets. Of the genes identified with altered expression in cervical cancer, KpnB1 showed elevated expression levels in cervical cancer patient tissue (Ward et al. 2011; van der Watt et al. 2009). This observation evoked further interest when it was shown that inhibition of KpnB1 using siRNA results in cell death (van der Watt et al. 2009; Angus et al. 2014). This effect of siRNA-related cell death appeared more specific in cancer cells compared to non-cancerous cells (Figure 1.1) (van der Watt et al. 2016) .

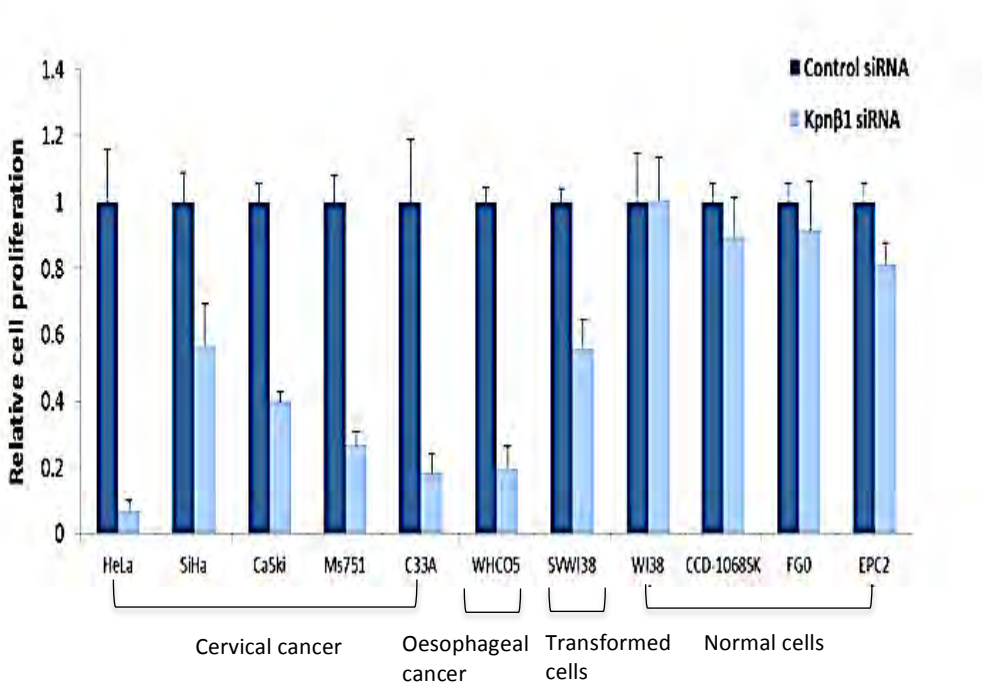

Figure 1.1: siRNA induces cell death specific to cancer and transformed with little effect on normal cells. Effects on relative proliferation after treatment with KpnB1 siRNA, shown by light blue bars, dark blue bars represent relative proliferation following treatment with control siRNA (from van der Watt et al., 2016).

Karyopherins are a family of proteins involved in the nucleo-cytoplasmic shuttling of proteins and RNA molecules into the nucleus of eukaryotic cells. Including the process of nuclear import, KpnB1 has been shown to be important for a range of cell processes, one such being the organisation of microtubules, where it is associated with the spacial and chronological distribution of those proteins associated with microtubule assembly, formation and organisation throughout the cell cycle (Timinszky et al. 2002; Angus et al. 2014; Cavazza & Vernos 2016). KpnB1 is thus important for processes such as mitosis and replication (Timinszky et al. 2002; van der Watt et al. 2009; Angus et al. 2014). Previous work conducted in our laboratory has shown that the knocking down of KpnB1 with siRNA results in mitotic abnormalities and errors in spindle assembly (Angus et al.

2014). KpnB1 has also been implicated in nuclear envelope (NE) assembly, as it has been shown to play a role in RanGTP, binding and attracting membrane vesicles and hence forming the NE (Cavazza & Vernos 2016).

Our laboratory has shown KpnB1 to be up-regulated in cervical cancer cells (van der Watt et al., 2011) we and others propose that nuclear import pathways and KpnB1 are potential targets for anti-cancer therapy (van der Watt et al. 2013; Kau et al. 2004). The premise of our research is thus that the nuclear import protein KpnB1 is important for the growth and survival of cancer cells, and that small-molecule inhibitors targeted against KpnB1 may yield possible anti-cancer treatments. This project was aimed at evaluating small molecules identified using a rational drug-design approach for their ability to inhibit cancer cell proliferation and their potential to bind to KpnB1.

1.4 Karyopherin B1 and the Nuclear Pore Complex

The mechanism by which KpnB1 transports molecules into the nucleus of cells is via the nuclear pore complex (NPC). A key function of the NPC is regulating the movement of molecules between the nucleus and the cytoplasm of eukaryotic cells. Structurally, NPCs are one of the larger, more complex multi-protein complexes within eukaryotic cells (Hoelz et al. 2011). These structures penetrate the nuclear envelope (NE) at specific sites at which the inner nuclear membrane, and the outer nuclear membrane fuse (Lott & Cingolani 2011). Molecules larger than 40 kDa are actively transported through the NPC by the Karyopherins (Figure 1.3 a) (D'Angelo,M and Hetzer M. H 2008).

The NPC is arranged into an eightfold-symmetrical structure composed of small proteins called nuleoporins or Nups (Figure 1.2 b) (Koh & Blobel 2015). It has a scaffold structure, embedded within the NE, which surrounds a central transport channel and two ring-structural features (Lim 2007). The first ring structure is localised within the cytoplasm environment, where eight filaments are attached to it (D'Angelo & Hetzer 2008; Hoelz et al. 2011), while the other ring, known as the nuclear or distal ring, also containing filaments, is positioned in the nucleus (D'Angelo & Hetzer 2008).

The cytoplasmic filaments have loose ends, while the nuclear filaments are joined in a distal ring, forming a structure known as the nuclear basket (Figure 1.2 a) (D'Angelo & Hetzer 2008). Functionally, the nuclear pore facilitates the movement of transport proteins such as KpnB1 and KpnA2 and their cargo into the nucleus. In the process of passing through the NPC, these proteins interact with the proteins of the NPC during transit through the structure (D'Angelo & Hetzer 2008).

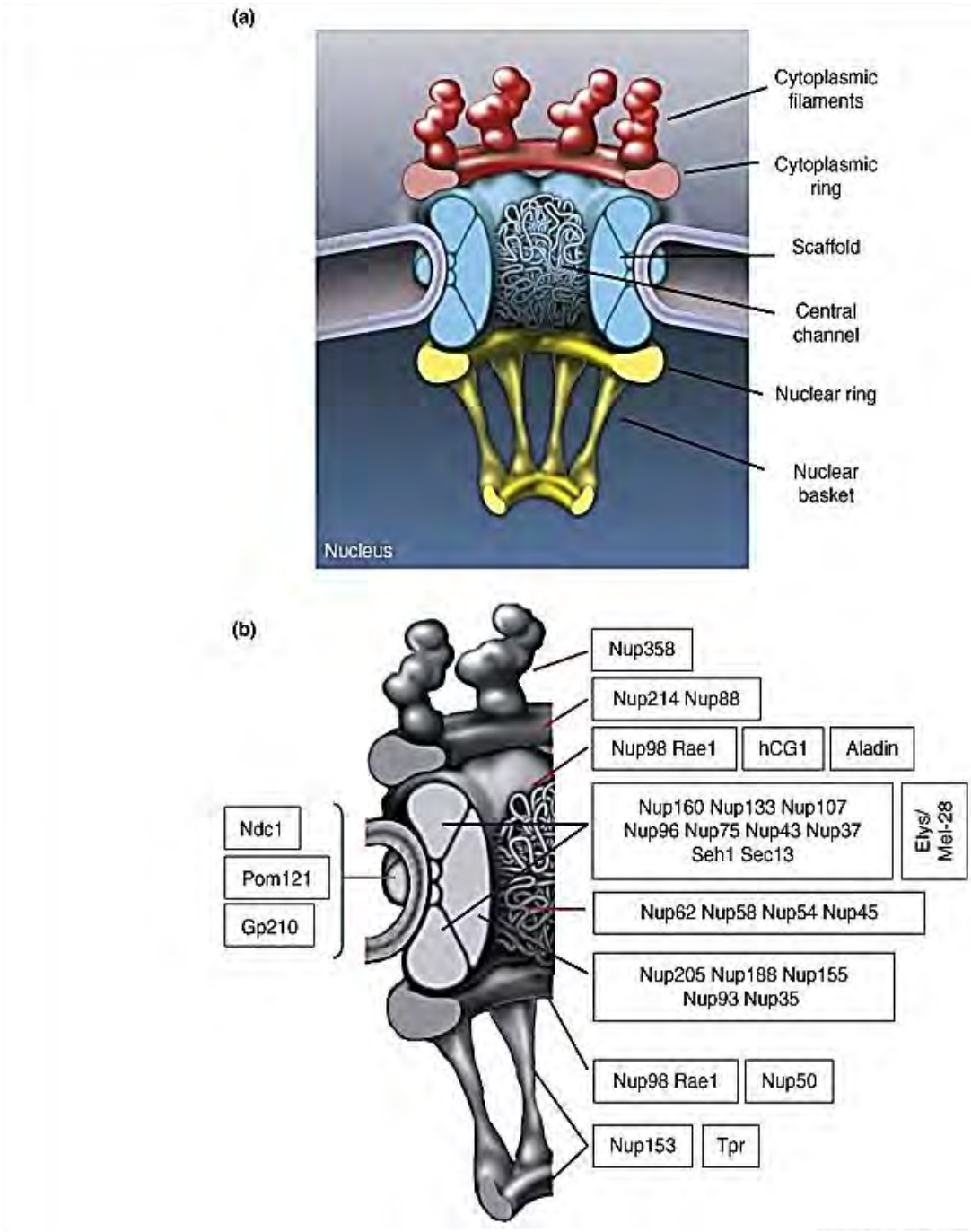

Figure 1.2: The nuclear pore complex (NPC) is a complicated structure comprised of smaller proteins known as nucleorporins (Nups). (a) Schematic diagram of the NPC showing the fundamental structures; (b) Location of the various Nups and how they are organised within the NPC (from D'Angelo & Hetzer, 2008).

Before cargo molecules can be docked and translocate through the NPC, they first require recognition by the shuttle molecules (Lim 2007). Recognition takes place via the identification of the nuclear translocation sequence (NLS) (Ferenczy & Keserũ 2010; Lim 2007).

The mechanisms involved in the translocation of the Karyopherin proteins with associated cargo remains uncertain. Within the NPC are a group of proteins, which are rich in phenylalanine and glycine (FG repeats) (Ma & Yang 2010). These FG repeats most likely assist in the transport process, because of their interaction with the cargo molecules as they pass through the NPC (Ma & Yang 2010; Koh & Blobel 2015).

1.5 Karyopherin B1 and Transport Through the Nuclear Pore Complex: Nucleocytoplasmic Transport

The nuclear envelope (NE) provides a protective barrier for the nuclear material. Movement through this channel is controlled by the NPC (Liu & York 2001). Shuttling proteins such as KpnB1 are able to enter and exit the nucleus along with their respective cargo molecules via this channel (Lott & Cingolani 2011). This structural feature maintains and protects the quality of the genetic material of the cell (Liu & York 2001). It also enables stringent regulation of genetically controlled processes within cells such as the transcription of NFAT in response to intracellular calcium release in T-cells (Feske et al. 2007; Gwack et al. 2007). Such control allows transcription factors access to the nucleus in response to certain stimuli, allowing cells to produce mRNA for protein translation in a

discriminant and/or regulated fashion (Hetzer & Wente 2009; Akhtar & Gasser 2007).

For a cell to respond to stimuli, signalling molecules must enter and leave the nucleus (Akhtar & Gasser 2007). This is done through the NPC, selectively allowing certain molecules entry and exit through the NE (Akhtar & Gasser 2007). The well-described method of transportation into the nucleus, the 'classical' pathway, involves interaction of KpnB1 with the adaptor protein KpnA2 (Figure 1.3 b) (Timinszky et al 2002). In this mode of importation, the nuclear localisation sequence (NLS) on the cargo molecule is recognised and subsequently binds to the adaptor protein KpnA2, which itself binds to KpnB1 (Conti, E., Muller, C. W. and Stewart M. 2005). This initial stage of the process takes place in the cytoplasm. Once in this bound conformation, the Karyopherin complex is able to dock on the outside of the NPC; following this, transport of the complex through the NPC into the nucleus via the interaction of KpnB1 with several nucleoporins is facilitated (Clarke P. L. and Zhang C. 2008). Once in the nucleus, disassociation of the cargo occurs upon binding of RanGTP and the cargo is freed to carry out its function within the nucleus (Conti, E., Muller, C. W. and Stewart M. 2005). The importer proteins are eventually recycled into the cytoplasm, with KpnB1 coupled to RanGTP and KpnA2 complexed to RanGTP and its export factor Crm1 (Clarke P. L. and Zhang C. 2008). In the cytoplasm, the hydrolysis of RanGTP by RanGAP releases the importer proteins for another round of protein importation (Clarke P. L. and Zhang C. 2008). The hydrolysis of

GTP provides the necessary energy for these transport cycles and is therefore the energy source for this process.

The transport of cargo through the NPC is dependent on the concentration gradient of RanGTP (Chook & Katherine E Süel 2011). In the cytoplasm, the import factors bind to their cargo in the absence of RanGTP (Chook & Katherine E Süel 2011; Yuh & Blobel 2001). The nuclear exporters will however only bind to their cargo if RanGTP is present, which thus constitutes an energy-requiring process (Chook & Katherine E Süel 2011; Clarke & Zhang 2004). The recycling of RanGTP is necessary if transport is to continue (Figure 1.3 a) (Chook & Katherine E Süel 2011; Yuh & Blobel 2001). In the nucleus, Ran combines with GTP via the guanidine nucleotide exchange factor RCC1, allowing it to provide the energy for transport of the KpnB1 and KpnA2 back to the cytoplasm (Chook & Katherine E Süel 2011; Clarke & Zhang 2004). During transport to the cytoplasm, GTP is hydrolysed by Ran GTPase activating protein 1 (RanGAP1), following which GDP is recycled into the nucleus (Conti, E., Muller, C. W. and Stewart M. 2005). The cycle is complete and another round of transport can take place.

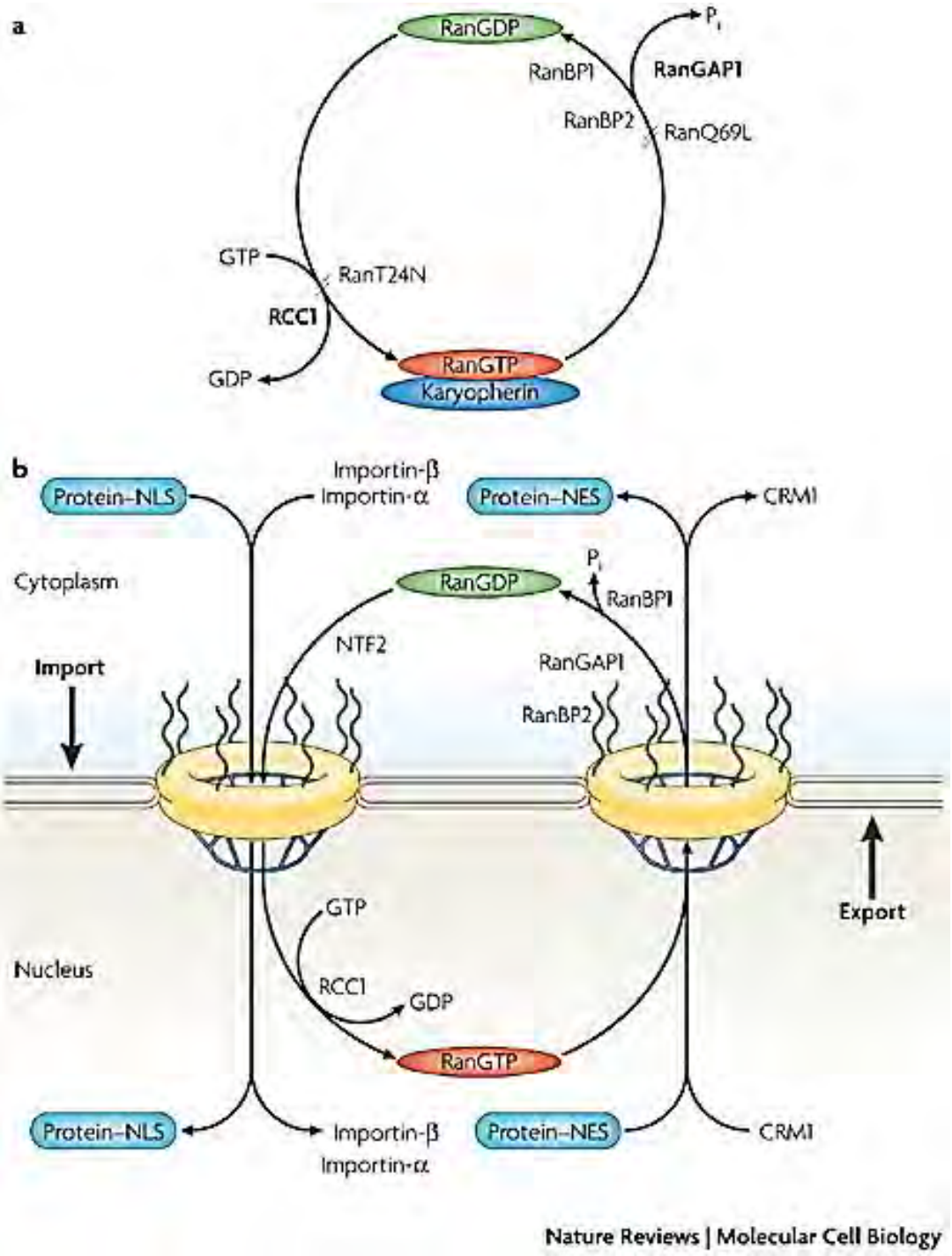

Figure 1.3: The classical nuclear import pathway: a) recycling of RanGTP to RanGDP via RCC1; b) Classic import pathway of KpnB1 (Importin-β) using KpnA2 (Importin-α) as an adaptor protein and GTP as the energy source (from Clarke & Zhang, 2008).

An additional mechanism by which molecules are able to enter the nucleus involves the direct interaction of the NLS located on the cargo with KpnB1. This non-classical transport mechanism happens independently of the binding of KpnA2 (Lott & Cingolani 2011). The cargo still requires RanGTP to bind to KpnB1 so that it can dissociate, and the recycling of KpnB1 and RanGTP is seen to occur in the same manner as it does in the classical pathway, only in the absence of KpnA2 (Lott & Cingolani 2011). An example where such a protein is transported in this way is Snuportin (Lott & Cingolani 2011).

1.6 The Nuclear Localisation Sequence

The nuclear localisation sequence (NLS) on the cargo molecule is the signal that promotes binding of the cargo to either the adaptor molecule KpnA2 (in the classic pathway) or directly to KpnB1 (in the non-classic pathway), thereby allowing the molecules to pass through the NPC into the nucleus (Yoneda et al. 1999). The NLS was first documented in 1984, when it was reported that a molecular sequence existed which was responsible for transporting the SV40 large-T antigen into the nucleus (Kalderon et al. 1984). After its discovery the sequence became known as the nuclear localisation sequence (NLS) and was known to have two important characteristics. Firstly, it is small (about seven residues), and secondly, it consisted mainly of highly basic amino acids such as arginine and lysines (Lott & Cingolani 2011; Kalderon et al. 1984).

This particular group of NLS became known as the classical NLS. Classical NLS can be either monopartite (single amino acid sequence) or bipartite (double amino acid sequence) (Kobayashi & Matsuura 2013; Cautain et al. 2015). This group of NLS interact with KpnA2 and function in the classical import pathway (Lott & Cingolani 2011).

The non-classical NLS differ in that they have more complex amino acid sequences, and their tertiary structure may also be important for the recognition of their target sequences (Lott & Cingolani 2011; Conti et al. 1998). The Importin B binding domain (IBB domain) on KpnA1, for example, has many basic amino acids, which facilitates the binding to KpnB1. This IBB domain has three defining characteristics. It adopts a favourable three-dimensional conformation when in complex with KpnB1, it is located on the N-terminus of Snuportin, and it is able to bind to KpnB1 with high (nanomolar) affinity (Lott & Cingolani 2011; Cingolani et al. 1999).

1.7 Structure and Function of Karyopherin B1

As previously described, KpnB1 is a nuclear transport factor which mediates the import of proteins and mRNA molecules into the nucleus of eukaryotic cells (Chook & Katherine E Süel 2011). In humans, this transport process is unidirectional and requires different transport proteins to control and maintain the export process. The bound crystal structure of KpnB1 has been determined, which allows insight into the three-dimensional structure of the protein and provides some clues as to how flexible the structure is when found in a bound

state (Yuh & Blobel 2001). To date the unbound crystal structure of KpnB1 has not been determined (Cingolani et al. 1999).

KpnB1 is a relatively large protein of around 100 kDa in molecular weight. It is comprised of 19 HEAT repeats (Huntingtin, elongation factor 3, PR65/A sub-unit of protein phosphates 2A, and the TOR lipid kinase). HEAT repeats are paired antiparallel alpha helices linked by a tandem loop, the pitch of which could change dramatically with the binding of substrates (Lee et al 2000). This flexibility is believed to be a key factor in allowing KpnB1 to interact with not just multiple different nuclear localisation signals on cargo molecules but also the adaptor protein KpnA2, the nuclear pore complex, and Ran (Conti et al. 2006).

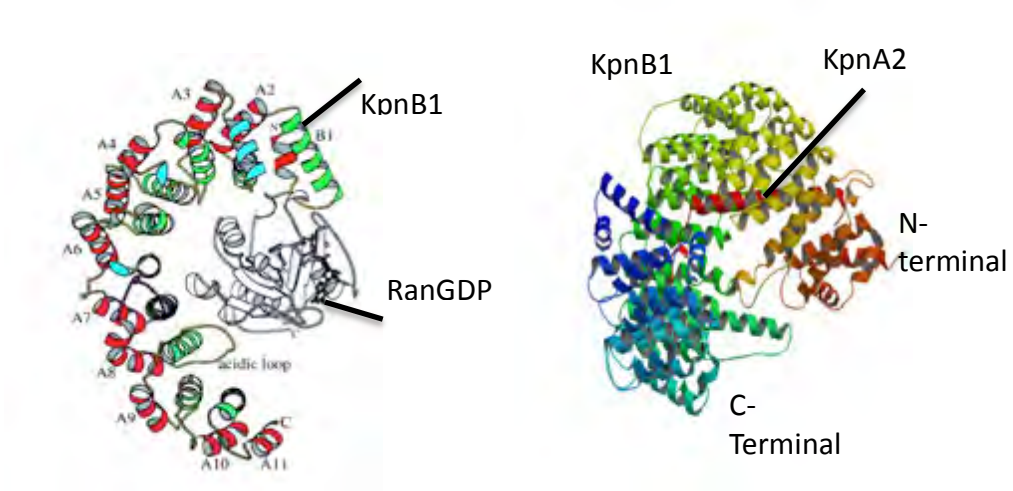

Figure 1.4: Crystal structure of KpnB1 bound to forms: A) KpnB1 bound to Ran: KpnB1 is a large superhelical structure binding Ran at the N-terminus (from Vetter, et al. 1999)(PDB ID: 1IBR). B) KpnB1 bound to the IBB binding domain of KpnA2: KpnB1 is a large superhelical structure binding the IBB domain of KpnA2 toward the N-terminus of KpnB1 (Cingolani et al. 1999)(PDB ID: 1QGK).

The HEAT repeats stack together with a slight clockwise twist, creating a superhelical structure with an inner concave surface and outer convex edge (Figure 1.4) (Conti et al. 2006; Chook & Katherine E. Süel 2011; Lee et al. 2000). The adaptor protein KpnA2 binds to the C-terminal arch of KpnB1, while RanGTP binds to the N-terminus (Figure 1.4) (Conti et al. 2006; Chook & Katherine E. Süel 2011). During the nuclear transport, either the 'classical' or the 'non- classical' pathways are activated to shuttle cargo molecules into the nucleus (Conti et al. 2006; Lee et al. 2000; Cautain et al. 2015). The adaptor and cargo proteins are seen to interact with the inner concave surface of KpnB1, while the Nups, which facilitate transport through the NPC, are seen to interact with the outer convex surface of KpnB1 (Lee et al. 2005).

Work done in our laboratory and elsewhere has shown that one of the key functions of KpnB1 is its role in maintaining cancer cell survival and for participating in cellular replication (van der Watt et al. 2009; Angus et al. 2014; Ciciarello et al. 2004). As discussed previously, we showed that KpnB1 expression is elevated in cervical cancer cells and KpnB1 siRNA – results in cancer cell death suggesting that KpnB1 is a possible candidate for targeting with small-molecule inhibitors (van der Watt et al. 2009; Angus et al. 2014; van der Watt et al. 2013). The design of the small-molecule inhibitor used in this project was based on the published crystal structure of KpnB1 bound to RanGTP and KpnA2. When bound to KpnA2, KpnB1 takes on a twisted 'snail-shell-like' conformation (Lee, S. J. et al 2000). The residues within HEAT repeats 1 to 3 and 4 to 7 are most likely responsible for generating flexibility within the protein structure, with

alpha helices able to rotate, avoiding steric interactions, in the case of RanGTP interactions (Lee, S. J. et al 2000). The acidic loop, on HEAT repeat 8, is important for substrate binding and disassociation (Cook et al, 2007). The unbound form of KpnB1 has not been determined and all compounds used in this study have been designed based on the bound form of KpnB1 (Lee et al. 2000). It is anticipated that targeting KpnB1 be effective in inhibiting its action (Cingolani et al. 1999; van der Watt et al. 2013).

1.8 Discovery of Small-Molecule Inhibitors with Anti-Cancer Activity

Paul Ehrlich first devised the term 'magic bullet' in the 1800s as a chemical therapy which was extremely specific in its action and interacted directly with its target (Imai & Takaoka 2006). Since then, targeted drug therapies have been successfully integrated into conventional cancer treatment in the form of small-molecule inhibitors, and the manner in which cancer is being treated now includes combination therapies (Imai & Takaoka 2006). As there is a high demand for treatments with reduced side effects and low cross-resistance, the need for novel compounds that are effective anti-cancer agents is equally urgent. The advent of technologies such as x-ray crystallography and genomic and proteomic sequencing has aided the discovery and production of new compounds with specific targets (Durrant & McCammon 2011).

Novel cancer therapeutic agents can take the form of small-molecule inhibitors, monoclonal antibodies, peptide mimics and antisense nucleotides (Imai & Takaoka 2006). Small-molecule inhibitors, which target kinases, have proven to be very useful in the treatment of various cancers. An example of where these

types of drug therapies have been very successful is in protein kinase inhibitors. Protein kinases catalyse intracellular reactions by transferring a terminal phosphate of ATP to substrates frequently on a serine or a threonine residue (Weisner et al. 2015). Kinases are important for signalling in the proliferation, survival and transformation of various oncogenes (Zhang et al. 2009). Drugs that target kinases are very specific in their action as they bind directly to the target protein attaching to a specific binding pocket. Their specificity means that they have been shown to reduce side effects when compared to chemotherapy and are therefore, often better tolerated by patients (Zhang et al. 2009).

An example of a well-known small-molecule kinase inhibitor in use today is Imatinib (Gleevec, GSK) (Druker 2002a). Imatinib is a tyrosine kinase inhibitor targeted at the mutant kinase created by the inversion of the BCR:ABL genes on the Philadelphia chromosome in chronic myeloid leukaemia patients (Druker 2002b; Druker 2002a). Figure 1.5 shows Imatinib (pink) bound to its target tyrosine kinase in the ATP binding pocket (Van Montfort & Workman 2009; Zhang et al. 2009). Imatinib binds to the glycine rich region (yellow) with hydrogen bonds and in so doing prevents the activation segment (red) from taking its active conformation and shutting down the signalling cascade responsible for uncontrolled cell reproduction (Van Montfort & Workman 2009; Zhang et al. 2009). A similar drug, known as Gefitinib (Iressa, Astra Zeneca), also binds to the ATP binding pocket of the epidermal growth factor tyrosine kinases inhibiting cancer cell proliferation (Van Montfort & Workman 2009). Gefitinib has been shown to be effective with Her1, Her2 and Her3 overexpressing cancer

patients, including breast and non-small-cell lung cancers (van Montfort and Workman 2009). These targeted therapies have been shown to be markedly successful because they function in such a specific manner. They inhibit the cancer cell's own molecular machinery which is mandatory for its survival, thus leading to cell death (Van Montfort & Workman 2009; Zhang et al. 2009).

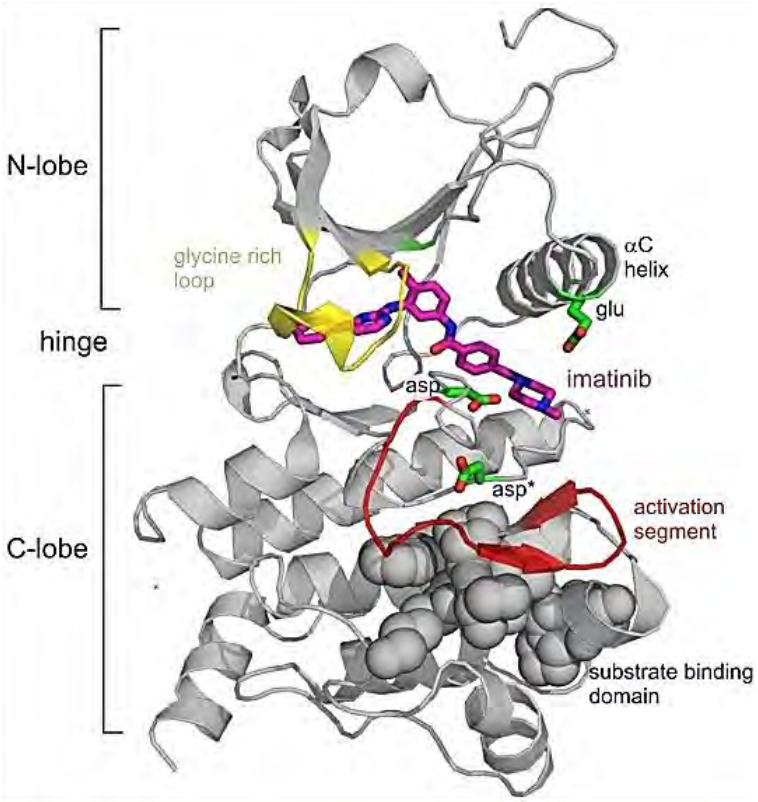

Figure1.5: Imatinib binds specifically to the mutant Tyrosine Kinase forcing it into the inactive conformation. Imatinib (pink) binds to the ATP binding pocket of the mutant tyrosine kinase via hydrogen bonds. The target activation segment (red) is forced into the inactive conformation (Van Montfort & Workman 2009)**.**

1.9 Inhibitors of Nuclear Transport as Anti-Cancer Approaches and rationale to this study

Chromosome region maintenance 1 (CRM1) is a nuclear export molecule, which controls the movement of molecules out of the nucleus. Like KpnB1, CRM1 has been observed to be up-regulated in some forms of cancer (Gerecitano 2014; van der Watt et al. 2009). It has been suggested that the increased export of tumour-suppressor proteins, including p53, p21, p27, pRb, FOXO and IKB, may play an important role in the maintenance of the cancer phenotype (Sun et al. 2013; Abdul Razak et al. 2016). Selective inhibitors of nuclear export (SINE) are new therapeutic compounds which are able to inhibit nuclear export by binding to the nuclear export sequence (NES) binding groove on CRM1 (Gerecitano 2014; Abdul Razak et al. 2016). By inhibiting the nuclear export machinery of tumour cells, SINE compounds are able to inhibit cancer cell proliferation and induce cell death by apoptosis. The compound Selinexor has been used in phase I clinical trials for use in multiple myeloma, AML, CLL, and various subtypes of NHL (Abdul Razak et al. 2016). These compounds may have use not just in cancer treatment; for example, Verdinexor, another SINE, is currently being tested as an antiviral treatment. The NES binding groove is located towards the N-terminus of CRM1 and contains several hydrophobic pockets. Crystal structures have revealed that SINES interact covalently with the NES binding groove, with cysteine 528 playing a major role in the binding of the compounds (Gerecitano 2014).

There is thus evidence that inhibiting nuclear transport has potential as an anti-cancer approach. In our laboratory, we aimed to identify small-molecule

inhibitors of nuclear import by targeting KpnB1 as an anti-cancer approach. Research in our lab has previously identified a parent compound using a rational drug-design approach which is a method commonly used to identify small-molecule inhibitors (Huggins et al. 2012). There are two types of rational drug design: ligand-based methods and structure-based methods (Huggins et al. 2012). In this approach a structure-based method was used: a technique which involves a process of 'reverse engineering' drugs, based on the known crystal structure of a target protein, using *in silico* modelling methods together with a large database of possible drug candidates to identify suitable test compounds (Huggins et al. 2012). Compounds identified as having potential to bind a specific target are tested *in vitro* and *in vivo* to assess the biological effects of the drugs and the binding affinities (Huggins et al. 2012). This may include making small changes to candidate molecules having the desired qualities, which are then pursued further. The chemical structure of the parent drug compound is altered to improve the efficacy of the compound and in some cases reduce undesired side effects (Huggins et al. 2012). The use of rational drug design in recent years has given rise to several major advances in cancer therapy. Such advances provide much hope for the field of drug design, as these new types of drugs have had success against certain cancer types. There are, however, still many forms of cancer, which remain difficult to treat and continue to have a high mortality rate, and for these cancer types the search for 'drugable' targets continues.

This project examines a novel previously identified small-molecule inhibitor and the way it functions *in vitro.* Of particular interest was whether the small-

molecule inhibitor being examined was directly interacting with KpnB1. The drug design process completed by our collaborators at the University of Louisville Kentucky, made use of the known crystal structure of KpnB1 bound to KpnA2 and Ran to screen an *in silico* library for small molecules with the potential to bind to KpnB1. The region of KpnB1 targeted was based on mutagenic studies that showed a loss in function of KpnB1 when alterations are incorporated into the regions where the binding site overlap of KpnA2 and RanGTP occurs between HEAT repeats 5 and 6 on the protein (Figure 1.6) (Cingolani et al. 1999).

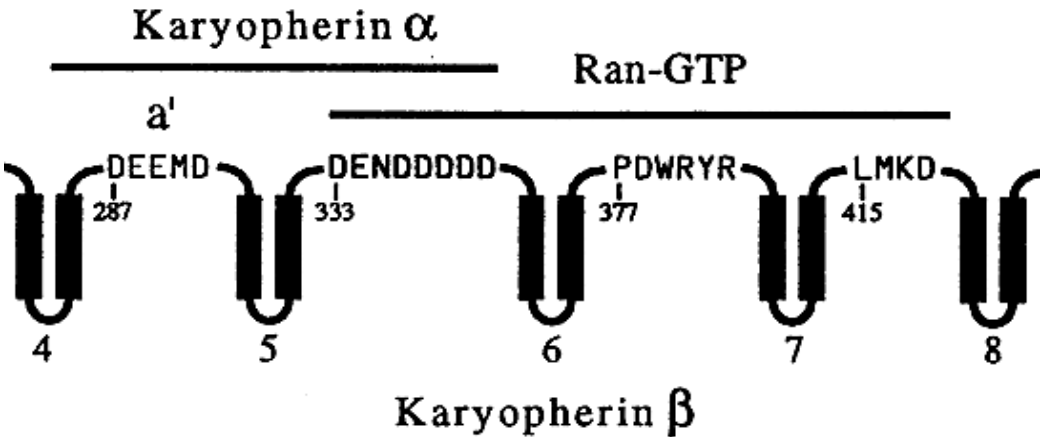

Figure1.6: Region of interest for drug binding is between HEAT repeats 5 and 6 of KpnB1. Schematic diagram of KpnB1 showing HEAT repeats 4 to 8 and the overlapping regions where RanGTP and KpnA2 bind (from Moroianu, Blobel, & Radu, 1996)**.**

1. The known crystal structure of bound KpnB1 was screened by our collaborators against an *in silico* library of 12 662 570 compounds for its ability to bind to small molecules. Of the compounds identified with potential to bind KpnB1, previous members of our laboratory tested forty-seven in *in vitro* experiments using CaSki cervical cancer cells. Compounds identified by the *in silico* screen were first tested for their effects on cell death and proliferation. Following this, compounds with the lowest IC_{50} (i.e. <50µM) were tested for their ability to block nuclear membrane transport. Only ten, of the compounds tested had an IC_{50} <50uM, and of these only three compounds – including one named inhibitor of nuclear import 43 (INI-43), 3-(1H-benzimidazol-2-yl)-1-(3-dimethylaminopropyl)pyrrolo[5,4-b]quinoxalin-2-amine – showed both cytotoxic effects and the ability to block nuclear transport as demonstrated by immunofluorescence microscopy and cell fractionation studies (van der Watt et al. 2016). The long-term goal of his research is to examine candidate KpnB1 targeted small molecules which were previously identified using a rational drug design approach and if they could have potential as future anti-cancer agents. This particular study is focused on investigating whether or not the lead compound INI-43 interacts with KpnB1 and attempts to examine the mechanisms and characteristics, which are responsible for enabling this possible interaction. If INI-43 was found to be interacting with the target protein KpnB1, it is possible that small changes could be make to the structure of INI-43 to improve the binding interactions between KpnB1 and INI-43.

Our objectives are as follows: Chapter 2 of the study outlines the *in vitro* effects of INI-43 on HeLa and CaSki cervical cancer cells. In this chapter a study of the effects of INI-43 on cancer cell proliferation, nuclear import as well as visualising changes to the localisation of KpnB1 in cells using confocal microscopy was performed. We examined the effects of INI-43 on cells expressing endogenous and exogenous KpnB1 and with the use of the far red fluorescent protein labelled KpnB1, and attempted to perform FRET photo bleaching to see if there was a direct interaction between KpnB1 and INI-43.

Chapter 3 outlines the production of purified protein and how this process was optimised using various chromatographic techniques. The methods used included His-affinity tag protein purification, anion exchange chromatography, gel filtration chromatography and GST-affinity tag protein purification. The final protein product was isolated on SDS-PAGE and confirmed via mass spectrometry.

Chapter 4 is a biophysical analysis of the in house purified protein with the experimental drug INI-43 to determine whether there is a direct interaction between the drug and the purified protein. We used various biophysical techniques including circular dichroism and isothermal titration calorimeterty in an attempt to characterise the possible interaction.

Detailed methodologies of all techniques used throughout this study are found in chapter 6.

1.10 Project Aims and Objectives

The aim of this study was to investigate the small molecule INI-43 as an anti-cancer agent and its ability to interact with the nuclear transport protein KpnB1. The objectives were:

2. To investigate the effects of INI-43 on HeLa and CaSki cancer cell biology by:

a. Determining INI-43 IC_{50} values.

b. Determining the effects of INI-43 on HeLa and CaSki cell proliferation and the induction of cell death.

c. Investigating the effects of INI-43 on the activity of NFAT, a KpnB1 cargo protein.

d. Investigating the effect of INI-43 on KpnB1 sub-cellular localisation.

3. To generate KpnB1 clones to be used in the preparation of purified KpnB1 for biophysical analysis of drug–protein interaction.

4. To investigate KpnB1-INI-43 interaction using circular dichroism (CD) and Isothermal calorimetry (ITC).

Chapter 2

Investigating the effects of a potential small molecule inhibitor of nuclear import, INI-43, on cervical cancer cells

2.1 Introduction

Previous studies have shown that the nuclear trafficking protein KpnB1 is upregulated in cervical cancer and transformed fibroblasts (van der Watt et al. 2009). Studies using siRNA showed that the knock-down of KpnB1 expression inhibits proliferation of cervical cancer cells and is associated with cell death via apoptosis (van der Watt et al. 2009; van der Watt et al. 2011; Angus et al. 2014); KpnB1 is implicated in mitosis and spindle assembly and its inhibition has thus been shown to affect cell cycle progression.

While no currently known therapeutic drugs specifically target KpnB1 as an anti-cancer agent, there are two experimental compounds, Karyostatin and Importazole, that inhibit the KpnB1–RanGTP interaction in the classical import pathway (Jonathan F Soderholm et al. 2011; Bird et al. 2013; Jans et al. 2011). Both compounds have been used to study cell cycle and chromatin assembly (Jans et al. 2011). Importazole is a 2,4-diaminoquinoxaline (Figure 2.1 A) and Karyostatin is a pyrole compound, which is a larger molecule (and subsequently reported also to be bulkier) (Figure 2.1 B) (Jonathan F Soderholm et al. 2011) (Bird et al. 2013). There is limited knowledge of the anti-cancer potential of these molecules.

As our laboratory has an interest in targeting KpnB1 as an anti-cancer approach, we aimed to identify novel small molecules with potential to bind to, and inhibit KpnB1

function (van der Watt et al. 2013).

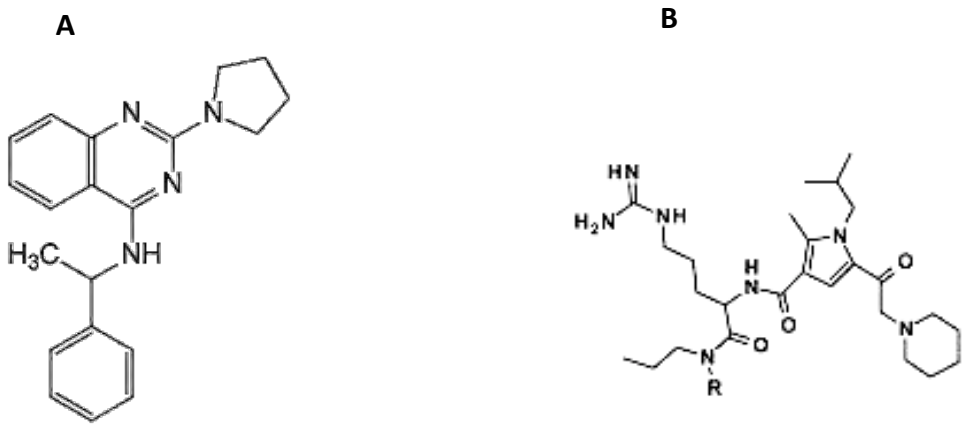

Importazole **Karyostatin**

Figure 2.1: Current experimental compounds which inhibit KpnB1 A) Chemical Structure of Importazole B) Chemical structure of Karyostatin.

Mutagenic studies of KpnB1 have shown a loss in function of KpnB1 when there are alterations to the regions where overlap occurs at the binding sites of KpnA2 and Ran-GTP, specifically between HEAT repeats 5 and 6 (Moroianu et al. 1996b). We therefore hypothesised that if a drug-like molecule was engineered to bind to the region of overlap, similar effects of loss in protein function may be observed.

An *In-silico* library of small molecules were screened based on their ability to bind to the KpnB1 target region of interest. The computational screening analysis was performed by our collaborators at the Molecular Modelling Facility of the James Graham Brown Cancer Centre, University of Louisville, Kentucky, USA, using a structure-based drug design approach. The aim was to identify compounds that bind the overlapping Ran- and KpnA2-binding region of KpnB1, (specifically between HEAT repeats 5 and 6) based on their crystal structures (PDB codes 1ibr, 2bku and

1qgk). A library of 12 662 570 distinctive chemical compounds in the ZINC drug-like database (Irwin & Shoichet 2005) was investigated against the regions of interest using the 1ibr structure, based on the methods described in (Holt et al. 2009). The compounds were ranked according to their predicted KpnB1-binding affinity and forty-seven of the top-scoring candidates were subsequently purchased from MolPort (Riga, Latvia), ChemBridge (San Diego, CA, USA) and Enamine (Kiev, Ukraine). Our laboratory screened these compounds for their ability to block nuclear import, as well as their cytotoxic effects on normal and cancer cells (van der Watt et al. 2016). Inhibitor of Nuclear Import-43, INI-43 (3-(1H-benzimidazol-2-yl)-1-(3-dimethylaminopropyl)pyrrolo[5,4-b]quinoxalin-2-amine) (Figure 2.2) exhibited both cytotoxic and nuclear import inhibitory effects and was obtained from Chembridge (ZINC identification no. 20547783) (van der Watt et al. 2013) and Stowell, 2011, MSc Dissertation.

INI-43 is a quinoxaline based compound and previous research has shown that quinoxaline based compounds have potential as anti-proliferative on cancer cells, (Pereira et al. 2014). INI-43 was one of three compounds identified to have both cancer cell killing effects and inhibitory effects on nuclear import pathways (Stowell, 2011). In this study, we aimed to further investigate the cell cancer killing effects and the nature of INI-43-KpnB1 interactions as a follow on to the Stowell study.

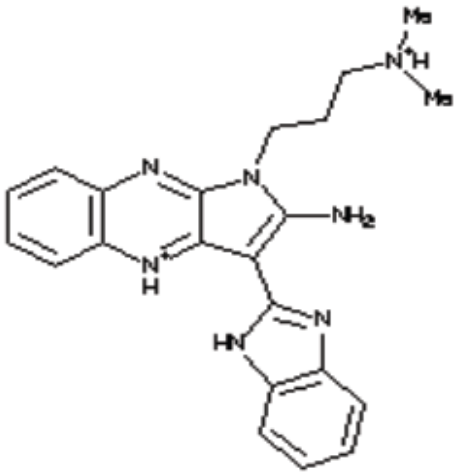

Figure 2.2: Inhibitor of nuclear transport 43 (INI-43). Chemical structure of INI-43 molecule; chemical name: (3-(1H-benzimidazol-2-yl)- 1-(3-dimethylaminopropyl)pyrrolo[5,4-b]quinoxalin-2-amine).

2.2 Results

2.2.1 Effects of INI-43 on cervical cancer cell proliferation

Full methods are found in chapter six, however briefly, studies were conducted in order to establish the IC_{50} of INI-43 in HeLa and CaSki cervical cancer cell lines, as well as examining the effects on cellular proliferation using the 3-(4,5-Dimethylthiazol-2-yl)-2,5-diphenyltetrazolium bromide (MTT) assay. This assay has been well characterised in the past as a colorimetric assay, able to determine cellular viability based on the colour change of the MTT based on the cells metabolic activity. This therefore allows for analysis of the potency of the anti-proliferative effects of the compound being tested. We used absorbance at 595nm as a direct measure of cellular proliferation.

Cell growth was analysed by measuring optical density at 595nm in the absence and presence of increasing concentrations of INI-43 (0, 1, 5, 8, 10, 15, 20 and 40μM) over a period of 48 hours. An IC_{50} of 6.23 μM was found in HeLa (Figure 2.3A) and 6.82 μM in CaSki (Figure 2.3B). These results were in line with that obtained by Stowell, 2011, MSc thesis, where an IC_{50} value of approximately 10 μM was obtained.

To monitor the effects of INI-43 on proliferation we again used the MTT assay using both HeLa and CaSKi cells. Cells were grown in 0, 5, 10 and 15 μM INI-43 over a period of five days. Our results show that 5, 10 and 15 μM concentrations of INI-43 have a significant inhibitory effect on cell proliferation in HeLa (Figure 2.4A) and 10 and 15 μM in CaSki (Figure 2.4B) cells. INI-43 thus has a clear cytotoxic effect on both cell lines.

2.2.2 INI-43 induces cell death via apoptosis.

Having shown that INI-43 is cytotoxic, we next investigated whether cell death induced via INI-43 treatment occurred via the apoptotic pathway. To monitor whether cell death occurred via apoptosis, we used the standard method of measuring apoptotic cell death using Poly (ADP-ribose) polymerase-1 (PARP-1) cleavage in HeLa and CaSki cells. Increasing doses of INI-43 (0 μM, 5 μM and 10 μM) were selected and used to treat both cell lines for a period of 24 hours. A dose of 15 μM INI-43 resulted in substantive cell death and degradation of all proteins including the loading control (data not shown). When cells treated with 15 μM INI-43, were viewed under the inverted light microscope, we observed no live cells, only floating dead cells. We thus assumed that by the time the cells were harvested for the assay any proteins would

have been degraded by the apoptotic pathway.

PARP-1 is downstream of caspase 3/7 which activates the cleavage of PARP-1 on upstream signals from the cell's mitochondria. Once PARP-1 becomes cleaved it initiates fragmentation of the DNA and the cells die via apoptosis. Western blot analysis for PARP shows a clear presence of cleaved PARP-1 in the presence of INI-43 in both HeLa (Figure 2.5 A) and CaSki (Figure 2.5 B) cells, confirming that INI-43 induces cell death via apoptosis. PARP cleavage was most pronounced at 10 µM INI-43. These results have also been supported by caspase 3/7 assays (van der Watt *et al.,* 2016).

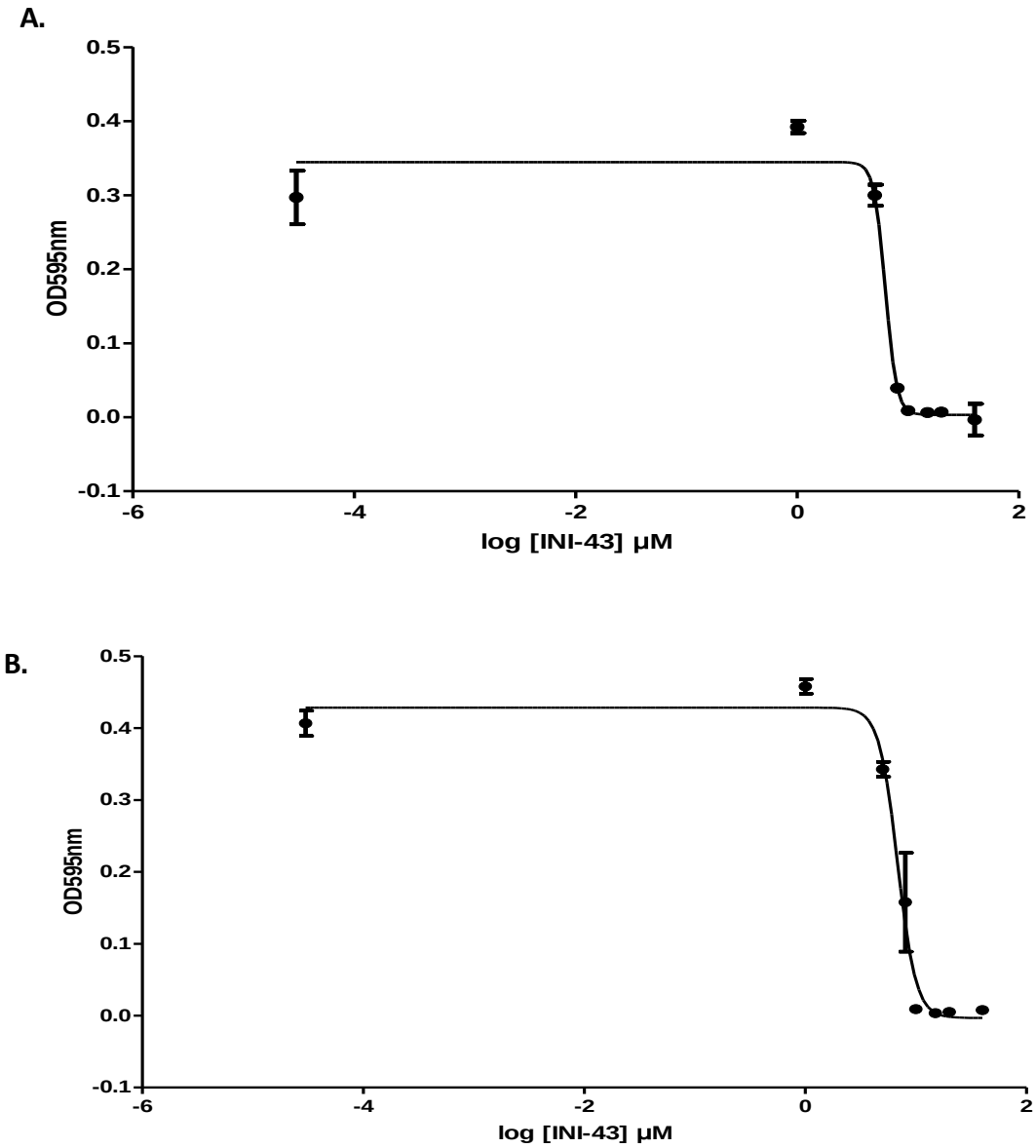

Figure 2.3: Dose-response curves showing HeLa (figure 2.3A) and CaSKi (figure 2.3B) response to increasing concentrations of INI-43. Half maximal inhibitory concentration (IC_{50}): IC_{50} of INI-43 in HeLa cells found to be 6.23µM (Figure 2.3A). The IC_{50} of INI-43 in CaSKi cells found to be 6.82 µM (Figure 2.3B).

A

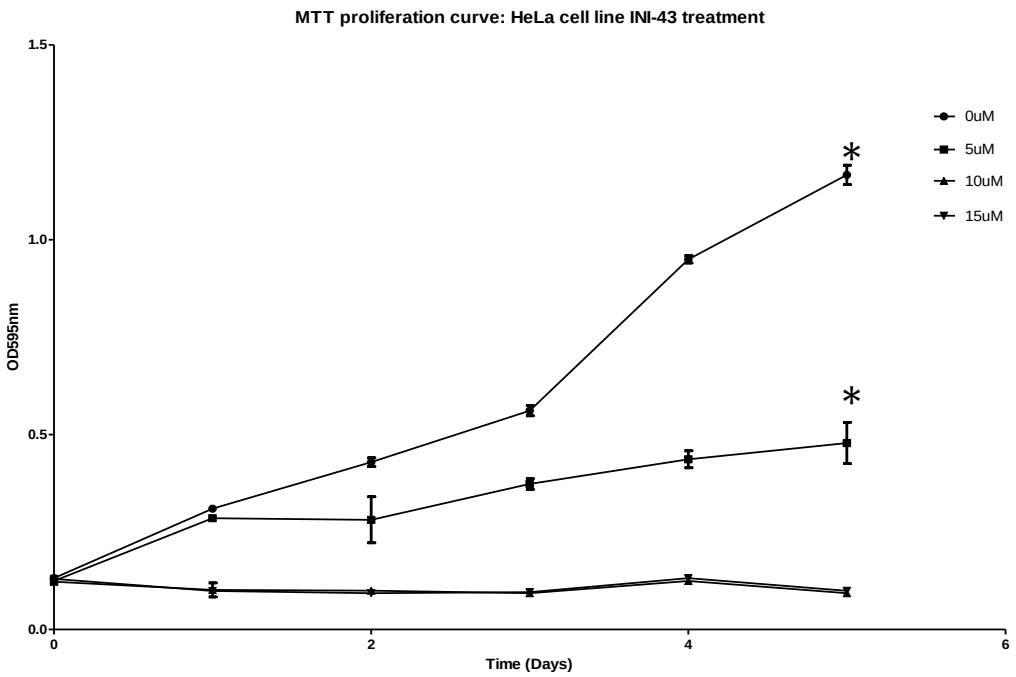

Figure 2.4: (A) Effect of INI-43 on HeLa cell proliferation. HeLa cells were treated with 0, 5, 10 and 15 µM INI-43, and proliferation monitored over five days using the MTT assay. Results shown here are the mean ± SEM of experiments performed in quadruplicate and repeated at least three independent times. (*p<0.05).

B

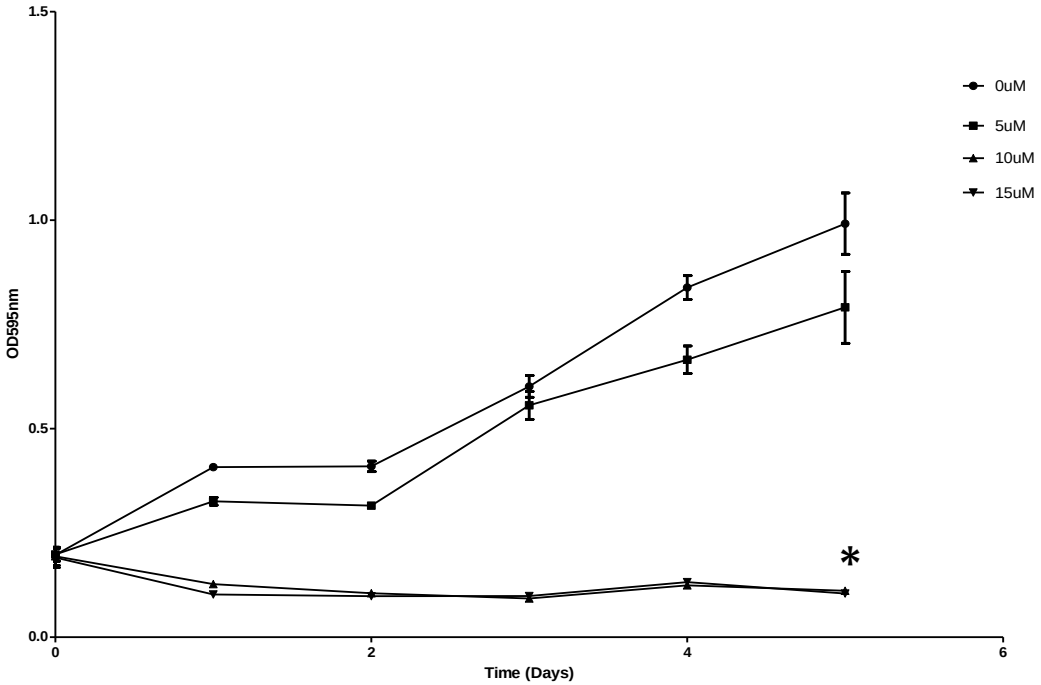

Figure 2.4: (B) Effect of INI-43 on CaSKi cell proliferation. CaSKi cells were treated with 0, 5, 10 and 15 µM INI-43, and proliferation monitored over five days using the MTT assay. Results shown here are the mean ± SEM of experiments performed in quadruplicate and repeated at least three independent times. (*p<0.05)

C

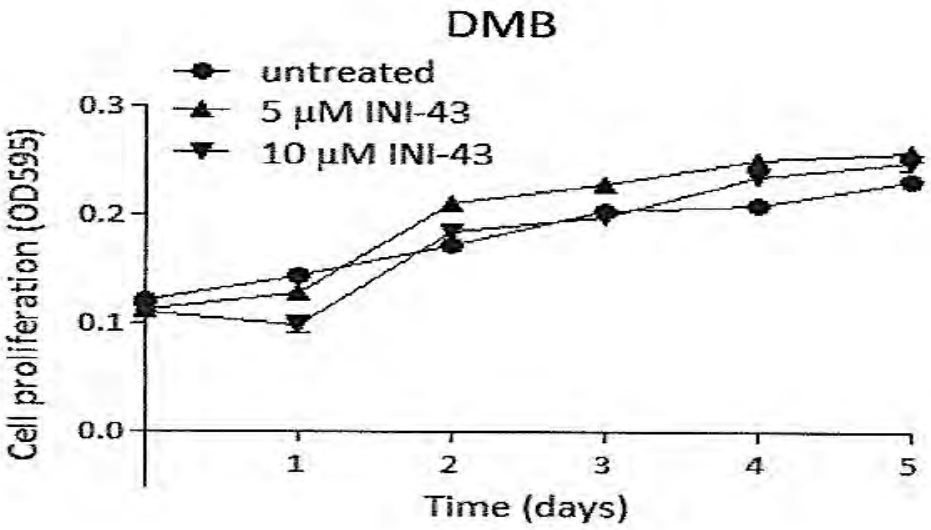

Figure 2.4: (C) Effect of INI-43 on DMB cell proliferation. DMB cells were treated with 0, 5, and 10 µM INI-43, and proliferation monitored over five days using the MTT assay. Results shown here are the mean ± SEM of experiments performed in quadruplicate and repeated at least three independent times (van der Watt et al. 2016).

D

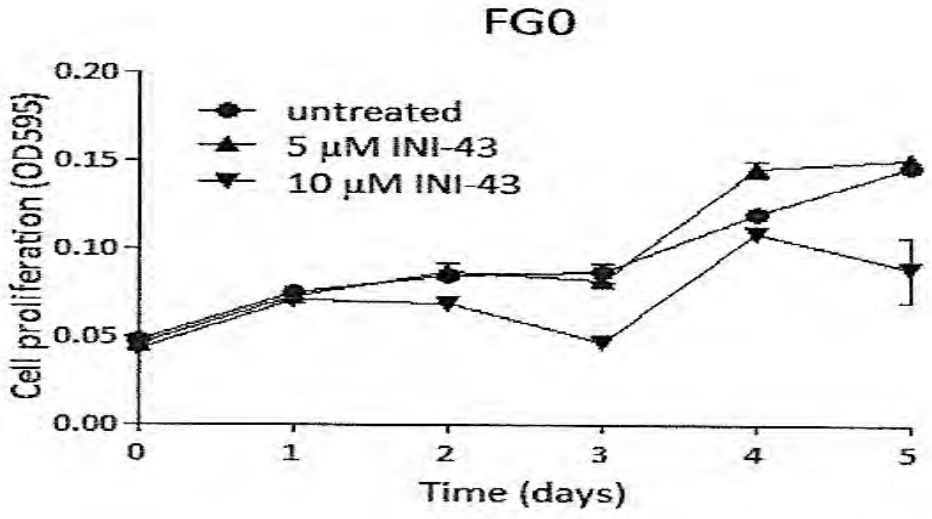

Figure 2.4: (D) Effect of INI-43 on FGO cell proliferation. FG0 cells were treated with 0, 5, and 10 µM INI-43, and proliferation monitored over five days using the MTT assay. Results shown here are the mean ± SEM of experiments performed in quadruplicate and repeated at least three independent times. (*p<0.05) (van der Watt et al. 2016).

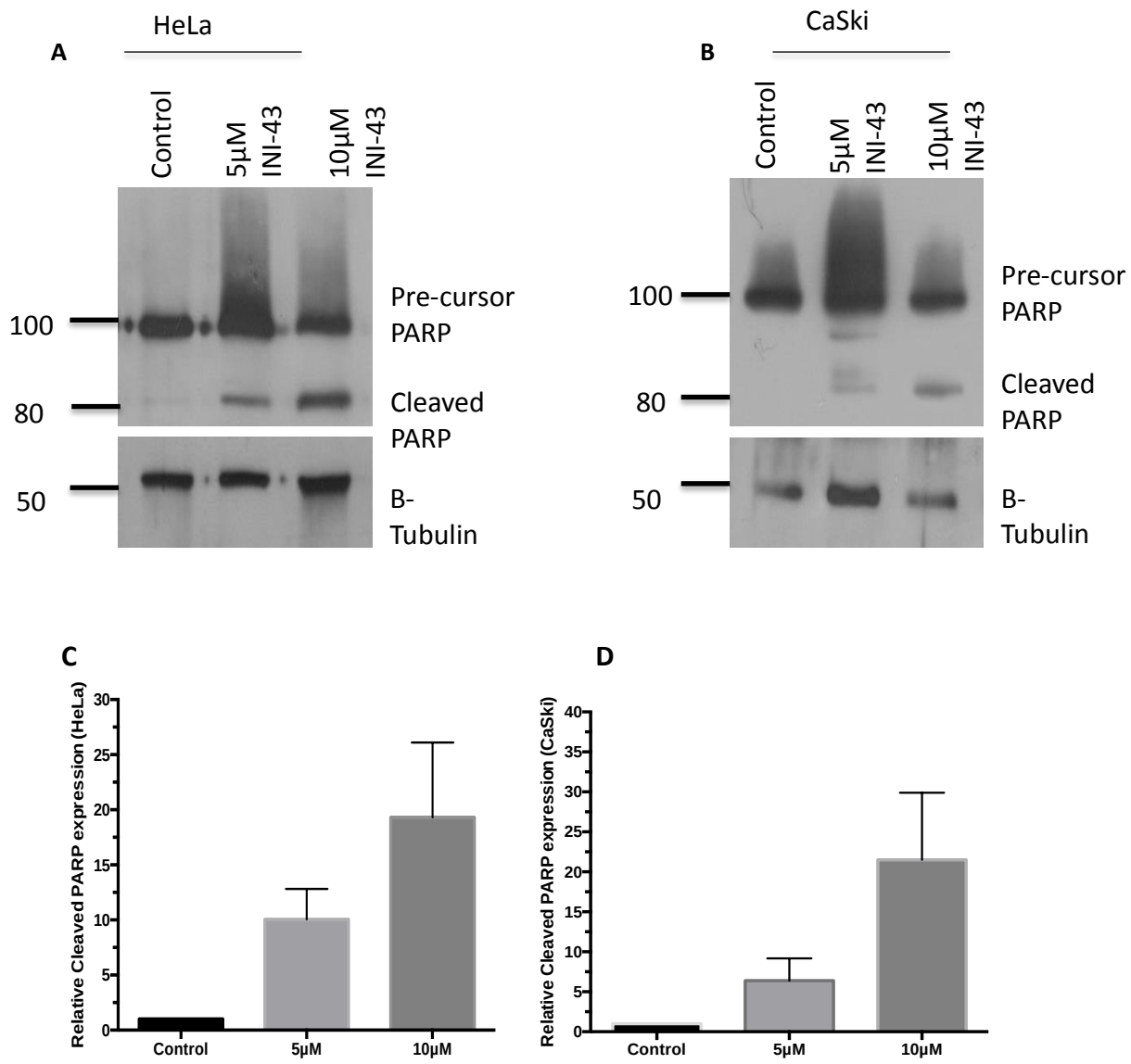

Figure 2.5: INI-43 induces cells death via apoptosis as shown by PARP-1 cleavage: Western blot analysis showing and increase in cleavage of pre-cursor PARP-1 with increasing doses of INI-43 in both HeLa and CaSki cell lines. (A) PARP-1 cleavage in HeLa cells; (B) PARP-1 cleavage in CaSki. Western blot analysis of PARP cleavage in cell lysates obtained from control, 5 µM and 10 µM INI-43 treated CaSki and HeLa cells. Cells were treated for 24hrs. β-Tubulin was used as a loading control. Results shown are representative of experiments performed at least three independent times. (C) Histogram showing quantification of cleaved PARP-1 relative to tubulin in HeLa. (D) Histogram showing quantification of cleaved PARP-1 relative to tubulin in CaSki.

2.2.3 Effects of INI-43 on Nuclear import of KpnB1 target proteins, NFAT

Having established that INI-43 induced a cytotoxic effect on the cervical cancer cell lines and cell death via apoptosis, we next examined the effect of INI-43 on nuclear import. This was done by (i) investigating the nuclear import of a KpnB1 target protein and (ii) investigating KpnB1 localisation after INI-43 treatment. The activity of NFAT, a known KpnB1 target protein, was investigated as a marker of KpnB1-mediated nuclear import. A NFAT-luciferase reporter plasmid containing three tandem repeats of a 30 bp fragment of the IL-2 promoter known to bind NFAT was used in luciferase assays as a measure of NFAT nuclear import (Addgene plasmid #10959). HeLa cells were transfected with the NFAT-responsive plasmid and treated with 5, 10 and 15 μM. Cells were treated with Ionomycin and PMA to induce NFAT nuclear translocation and associated transcriptional activity. Ionomycin induces the release of intracellular calcium stores and stimulates NFAT translocation to the nucleus (Beals et al. 1997).

Our data shows that PMA/Ionomycin treatment resulted in NFAT activation (i.e. nuclear translocation). A dose-responsive decrease in NFAT activity was observed with increasing concentration of INI-43 (Figure 2.6). From this we inferred that the decrease in NFAT activity was a result of decreased import of NFAT in the presence of INI-43. Since NFAT relies on KpnB1 to gain entry into the nucleus, these results suggest that INI-43 interferes with the nucleus-import activity of KpnB1.

Alternatively this observation could be as a result of the INI-43 is preventing upstream calcium dependent phosphatases from dephosphorylating the NLS of NFAT thereby preventing the recognition of the NLS by KpnB1 resulting in an inhibition of NFAT activity.

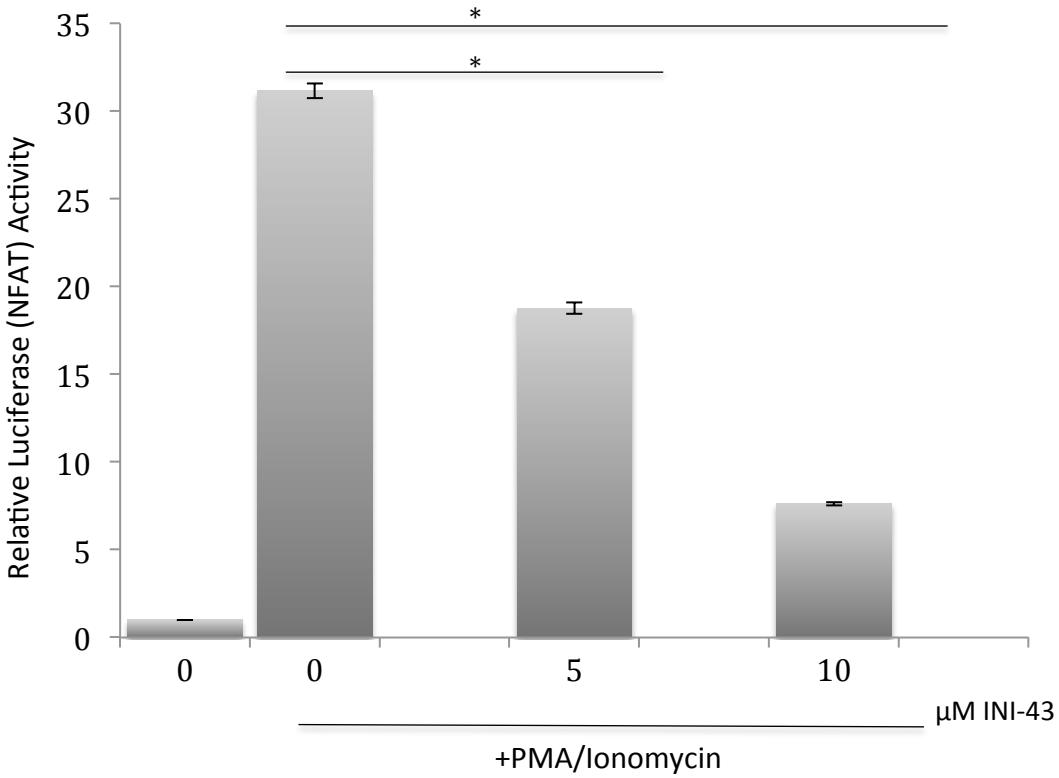

Figure 2.6: INI-43 inhibits nuclear import of the KpnB1 target protein NFAT. HeLa cells were transfected with the NFAT-luciferase reporter plasmid (Addgene plasmid #10959), then treated with 5 and 10 µM of INI-43. After stimulating with Ionomycin and PMA, the relative NFAT activity was quantified by expressing luminescence relative to that of the transfection control, TK-renilla-luciferase. Results shown are the mean ± SD of experiments performed in triplicate. ($p<0.05$).

2.2.4 Effects of INI-43 on the endogenous KpnB1 localisation

Previous studies demonstrated that endogenous levels of KpnB1 expression are elevated in cervical cancer cells. A major function of this protein is aiding the transport of cargo molecules through the NPC. Earlier experiments referred to in this chapter have shown that the small molecule inhibitor INI-43 is able to inhibit the activity of the KpnB1 target protein NFAT.

Having observed the ability of INI-43 to inhibit the activity of KpnB1 target proteins, we also investigated the effects INI-43 of on the localisation of KpnB1 itself in HeLa cells, using confocal microscopy. Control and HeLa cells treated with 5 μM INI-43 for 45, 60 and 180 minutes using immunofluorescence analysis for KpnB1. Cell nuclei were stained with DAPI and images were captured using a Zeiss fluorescence microscope.

Our results show that in control untreated cells, KpnB1 was mainly located in the nucleus (Figure 2.7A). Treatment of cells with INI-43 for 45 minutes resulted in relocation of KpnB1 towards the peri-nuclear and cytoplasmic areas of the cells (Figure 2.7B). Similar observations were made with the 60-minute treatment, with cells showing an intense peri-nuclear localization of KpnB1 forming a "ring-like" structure (Figure 2.7C). With the 180-minute INI-43 treatment, KpnB1 localisation appeared to be predominantly cytoplasmic (Figure 2.7D). These results provide evidence that the small molecule INI-43 interferes with the nucleus localisation of KpnB1. By inhibiting the normal transport mechanism of KpnB1, INI-43 appears to interfere with the nuclear localisation of KpnB1 and to

block its nuclear entry, subsequently preventing the import and activity of KpnB1 target proteins such as NFAT.

2.2.5 Effects of INI-43 on Cells Expressing Red Fluorescent Tagged KpnB1

Preparation of Red Fluorescent Tagged KpnB1

In addition to investigating the effects of INI-43 on endogenous levels of KpnB1, we also explored the effects of INI-43 on the localisation of exogenously expressed far-red fluorescent-labelled KpnB1. The first step was to prepare a fluorescent-labelled KpnB1 construct (FRFP-KpnB1), accomplished by cloning the KpnB1 insert into the pmKate-2c plasmid. Full-length KpnB1 was amplified using PCR from pGEX6-KpnB1 (a plasmid constructed in this project for protein purification methods). Restriction sites (Sac11 and BamH1) were incorporated into the 5' and 3' end primers to facilitate the cloning of the KpnB1 fragment into the final plasmid.

A PCR product of approximately 2.5 Kb was obtained (Figure 2.8A). The 2.5 Kb product was cloned into pmKate-2C, and the fragment was released and checked by enzymatic digestion using Sac11 and BamH1 (Figure 2.8B). The presence of the insert was also confirmed by sequence analysis. To confirm expression of the tagged protein, the plasmids were transfected into HeLa cells and protein lysates extracted followed by western blot analysis. Results showed that transfected cells were positive for both endogenous KpnB1 and tagged FRFP-KpnB1 (Figure 2.8C). Cells transfected with FRFP-KpnB1 and treated with INI-43 were subsequently used to monitor the effects of INI-43 on the FRFP-KpnB1 sub-

cellular localisation using confocal microscopy. Our results show that INI-43 treatment results in peri-nuclear and cytoplasmic localisation of FRFP-KpnB1 (Figure 2.9), very similar to that observed with endogenous KpnB1. The chemical structure of INI-43 makes the molecule fluoresce between 488nm and 540nm, and hence its localisation could be monitored by fluorescent microscopy. INI-43 appeared to localise throughout the cell (figure 2.9).

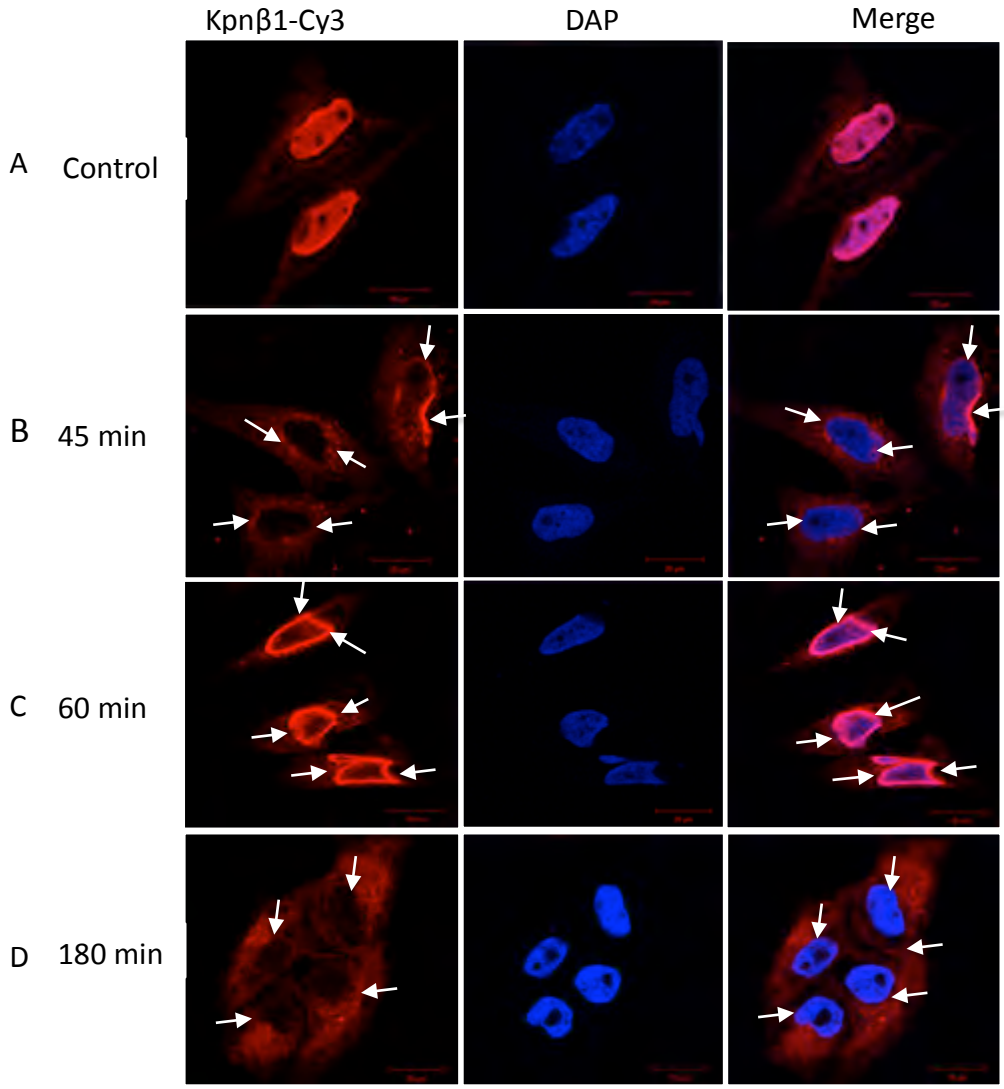

Figure 2.7: Effects of INI-43 treatment on localisation of endogenous KpnB1. Immunofluorescent analysis showing INI-43 treatment alters KpnB1 subcellular localisation. HeLa cells were treated with 5 µM INI-43 for 45 minutes, 60 minutes and 120 minutes, and fluorescent images captured by confocal microscopy. **(**A) Control/untreated cells. (B) 45 min treatment with 5 µM INI-43. (C) 60 min treatment with 5 µM INI-43. (D) 180 min treatment with 5 µM INI-43. The arrows show how the protein re-localises from the nucleus in control/untreated cells to create intense peri-nuclear relocation of KpnB1 forming a distinct ring as described previously.

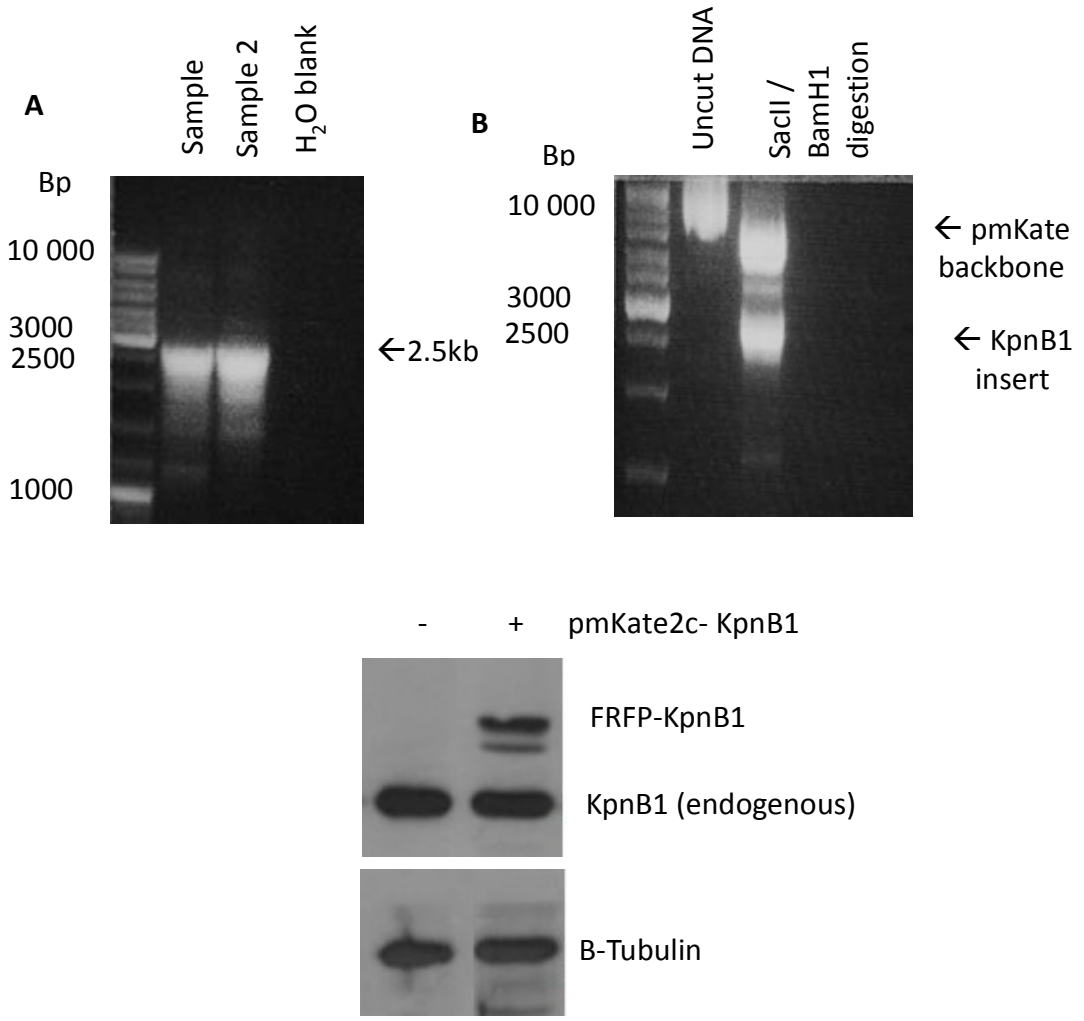

Figure 2.8: Preparation of FRFP-pmKate2c plasmid. (A) PCR amplification of 2.5 kbp KpnB1. (B) Restriction digestion to visualise KpnB1 release from the final plasmid using SacII and BamHI. (C) Western blot to visualise successful expression of FRFP-KpnB1 in HeLa cells post transfection with gencellin.

2.2.6 Visualising the timing of INI-43 uptake in HeLa cells via confocal microscopy

Having found that INI-43 displays fluorescent characteristics, we monitored INI-43 fluorescence and FRFP-KpnB1 concurrently over a period of 20, 30, 40, and 45 minutes of drug treatment. HeLa cells were grown on glass coverslips, and, following transfection with FRFP-KpnB1, the cells were then treated with INI-43 and were observed at various different time intervals using confocal microscopy.

Our results show that INI-43 fluorescence is detected in the cells at 20 minutes (Figure 2.10A). At this time point there seems to be little effect on FRFP- KpnB1 localization, which is predominantly nuclear (Figure 2.10B). By 30 minutes, INI-43 treatment appears to have an effect on the FRFP-KpnB1 localisation and there is a less intense localisation in the nucleus than at the 20-minute treatment. A peri-nuclear "ring-like" localisation of FRFP-KpnB1 is observed (Figure 2.10C). Within 40 minutes of INI-43 treatment, the cytoplasmic and a more intense peri-nuclear localisation of FRFP-KpnB1 is observed (Figure 2.10D). A 45-minute INI-43 treatment period showed localisation of FRFP-KpnB1 similar to that observed at 40 minutes (Figure 2.10E). These findings support our earlier data on the effects of INI-43 on endogenous KpnB1 localisation, showing a similar pattern in which treatment with INI-43 results in peri-nuclear and cytoplasmic KpnB1 localisation.

Our data on the effects of INI-43 on the localisation of KpnB1, suggest that INI-43 may be interacting and inhibiting KpnB1. Our next investigation was therefore to monitor the potential of INI-43–KpnB1 interaction using FRET photobleaching.

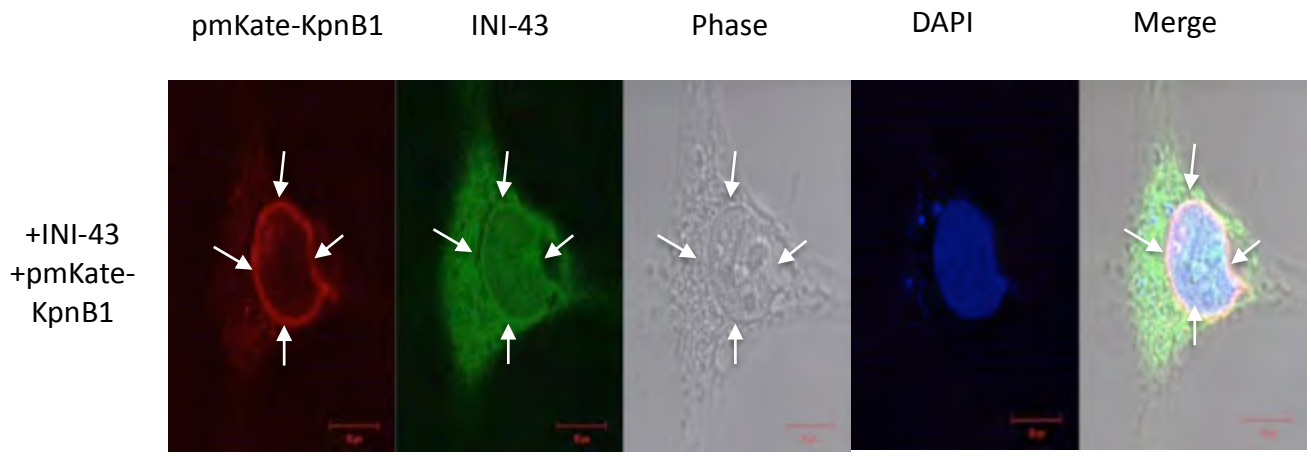

Figure 2.9: Confocal microscopy shows relocation of exogenously expressed KpnB1 post treatment with INI-43. HeLa cells transfected with FRFP-KpnB1 and treated for 24 hours with INI-43. A similar pattern to that of the endogenous KpnB1 (Figure 2.7) observed in that FRFP-KpnB1 localises in the peri-nuclear and cytoplasmic region. A distinct peri-nuclear "ring-like" structure is formed post treatment with INI-43 (distinguished by white arrows). INI-43 itself fluoresces, and appears to localise throughout the cell.

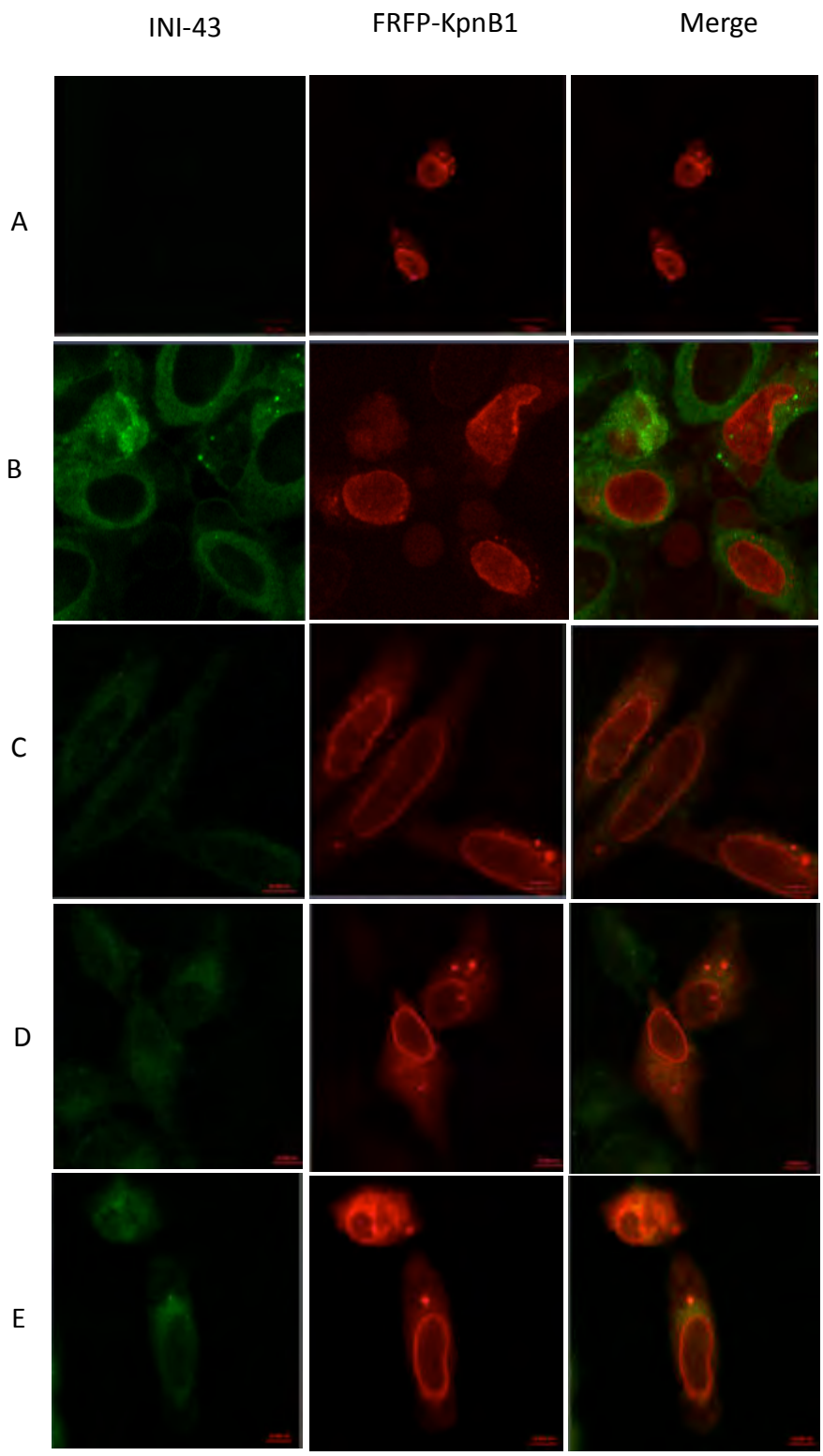

Figure 2.10: Immunofluorescent analysis of INI-43 and FRFP-KpnB1 in HeLa cells. (A) HeLa cells transfected FRFP only (scale 20µM). (B) HeLa cells treated with 5 µM INI-43 for 20 min (scale 10 000µM). (C) HeLa cells treated with 5 µM INI-43 for 30 min. (D) HeLa cells treated with 5 µM INI-43 for 40 min (scale 10 000µM). (E) HeLa cells treated with 5 µM INI-43 for 45 min (scale 10 000µM).

2.2.7 FRET Photobleaching analysis as an approach for measuring FRFP-KpnB1 and INI-43 interactions

We had earlier established the duration for treatment of cells with INI-43 that would show optimal effects on exogenously expressed FRFP-KpnB1 in HeLa cells. This optimal treatment duration was identified as being between 30 and 45 minutes - the duration within which the effects of changes in FRFP-KpnB1 localisation were visualised most clearly. We adopted this timing in using FRET photobleaching analysis to examine whether or not the KpnB1 was directly interacting with INI-43.

We used FRFP-KpnB1 in FRET photobleaching experiments, as spectral analysis showed that INI-43 and the red fluorescence in pmKate-2C had overlapping excitation and emission spectra, which is a necessary requirement for FRET (figure 2.11 A). When performing FRET photobleaching it is important that the excitation and emission spectra of the donor overlap with those of the acceptor. During the assay lasers to excite the donor fluorphore, causing it to fluoresce. Photons from the excited donor, of the correct wavelength are released and excite the acceptor, causing it too, to fluoresce. An initial image is taken providing a reading of both donor and acceptor fluorescence. Next, a region of interest (ROI) is selected, and within this ROI, the acceptor is bleached out using a high-intensity laser. The image is recaptured and the FRET efficiency is calculated. Upon bleaching the acceptor fluorophore, the donor, gives off higher intensity fluorescence when excited, as it is no longer sharing photons with the acceptor. Thus, if there is a direct interaction between donor and

acceptor, when the acceptor is bleached the donor produces a brighter signal than in the pre-bleach reading.

To determine whether FRET photobleaching was a feasible assay to monitor potential KpnB1-INI43 interactions, the excitation and emission scan of INI-43 was read in a fluorometer and compared to that of the spectra of FRFP in pmKate-2c (Figure 2.11 A). The spectra of INI-43 were also read inside cells to determine that the drug does not change its excitation and emission spectra after being taken up by the cells (Figure 2.11 B). The spectral scan of the drug in Figure 2.11 A produced the same results as the scan of the cells in Figure 2.11 B. These spectral scans suggested that INI-43 and FRFP-KpnB1 were compatible for use in FRET photobleach analysis.

Having established the required parameters for FRET photobleaching, we set up experiments post treatment with INI-43. HeLa cells grown on glass coverslips were transfected with FRFP-KpnB1. The cells were treated with 5 μM INI-43 for a period of time and then fixed, and fluorescent images were taken pre- and post-bleach and the FRET efficiency measured.

FRET photobleaching was performed at different time points (20, 30, 40 and 45 minutes), showing pre- and post-bleaching comparisons for the region of interest (Figure 2.12). After 20 minutes, a low FRET signal was observed in comparison to the 30, 40 and 45-minute drug treatments. At the 30, 40 and 45-minute time points a peri-nuclear ring formation was observed where protein was re-located from the nucleus. Based on these experiments, the ideal time to perform FRET photobleaching was between 30 and 40 minutes after INI-43 treatment (Figure

2.12 B and C). It was at these time points that the co-localisation of the FRFP-KpnB1 and INI-43 appeared as optimal for FRET efficiency.

The results for the FRET analysis were quantified and the change in fluorescence after photobleaching is shown in Table 2.1. Four individual cells were analysed of 30-minute and 45-minute INI-43-treated cells, and individual FRET photobleaching was performed. The average FRET efficiency was calculated to be 28.13 for the 30 min treatment and 33.37 for the 45 treatment which was significantly higher that the fret efficiency of the unbleached region.

Analysis for 30-minute INI-43 treated cells, and four individual FRET photobleaching analyses for 45-minute INI-43 treated cells, show comparatively similar in terms of average FRET efficiency for both time points that initially suggested a possible interaction between FRFP-KpnB1 and INI-43. This data was however found to be inconclusive, as control experiments using pmKate-2c only showed that the empty vector was only able to produce a colour shift from red to green on photobleaching (figure 2.13). Kremers et al., 2009, reported similar findings. While earlier experiments had shown immunofluorescent visualisation of INI-43 and FRFP-KpnB1, and co-localisation of the drug with the protein, we were unable to provide conclusive evidence of a direct interaction of INI-43 with KpnB1 using FRET photobleaching.

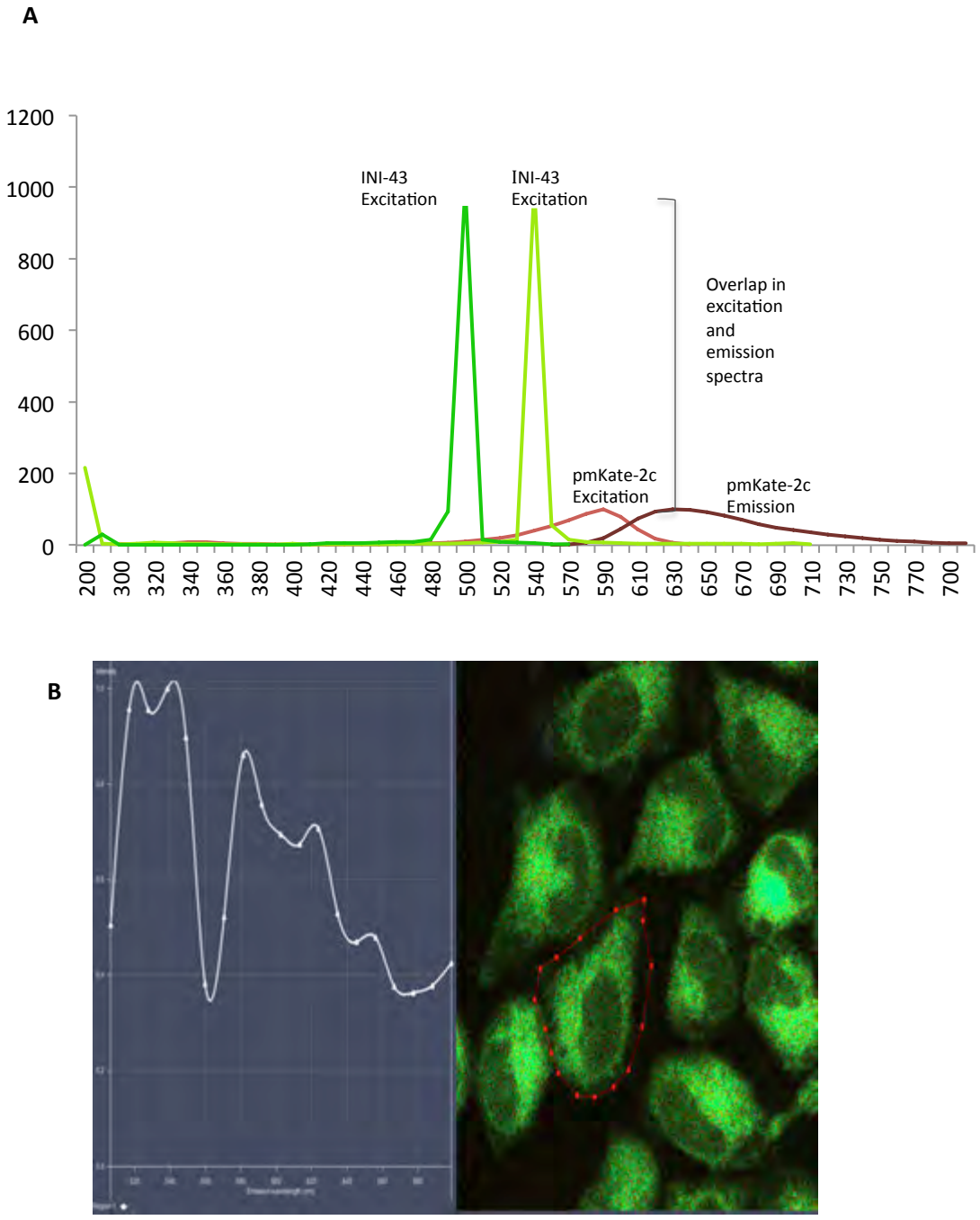

Figure 2.11: Excitation and emission spectra for INI-43 and pmKate-2C: (A) Measurements taken in a fluorometer showing overlap of the emission of INI-43 and excitation of pmKate-2c. (B) Excitation and emission spectra of INI-43 inside HeLa cells**.**

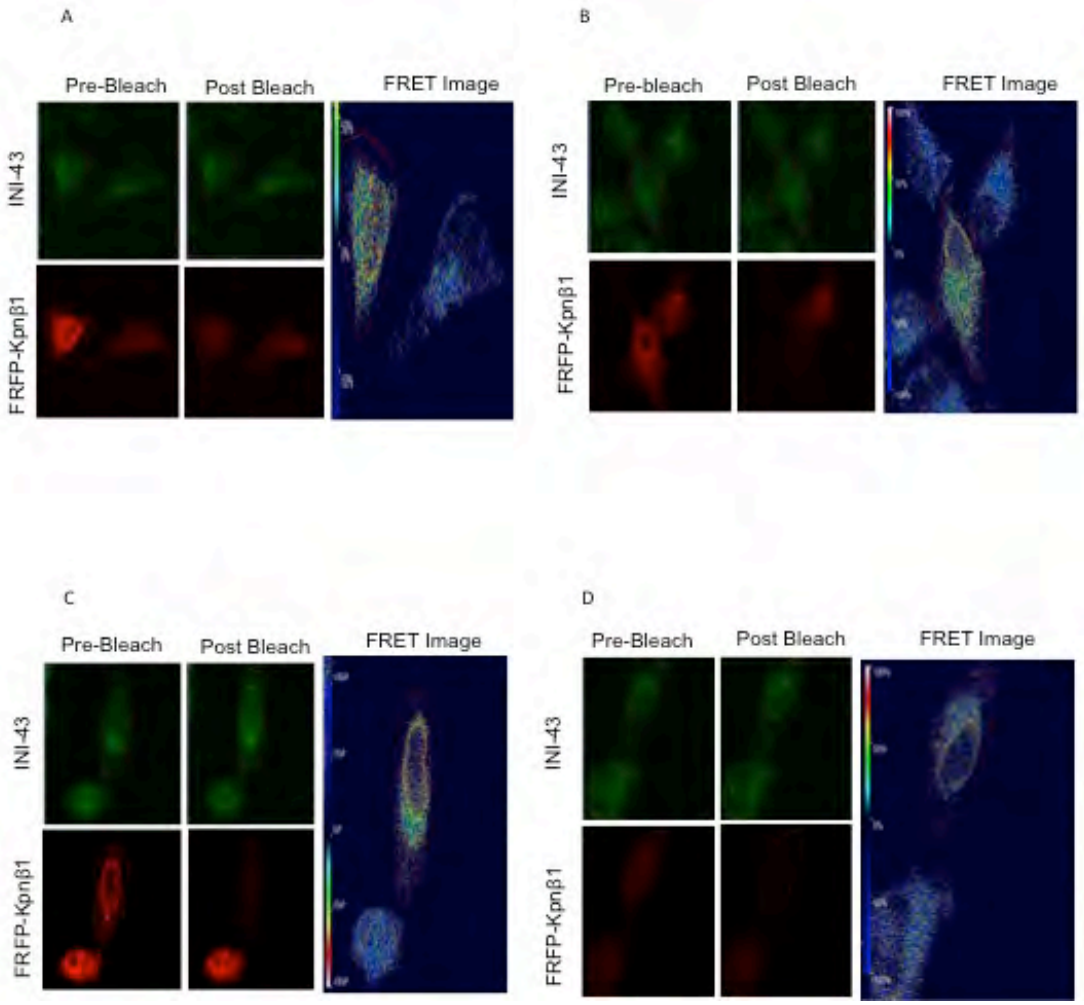

Figure 2.12: FRET photobleach experiments showing co-localisation between INI-43 and FRFP-KpnB1. (A) FRET photobleaching 20 minutes post treatment with INI-43. (B) FRET photobleaching 30 minutes post treatment with INI-43. (C) FRET photobleaching 40 minutes post treatment with INI-43. (D) FRET photobleaching 45 minutes post treatment with INI-43. Fluorescent image were captured using a Ziess confocal microscope.

Table 2.1: Summary of Results shows possible interaction between pmKate-KpnB1 and INI-43. Four individual readings for 30-minute INI-43 pre-treatment and four individual results for 45-minute INI-43 pre-treatment with average FRET efficacy.

		Bleached region			Unbleached region			
	Region of Interest	FRET efficiency	Delta Donor	Delta Acceptor	FRET efficiency	Delta Donor	Delta Acceptor	Net change
30 min INI-43 treatment	1	33.29	3.76	-51.8	12.09	0.2	-4.77	21.2
	2	31.13	2.75	-31.22	10.89	0.15	-5.74	20.24
	3	30.58	2.18	-28.91	10.04	0.17	-3.78	20.54
	4	17.5	2.24	-28.13	3.89	0.05	-3	13.61
	Average	**28.13**			**9.23**			**18.9**
	SD	**7.18**			**3.66**			
45 min INI-43 treatment	1	42.39	6.62	-44.3	28.89	0.94	-19.96	13.5
	2	16.32	1.62	-17.57	6.05	0.08	-2.57	10.27
	3	32.19	10.19	-59.25	23.5	1.29	-8.07	8.69
	4	44.57	13.36	-66.21	18.35	1.07	-6.5	26.22
	Average	**33.87**			**19.2**			**14.67**
	SD	**12.88**			**9.76**			

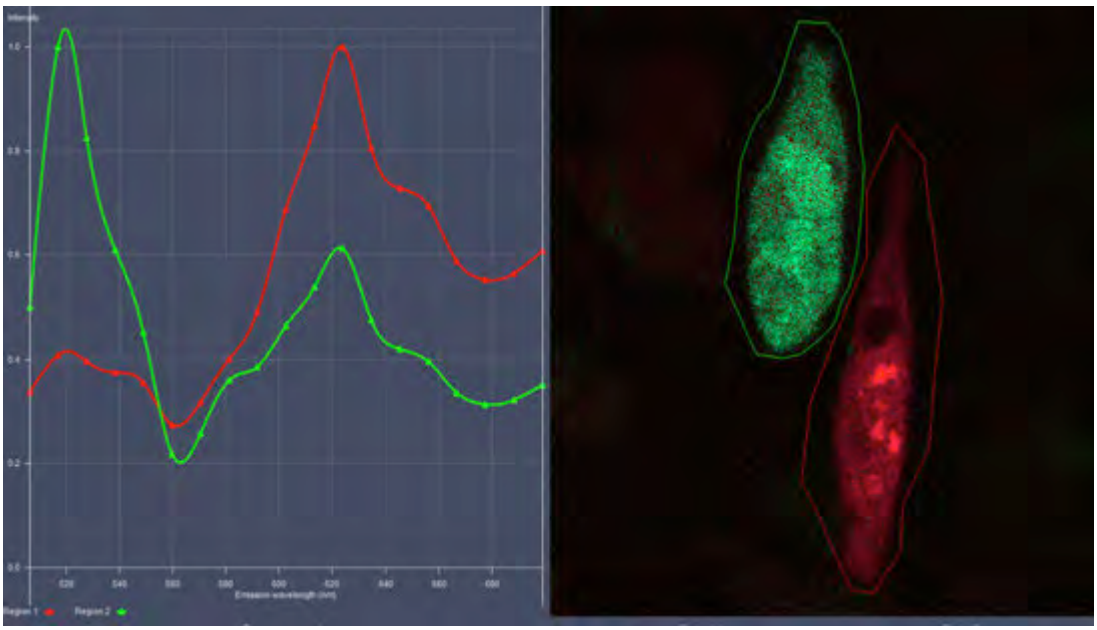

Figure 2.13 pmKate-2c only is able to undergo photo conversion from red to green. Control cells were transfected with pmKate-2c (no drug treatment) and observed post bleaching. Green line represents photo-conversion after photobleaching of the empty vector from red to green fluorescence; red line represents pmKate-2c where no photobleaching was used.

2.3 Discussion

In our laboratory we have generated evidence showing that KpnB1 is upregulated and required for the survival of cervical cancer cells (van der Watt *et al.,* 2009, 2011; Angus *et al.*, 2014). Small molecule inhibitors targeted to bind to and inhibit KpnB1 is therefore one of our major areas of interest. The study reported here centred on one experimental compound, INI-43, as an inhibitor with anti-cancer activity. This study investigated the mechanism of action for INI-43.

Our data indicates that INI-43 has a cytotoxic effect in cervical cancer cells with an IC_{50} ranging between 6 µM and 10 µM a much lower value than that of other available nuclear import inhibitors such as importazole which is reported to have and IC_{50} of 22.5 µM in HeLa cells (Jonathan F Soderholm et al. 2011). We also show that INI-43 initiates cell death by activating apoptotic pathways. This was observed using the PARP-1 cleavage assay. This result has been independently confirmed by others in our laboratory using PARP-1 cleavage and other assays such as caspase 3/7 assay (van der Watt *et al.,* 2016). PARP-1 is downstream of caspase 3/7 which activates the cleavage of PARP-1 on upstream signals from the cell's mitochondria. Once PARP-1 becomes cleaved it initiates fragmentation of the DNA and the cells die via apoptosis. Western blot analysis for PARP shows a clear presence of cleaved PARP-1 in the presence of INI-43 in both HeLa (figure 2.5 A) and CaSki (figure 2.5 B) cells, confirming that INI-43 induces cell death via apoptosis. These results have also been supported by caspase 3/7 assays (van der Watt *et al.,* 2016).

The results presented here also suggest that INI-43 affects the cell by interfering with nuclear import pathways. We report a significant decrease in NFAT promoter activity in the presence of INI-43. NFAT is a transcription factor, which gains access to the nucleus via KpnB1. Similarly Importazole is also shown to inhibit the ability of NFAT to gain access to the nucleus (Jonathan F Soderholm et al. 2011). Our data suggests that INI-43 inhibits KpnB1 import pathways and that this inhibitory effect has a negative impact on the activities of its cargo proteins such as NFAT.

INI-43 showed inhibitory activity against the translocation of endogenous KpnB1 into the nucleus. This was evident using confocal microscopy, which revealed a distinct difference in KpnB1 localisation in INI-43-treated cells compared to control cells, where a decrease in nuclear localisation was observed in treated cells. In INI-43-treated cells, KpnB1 was localised in the cytoplasm and also to the peri-nuclear region where it localizes in high concentrations. The fact that the presence of INI-43 interferes with KpnB1 localisation to the nucleus, suggests that KpnB1-associated nuclear import will be inhibited. It is unclear whether KpnB1 is remaining on the periphery of the nucleus or if it is becoming trapped in the endoplasmic reticulum. The only way to be of the location of the drug would be to perform tracking experiments. Previous cell fractionation studies have shown exclusion of INI-43 from the nucleus and relocation to the cytoplasm post treatment (van der Watt et al. 2016). Our results provide evidence that INI-43 interferes with nuclear import mechanisms associated with KpnB1. The nature of the KpnB1 INI-43 interaction will be explored in later chapters.

In examining exogenous FRFP-KpnB1 in HeLa cells we observed a result similar to that of endogenous KpnB1 was observed. After treating HeLa cells for 24 hours with INI-43 we observed an exclusion of FRFP-KpnB1 from the nuclear region, with localisation to the peri-nuclear region becoming more prominent. This was observed within 30 minutes of treatment with the drug. As INI-43 is a drug that exhibits fluorescence, we were also able to show changes in FRFP-KpnB1 localisation coincided with drug presence in the cells. If INI-43 is binding to the region of interest, it could be causing re-localisation of KpnB1 by possibly preventing the Ran interaction, similar to the function of importazole (Jonathan F. Soderholm et al. 2011). This deprives the system of cellular energy and the import process is no longer able to occur. Another possibility is that INI-43 is preventing the recognition and binding of KpnA2. Such inhibition would prevent KpnB1 from entering the nucleus causing KpnB1 to remain stuck in the cytoplasm (Yuh & Blobel 2001). Both of these explanations do not explain the very distinctive 'ring-like ' structure observed in the peri-nuclear region.

FRET photobleaching as a tool for looking at drug–protein interactions, although initially promising with results 30 and 45 min treatments producing encouraging FRET efficiencies, the final result was inconclusive. When we performed the control using cells expressing the empty vector pmKate-2c, we observed changes in fluorescent emission from red to green. Furthermore, pmKate-2c is one of only eight known fluorescent labels shown to change emission spectra on photobleaching (Kremers et al. 2009). To further investigate potential INI-43

interaction we next explored alternative biophysical methods that required purified KpnB1 protein.

Chapter 3

Optimization of KpnB1 Protein Purification

3.1 Introduction

Previous studies have shown that KpnB1 is able to maintain the intracellular trafficking of molecules from the cytoplasm into the nucleus of cells (Hintersteiner et al. 2010; Hetzer et al. 2005). Based on siRNA experiments, we have observed that KpnB1 knockdown results in cancer cell death via apoptosis (van der Watt et al. 2013; Angus et al. 2014). This effect has been shown to be more specific in cancer cells than in normal cells (Angus et al. 2014). Using an *in silico* approach to identify small molecules with potential to bind and inhibit KpnB1 function, we identified INI-43.

In this study and in our recently published work (van der Watt et al. 2016) we showed that INI-43 exerts its cytotoxic effects by targeting KpnB1-associated nuclear transport pathways. This chapter describes the procedure we used to generate purified KpnB1 for use in biophysical investigation of protein–drug interactions. More specifically we required purified KpnB1 for investigating whether INI-43 can interact directly with KpnB1. Methods of purification used included affinity chromatography and anion exchange chromatography. Affinity chromatography uses the recombinant expression of affinity tags such as GST

and His tags on the N- or C-terminus of the protein being purified (Arnau et al. 2006). In these purification methods the tagged protein becomes immobilized on a resin matrix, which binds specifically to the purification tag, allowing for separation from cellular debris. The protein can be released from the resin after washing away impurities, following which it can then be analysed for its level of purity using SDS-PAGE and western blot (Young et al. 2012).

High-resolution anion exchange is a method of protein purification that uses the native charge of the protein to purify it. Columns have size exclusion and a positively charged resin that enables the protein of interest to be immobilised by the resin due to the difference in charge. Cellular debris can be removed by washing, and a salt gradient is used to elute the protein from the resin; fractions are collected and analysed for protein content using SDS-PAGE and western blot analysis. This method requires knowledge about the protein's isoelectric point and optimal pH. It also involves a number of different steps, including a gel filtration for a final stage of purification based on size exclusion.

His tagged affinity chromatography uses IMAC (Immobilised Metal Affinity Chromatography) resins. The technique is based on the interaction between the exposed histadine residues, which have been recombinantly expressed on one of the terminal ends of protein of interest using an *E. Coli* expression system. The metal ion of choice e.g., Ni^{2+} in our case, is cross-linked in the agarose matrix via a chelating agent to create an environment to which the His tagged protein will become attached. Once the protein of interest becomes bound the resin

impurities can be removed using wash buffers, leaving the pure protein to be collected with the imidazole elution buffer (Rosano & Ceccarelli 2014).

The GST (glutathione-S-transferase) tag is a 26 kDa protein derived form *Schistosomo japonicum* (Rosano & Ceccarelli 2014). Like the His tag the GST tag is recombinantly expressed on one of the terminal ends of protein of interest using an *E. Coli* expression system. GST binds specifically to glutathione immobilized to sepharose beads in a resin matrix (Rosano & Ceccarelli 2014). This specific binding enables impurities to be washed away with wash buffer in the washing steps and the protein of interest can be collected during the elution steps with reduced glutathione which competes for binding to the glutathione sepharose.

At the time of this investigation, purified KpnB1 was not commercially available and it would not have been economically viable to purchase purified KpnB1 for use in biophysical analysis that requires substantial amounts of pure protein. Our objective was thus to clone KpnB1 in expression vectors that would enable protein purification methods for optimal expression.

3.2 Results

3.2.1 Cloning of KpnB1 into a vector allowing for N- and C-terminal His tagging

A His-tagged vector system (pET-28b+, kindly donated by Prof Sewell, UCT Structural Biology Unit) was initially used as a system to generate KpnB1 for purification. The human variant of KpnB1 was amplified by PCR from pGEX-

KpnB1 plasmid (see Appendix, Figure 2). Two sets of primers were constructed that allowed for one clone with an N-terminal His-tag and a second with a C-terminal His-tag. The amplified PCR products were run on a 1% agarose gel (Figure 3.1 A). These inserts were A-tailed, then cloned into the final vector pET-28b+ via the shuttle plasmid pGEM-T-EASY. Restriction enzyme digest was used to release the KpnB1 insert from pGEM-T-EASY, which was then cloned into pET28b+, allowing for N- and C-terminal His tagging. The inserts were mapped using restriction enzyme digest (figure 3.2. B and C), and DNA sequencing was performed to confirm the correct KpnB1 sequences.

3.2.2 Purification of C-His- KpnB1 and N-His-KpnB1

a) Nickel Affinity chromatography to obtain purified KpnB1

E. Coli BL21 (DE3) containing the plasmid pET28b-KpnB1 encoding either C-His- or N-His-tagged KpnB1 was grown and cultures were stimulated with IPTG to induce protein production. Protein lysates were then applied to affinity chromatography resin.

Both N-His- and C-His-tagged variants of KpnB1 had a low affinity for the IMAC resin. In an attempt to increase binding, the flow-through was re-run on the column using a wider imidazole gradient and slower run rate. This again demonstrated that the protein had very low affinity for the resin (Peak 2, Figure 3.2).

The binding traces observed in Figure 3.2 A and B clearly show that there is a large amount of protein in the flow-through (first peak) and then very little in the elution (second peak). Figure 3.2 A, shows the purification profile for the C-His-KpnB1 and Figure 3.2 B, for N-His-KpnB1. The N-His-KpnB1 did not show any protein being eluted off the column and the C-His-KpnB1 showed a very small amount of protein being eluted off in the form of the second peak between fractions 25 and 27. Since the His affinity tag chromatography proved to be unsuccessful we explored alternative methods of protein purification such as anion exchange chromatography.

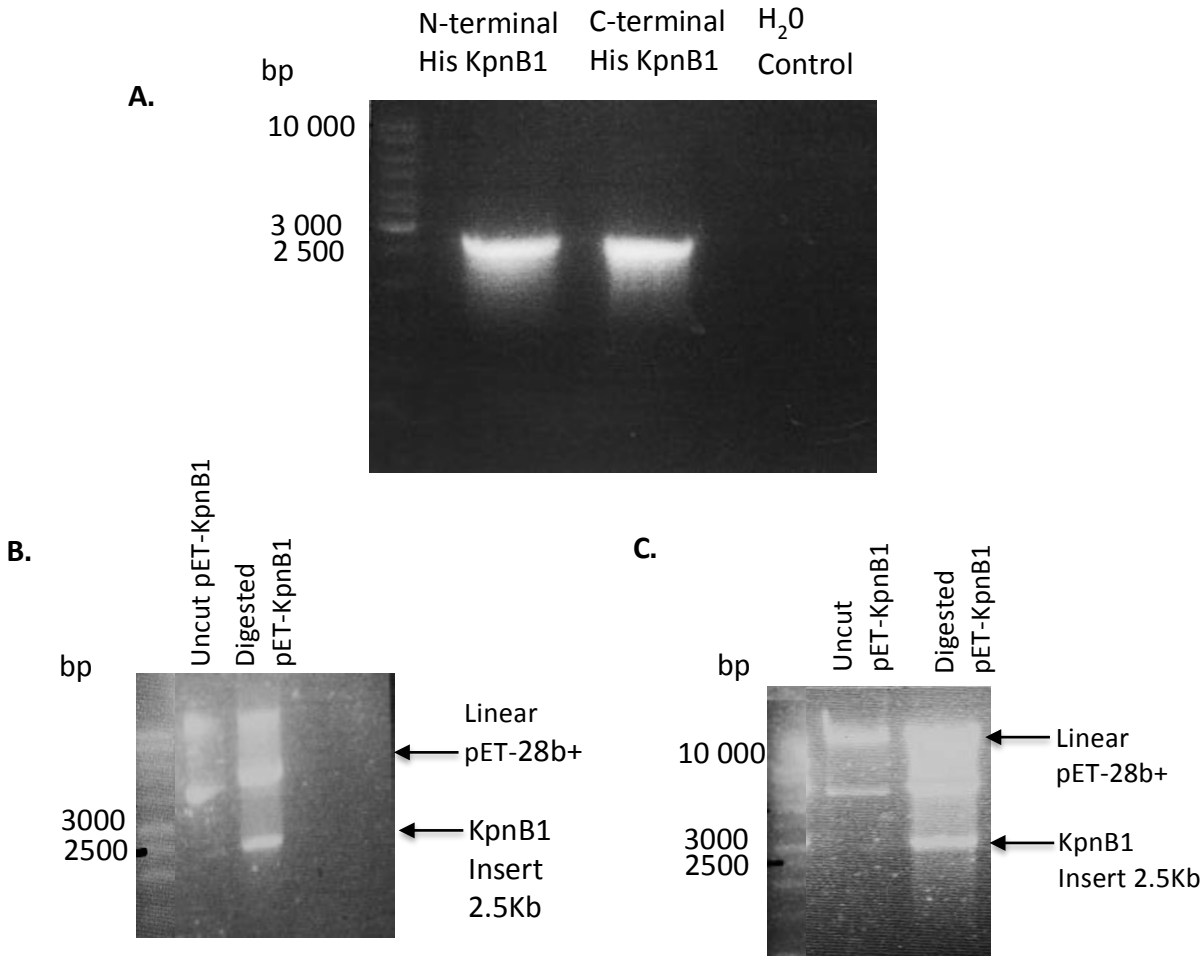

Figure 3.1: Cloning of KpnB1 into pET-28b+. (A) PCR amplification of KpnB1 for insertion into pET-21b+ a 2.5 kb fragment was obtained. (B) Visualisation of the 2.5 kb insert of C-His tagged KpnB1 using restriction enzymes BamHI and NotI. (C) Visualisation of the 2.5 kb insert of N-His tagged KpnB1 using restriction enzymes BamHI and NotI.

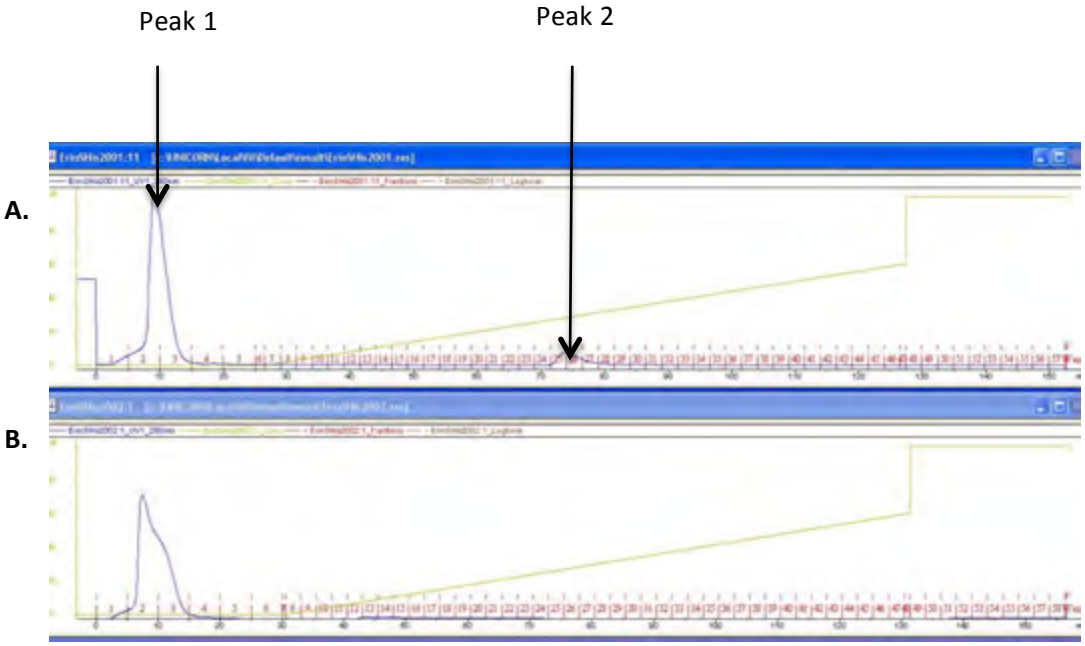

Figure 3.2: Nickel affinity chromatography was found to be unsuccessful in the purification for both N- and C-terminal HIS-KpnB1: Lysates were loaded onto the column and the protein concentration was measured using spectral analysis at 280nm throughout the process to measure the efficiency of the technique. The X-axis represents time and fraction number collected, while the Y-axis displays absorbance at 280nm; the concentration of the elution gradient is represented by the green line. (A) Examination of C-terminal His-tagged KpnB1 shows that most of the protein was lost in the flow-through (peak 1), while a small amount was collected in the elutions (peak 2). (B) Examination of N-terminal His-tagged KpnB1 shows that most of the protein was lost in the flow-through (peak 1), while a negligible amount was collected in the elutions (peak 2).

b) Anion Exchange Purification

KpnB1 protein was expressed using *E. Coli* BL21 (DE3) cells containing the plasmid pET28b-KpnB1 encoding C–His-tagged KpnB1. Protein lysates were loaded onto a high-resolution anion exchange chromatography column. After collecting the lysate, the induction and solubility of the protein was visualised using SDS-PAGE (Figure 3.3 A) and western blot using anti KpnB1 (rabbit polyclonal antibodies) for visualisation (Figure 3.3 B). This process was performed to ensure that the bacteria upon IPTG induction were producing the KpnB1 protein, and also that it was a soluble product. Un-induced as well as IPTG induced lysates from *E. coli* cells were examined. Proteins in the 97 kDa range were present after induction with IPTG, however a number of other bands were also detected (Figure 3.3 B).

Some cross reactivity was observed in the 97 kDa KpnB1 band region however, bands just above the 80 kDa marker and a protein band in the 60 kDa region was also detected. These bands were detected in both un-induced and induced cells, albeit to a greater extent in induced lysates. It is not clear whether these bands are degradation of KpnB1 or non-specific antibody interactions.

As we did detect some KpnB1 antibody cross reactivity, purification of His-KpnB1 protein was performed using a HiPrep 16/10 QHP (GE Health Sciences) with the intent to enrich for KpnB1 protein. The column was equilibrated and the crude lysate was loaded and eluted using a salt gradient. Select fractions were analysed using SDS-PAGE and western blot analysis (Figure 3.4 A and B).

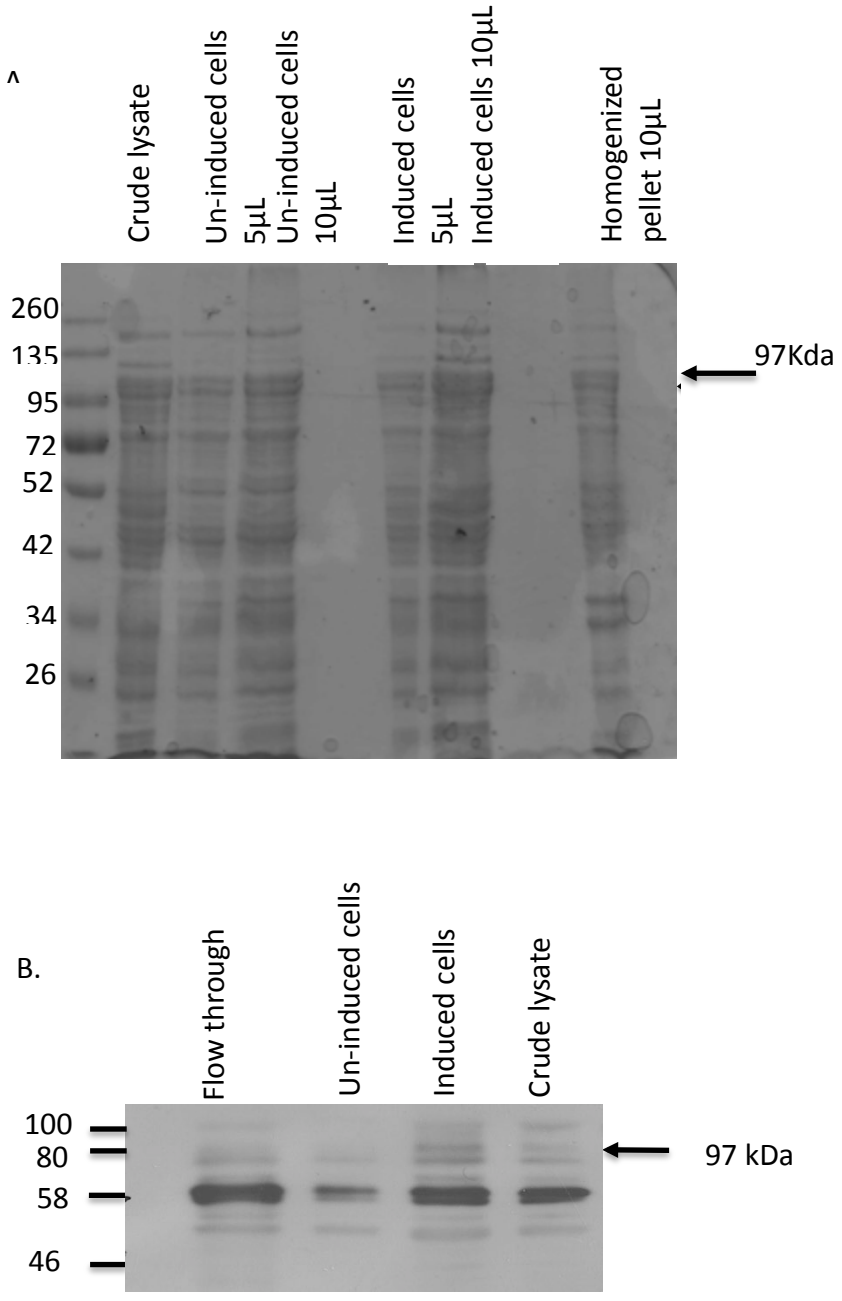

Figure 3.3: Bacteria expressing the pET-KpnB1 plasmid are able to produce soluble expression of His-KpnB1 protein and demonstrate IPTG-dependant induction of the protein. (A) Samples of the various stages of induction and lysis were electrophoresed using SDS-PAGE to examine the production of soluble protein (B) Western blot was used on the samples to determine IPTG-dependant induction of the His-KpnB1 protein.

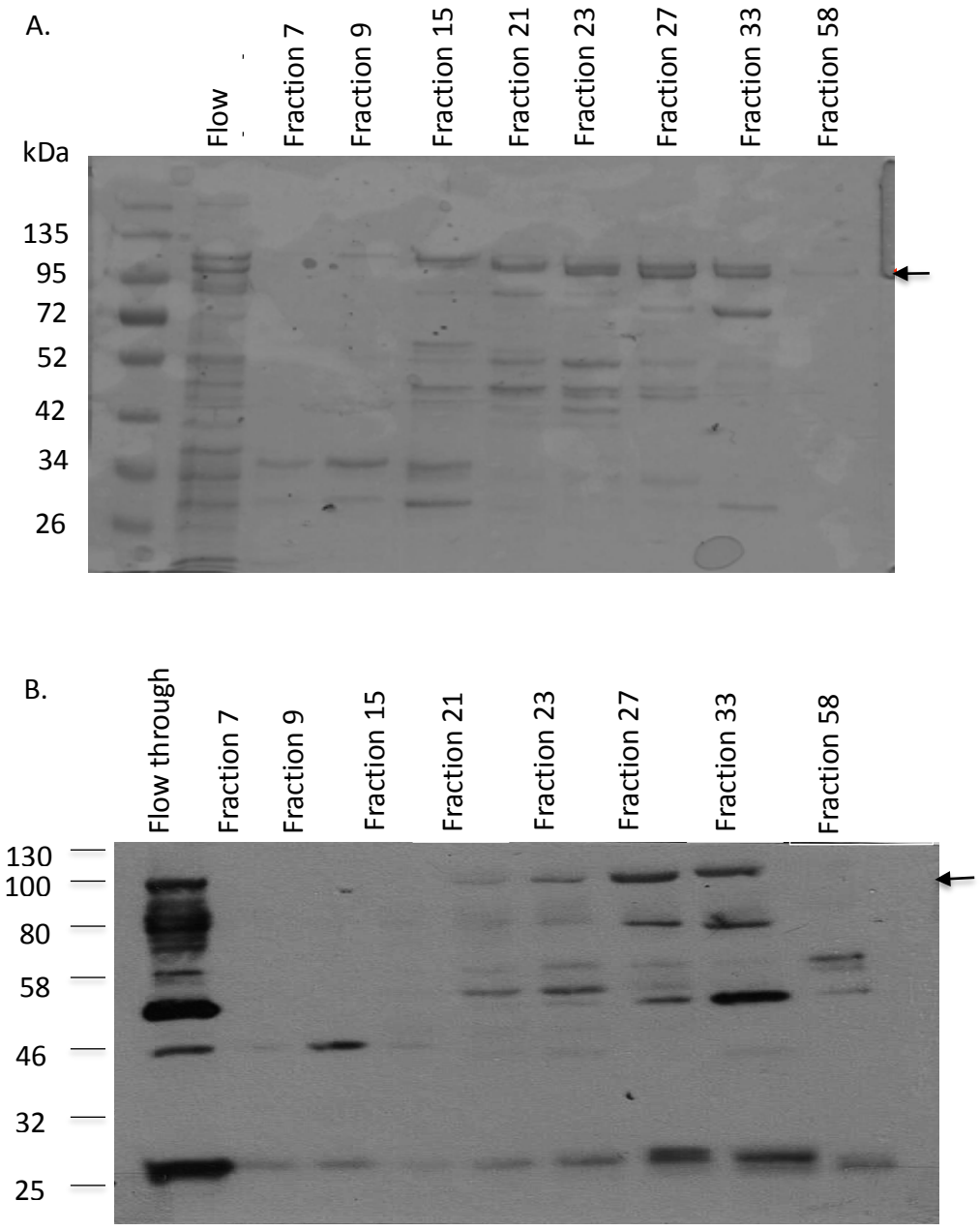

Figure 3.4: First round of anion exchange using HiPrep 16/10 QHP column. (A) SDS-PAGE analysis of fractions after anion exchange purification. (B) Corresponding western blot analysis of fractions from anion exchange purification, based on the blot fractions 21-27 displayed an enrichment in the 97 kDa protein however there was still lower molecular weight band contamination.

Western blot analysis on eluted fractions identified bands in the 97 kDa region (as expected for KpnB1); however, multiple other bands were also detected on both SDS-PAGE (Figure 3.4 A) and by western blots for KpnB1 (Figure 3.4 B). While the bands in the 97 kDa region were present on SDS-PAGE and western blot, bands of other sizes were detected. Fractions 24 to 60 were pooled and de-salted then re-run through a high-resolution ion exchange, using a narrower salt gradient to further eliminate impurities within the lower molecular weight range. Select fractions were analysed using western blot for KpnB1 in the fraction (Figure 3.5).

In total two rounds of anion exchange were performed and following anion exchange, fractions 28 to 35 (figure 3.5) showed a band in the ~97 kDa region and were pooled and concentrated, following which gel filtration was performed. Fractions from gel filtration were analysed using SDS-PAGE to enrich for proteins in the ~97 kDa region (figure 3.6 A). Fractions 31 to 35 and 36 to 55 were pooled, run on SDS-PAGE (figure 3.6 B) and western blot for analysis (figure 3.6 C).

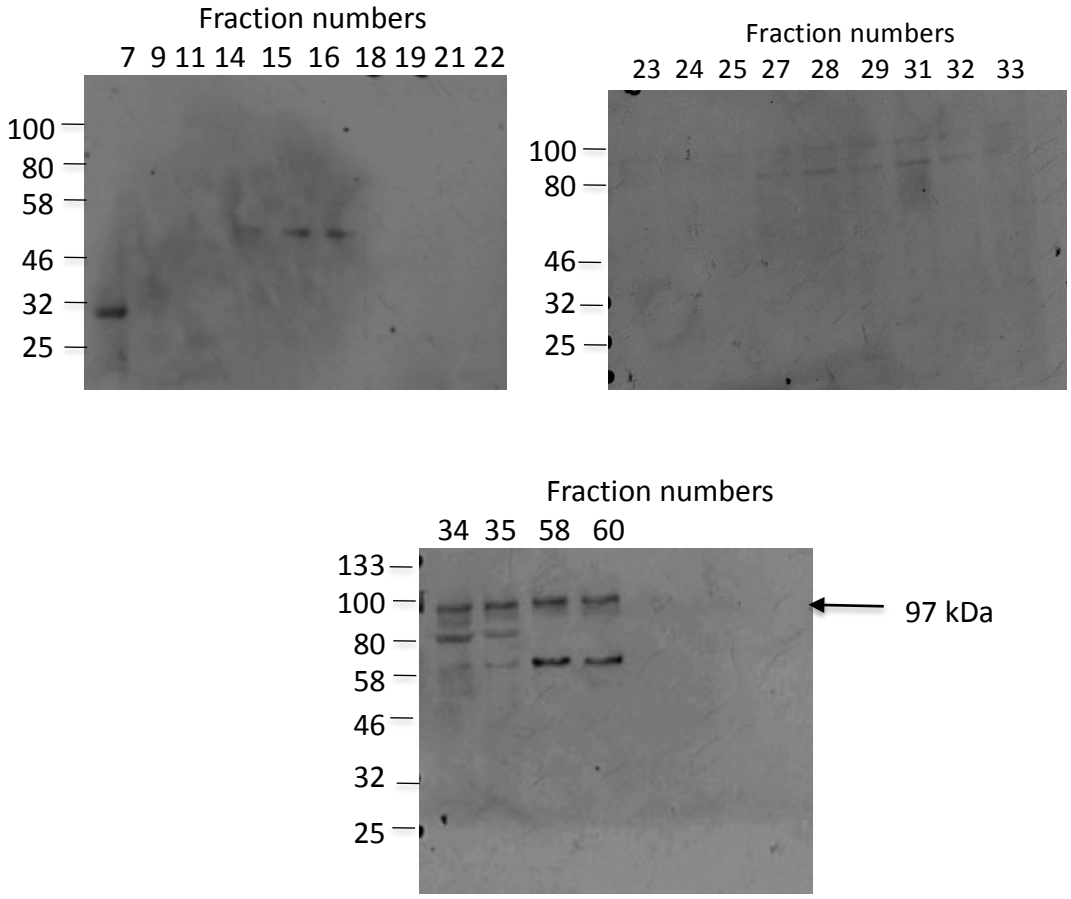

Figure 3.5: Western blot of fractions from second round of anion exchange. Selected fractions from the second round of anion exchange were probed for KpnB1. The blots show an increase in the level of enrichment and purity of His-KpnB1 around the fraction numbers 34 to 60**.** Fractions were run on 3 separate blots however only the third and final blot displays evidence of antibody cross reactivity with expected size of His-KpnB1 (97 kDa).

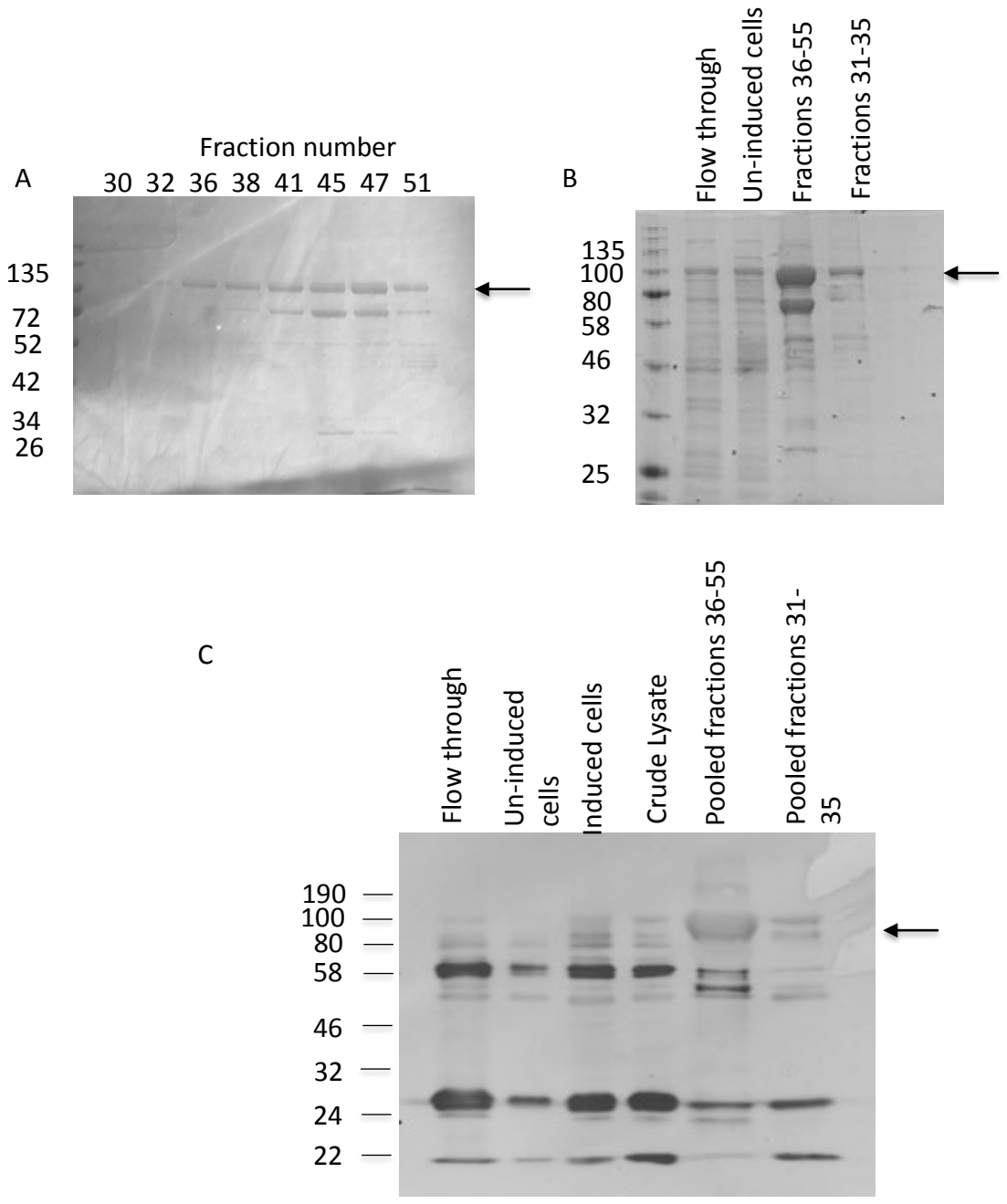

Figure 3.6: Results from gel filtration shows protein in the 97 kDa and lower molecular weight bands still present. (A) Fractions from gel filtration most likely to contain His-KpnB1 were analysed using SDS-PAGE showing fractions from gel filtration. (B) Fractions were pooled and re-analysed using SDS-PAGE showing enrichment for the 97 kDa band (C) Pooled fractions were analysed using western blot for KpnB1 to confirm purification of KpnB1.

3.2.3. Mass Spectrometry analysis of proteins collected in using gel filtration chromatography

After pooling the fractions that contained the proteins in the 97 kDa region from gel filtration, we prepared samples for mass spectrometry in order to determine whether KpnB1 was present. The pooled fractions were run on an SDS-PAGE gel, with HeLa lysates used as a positive control for KpnB1 in western blots. Surprisingly, after the pooling of fractions and performing western blots for KpnB1 we could no longer detect the prominent 97 kDa protein in purified fractions using SDS-PAGE (Figure 3.7 A). Western blot analysis for KpnB1 suggests possible degradation or contaminating non-specific proteins (Figure 3.7 B). This was confirmed when protein bands within the ~80 kDa region were excised and analysed by mass spectrometry. Mass spectrometry data showed that the only component of the sample that could be positively identified was human keratin, a likely contaminant (figure 3.7 C).

Based on these findings, we decided on and alternative approach to purification, as the methods tried thus far (His-tag affinity chromatography and anion exchange) did not provided optimal purified KpnB1 for use in biophysical analyses.

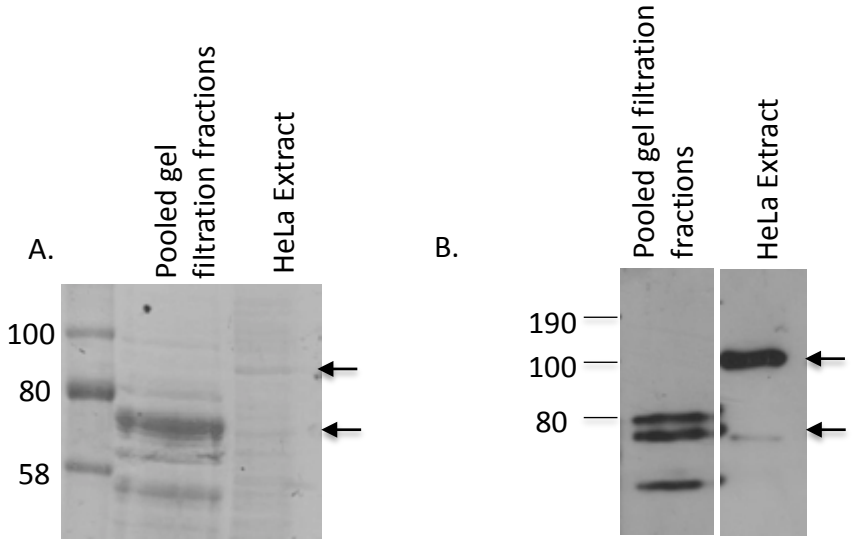

C.

Accession	Description	Sum (Coverage)	Unique Peptides	MW [kDa]
P13645	Keratin, type I cytoskeletal 10 OS=Homosapiens GN=KRT10 PE=1 SV=6 - [K1C10_HUMAN]	19.86%	6	58.8
P35908	Keratin, type II cytoskeletal 2 epidermal OS=Homosapiens GN=KRT2 PE=1 SV=2 - [K22E_HUMAN]	26.92%	2	65.4

Figure 3.7: SDS-PAGE, western blot and Mass spectronomy analysis show a possible degradation of the protein or contamination. (A) SDS-PAGE analysis of pooled gel filtration fractions 36-55 compared to HeLa cell extract. (B) Western blot comparing the pooled fractions 36-55 from gel filtration to HeLa extract. (C) Mass Spectronomy of proteins in the ~80 kDa region from the pooled fractions is negative for KpnB1 and contains human keratin.

3.2.4 Preparation of GST tagged KpnB1 as an alternative mode of purification

The plasmid pIB-GFP, containing (KpnB1-GFP) was kindly provided to us by M. Ciciarello and colleagues (see M. Ciciarello et al., 2004 and Appendix Figure 2). Primers were designed to allow for amplification of the KpnB1 fragment of interest using PCR. Restriction sites BamH1 and Xma1 were incorporated onto the 5' ends of the primers, facilitating the cloning of the KpnB1 fragment into the final plasmid pGEX-6p1.

The PCR products were electrophoresed on a 1% agarose gel (Figure 3.8 A) and the 2.5 kb product was cloned into pGex-6p1. Inserts were visualised using restriction enzyme digest with BamHI and XmaI (Figure 3.8 B). The insert was sequence confirmed and pGex-6p1-KpnB1 transfected into *E. Coli* (JM109) bacteria cells. Expression of GST-tagged KpnB1 was induced using IPTG. Our result showed that protein induction was occurring within one hour of IPTG treatment (Figure 3.8 C).

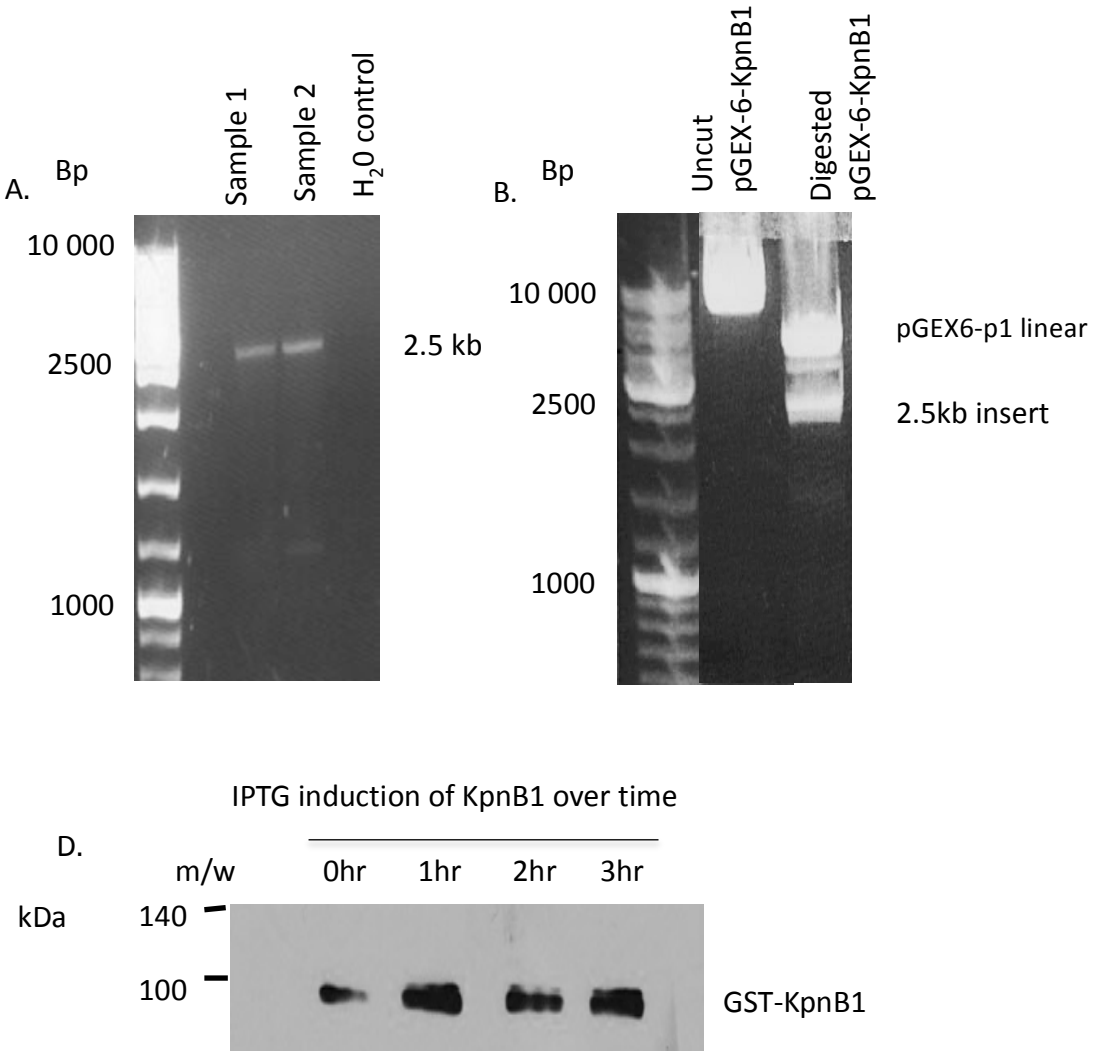

Figure 3.8: KpnB1 was successfully cloned into pGex-6p1. (A) PCR amplification of 2.5 kb KpnB1 for insertion into pGEX-6P1. (B) Visualisation of 2.5 kb KpnB1 insert excised from the plasmid using restriction enzymes BamHI and XmaI. (C) Western blot for KpnB1 demonstrating successful induction of GST- KpnB1 upon stimulation with IPTG over 1, 2 and 3 hours. Un-induced lane (0 hr) shows expression of KpnB1 albeit at a lesser quantity than the induced lanes. This is due to leakiness of the vector.

3.2.4 GST-KpnB1 protein purification using GST-tag affinity chromatography

E. Coli containing the plasmid pGex-6p-KpnB1 was grown and stimulated with IPTG to induce the expression of GST-KpnB1 protein. Lysates were loaded onto 2 mL of affinity chromatography resin (glutathione sepharose™ 4B GE Healthcare) and protein was purified using batch-binding techniques. Once the crude lysate was added to the resin, the mixture was placed on a rotator at room temperature for 4 hours then moved to the cold room (4˚C) where it continued to rotate overnight. Elution was performed using a solution of ice-cold 50mM reduced glutathion (Sigma) in water pH 7.5 – 8.

Purified protein was electrophoresed using SDS-PAGE and stained with coomassie brilliant blue to examine the efficiency of the purification performed (Figure 3.9 A). Crude fractions, flow-through, washes and all elutions were run on the gel, along with BSA standards. This enabled quantification of the amount of KpnB1 in our results showed the GST-tagged purification methods was substantially improved to the earlier methods attempted. While minor bands were still detected, a concentration of protein was observed in the ~123 kDa region of eluted fractions (Figure 3.9 A). This corresponds to the expected size of KpnB1 at 97 kDa fused to the GST-tag (26 kDa).

Western blot analysis showed KpnB1 cross reactivity at the correct size (Figure 3.9 B), and mass spectrometry confirmed the presence of KpnB1 as the predominant protein within the band with a purity of approximately 77% (Figure 3.9 C).

A.

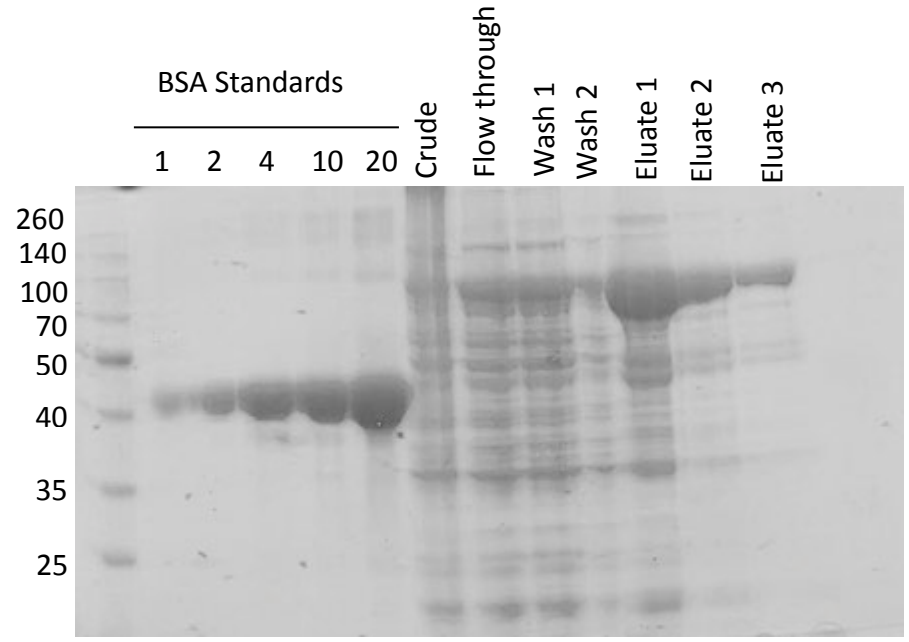

B.

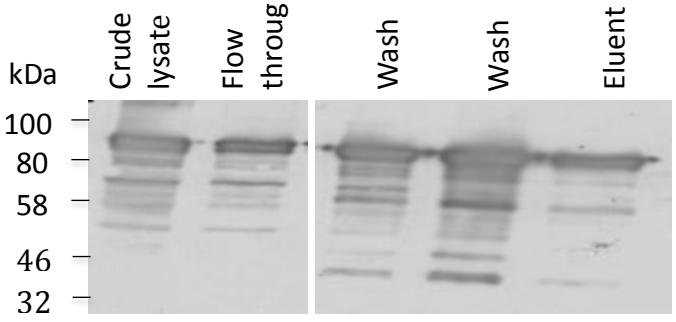

C.

Accession	Description	Sum (Coverage)	Unique Peptides	MW [kDa]
Q14974	Importin subunit beta-1 OS=Homosapiens GN=KPNB1 PE=1 SV=2 - [IMB1_HUMAN]	77.28%	106	97.1
P04264	Keratin, type II cytoskeletal 1 OS=Homosapiens GN=KRT1 PE=1 SV=6 - [K2C1_HUMAN]	40.22%	13	66

Figure 3.9: Purification of GST-KpnB1 was successful using glutathione sepharose resins and achieved a desired level of purity. (A) Various fractions from batch binding were analysed by SDS-PAGE using BSA standard (µg BSA). (B) Western blot to showing various fractions from batch binding. (C) Mass spectroscopy analysis of protein from Coomassie gel shows eluate 3 to have a purity of 77.28% GST-KpnB1.

The purification table (table 3.1) shows an increase in the amount of purified KpnB1 throughout the purification process, with a decrease in percentage yield, which is expected. Initially there is an increase in the yield however this is merely due to the increase in the volume from the washing steps. Eluate 3 was found to have the highest purity of protein, at 75.45%. Eluate 2 had the second highest purity. Protein samples were excised from the SDS-PAGE gel and sent for mass spectrometry analysis confirming its purity to be between 92.5 and 77.28%. There was however some keratin contamination observed in the mass spectrometry analysis, despite having all precautions in place to prevent contamination.

The purified GST-tagged KpnB1 was subsequently used to investigate KpnB1–INI43 interactions using biophysical analytical techniques including circular dichroism and isothermal calorimetry.

Table 3.1: Purification table of the various stages of purification of GST-KpnB1 using affinity tag purification. Figures in the table are based on densotometric analysis of the SDS-PAGE gel in figure 3.8 A.

Sample	Intensity	µg in sample	µg/µL	Total protein	% Yield	% Purity
Crude	18361.37	4.77	0.48	9544.86	100.00	22.73
Flow through	13393.24	3.44	0.69	13751.37	144.07	18.85
Wash 1	53847.87	143.05	1.43	14305.15	149.87	63.49
Wash 2	25045.40	6.57	0.66	6567.96	68.81	43.05
Elution 1	78434.87	15.18	1.52	1517.50	15.90	38.84
Elution 2	35648.32	4.85	0.49	485.09	5.08	42.07
Elution 3	17023.69	0.36	0.04	35.68	0.26	75.45

3.3 Discussion

To date, one of the most successful methods of purifying KpnB1 was carried out by the use of a column constructed of the IBB binding domain of KpnB1 binding partner KpnA2 (Cingolani et al. 1999). Optimisation of this method enabled those authors to obtain quantities of purified protein as high as 50mg/mL for use in crystallography studies. The success of this method was due to the naturally high binding affinity of KpnB1 for the IBB domain of KpnA2. KpnB1 partnered to this IBB domain was co-crystalized bound together, hence once KpnB1 was immobilized to the KpnA2 column it was unnecessary to separate the binding partners. This method is ideal for collecting large quantities of highly pure protein. We did not, however, have access to purified binding partners of KpnB1, and creating such an advanced purification system went beyond the scope of our studies at this time. We also required unbound KpnB1 for the biophysical drug-binding analysis, and separating KpnB1 from the IBB domain may have been problematic. We therefore chose to use simpler purification methods.

Other research groups have been successful in purifying KpnB1 using His-tag affinity chromatography (Ingrid R. Vetter et al. 1999). We however, did not have success in purifying KpnB1 using this method. One possibly for this could be that we were using the full-length protein 1-860 amino acids , whereas Vetter et al. (1999) used a fragment of 1-462 amino acids.

Having used a number of different protein purification methods, we were able to prepare sufficient quantities of purified KpnB1 using GST-affinity tag purification methods. Other methods, including anion exchange chromatography and His-

tag affinity chromatography, proved to be ineffective in that the protein did not have the required affinity for the resin under the conditions used, as observed in the case of His-tag affinity resin purification. Furthermore, due to the numerous time-consuming steps involved in anion exchange purification, protein degradation was observed, which meant that this technique failed to provide optimal results for the purification of KpnB1.

Our biggest challenge with the purification of KpnB1 was to obtain large quantities (µg amounts) of sufficiently pure protein without degradation. The use of GST-affinity tag purification methods enabled us to overcome some of these challenges. GST-affinity tag purification is a single-step purification system and therefore more suitable for the purification of KpnB1, thus suiting our requirements.

The mass spectrometry results we achieved revealed that the purified KpnB1 was sufficiently pure (~95%) suggesting it was of a quality that could be used in the biophysical analysis to examine drug–protein interactions as recommended by (Pihan et al. 2015). Purified KpnB1 was used to assess whether INI-43 was directly interacting with KpnB1 using biophysical methods including circular dichroisim and isothermal calorimetry.

Chapter 4

Biophysical characterisation of potential KpnB1-INI-43 interactions

4.1 Introduction

Purified KpnB1 was used to perform biophysical analyses in order to examine structural interactions between KpnB1 and INI-43. We used two methods of analysis, circular dichroism (CD) and isothermal calorimetry (ITC). CD is a form of spectroscopy which makes use of the differential absorption of left- and right-circularly polarised light (Rogers & Hirst 2004; Kelly & Price 2006). Linearly polarized light is observed when light travels in an oscillating electromagnetic wave with constant amplitude. Circularly polarised light is created when two waves of linear polarised light of equal amplitude are combined at 90° opposing phases to each other (Figure 4.1) (Rogers & Hirst 2004). The radiation generated by this light is used to produce a CD signal commonly measured in ellipticity. Optically active amino acids make it possible to use CD to measure the transitions of electrons within proteins to different levels of the excited state (Rogers & Hirst 2004). This method utilises a range of wavelengths to measure ellipticity of the protein being examined (Kelly et al. 2005) (Figure 4.1). A signature reading in terms of ellipticity can be deciphered (Greenfield 2006c) which gives insight into secondary structure (Kelly et al. 2005). Typically, CD spectra between 180nm and 260nm can be examined to analyse the secondary structure of a protein under investigation (Greenfield, 2006c). Secondary structures such as alpha helices, beta sheets, turns and random coils provide characteristic spectra; application of CD thus provides deeper insights into the

structural characteristics of proteins (Greenfield, 2006c). Three groups within the protein chromophores – peptide bonds, amino acid side chains and the prosthetic groups – are of particular interest when examining CD spectral analysis (Rogers & Hirst, 2004).

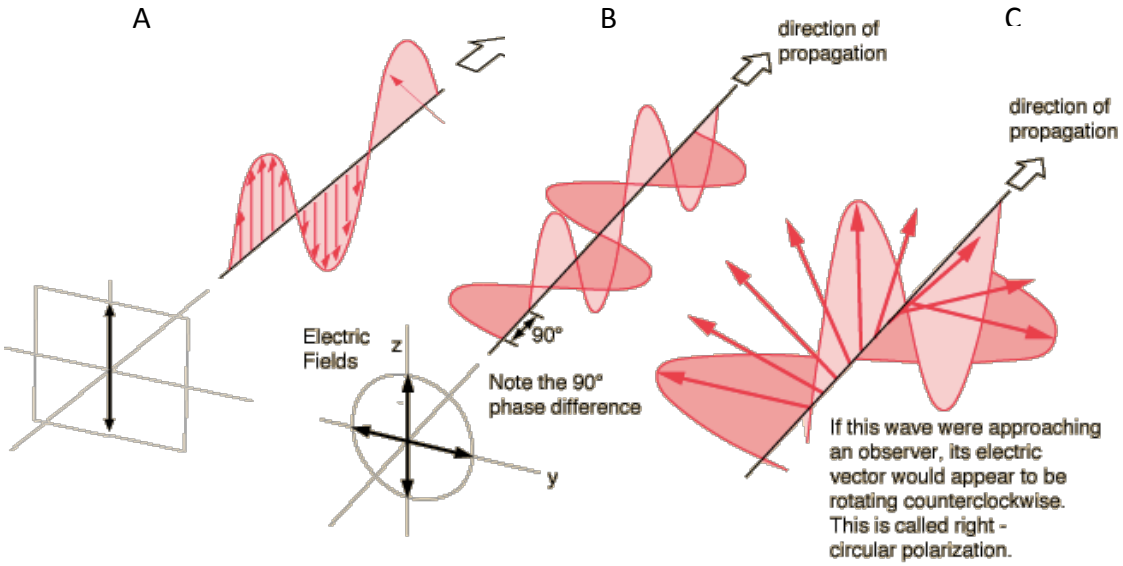

Figure 4.1: Circularly polarised light used in CD. (A) Linearly polarised light is produced by waves of constant amplitude. (B) Two waves of linearly polarised light in transverse planes of equal amplitude at opposing 90° phases are used to produce circularly polarised light. (C) Circularly polarized light can be left-circular or right-circular; both are used in CD analysis (From http://hyperphysics.phy-astr.gsu.edu/hbase/phyopt/polclas.html).

Factors which can influence the CD spectra of aromatic amino acids include the rigidity of the protein and the presence of hydrogen bonds (Kelly et al. 2005; Rogers & Hirst 2004). As mentioned, secondary structures within a protein have their own characteristic spectra (Figure 4.2). Proteins rich in alpha helices will

often display spectra similar to 1 in Figure 4.2 with a positive band at 190 nm and two negative bands at around 210 and 220 nm. Proteins rich in beta sheet will have a positive band at around 200 nm and a negative band at around 220 nm as seen by line number 2 in Figure 4.2. Disordered proteins have no distinct spectral pattern as seen by and as seen by line number 5 in Figure 4.2.

Examining the response of CD spectra under the influence of increasing heat gives insight into the protein's overall thermal stability (Kelly et al. 2005; Greenfield 2006b; Greenfield 2006a).

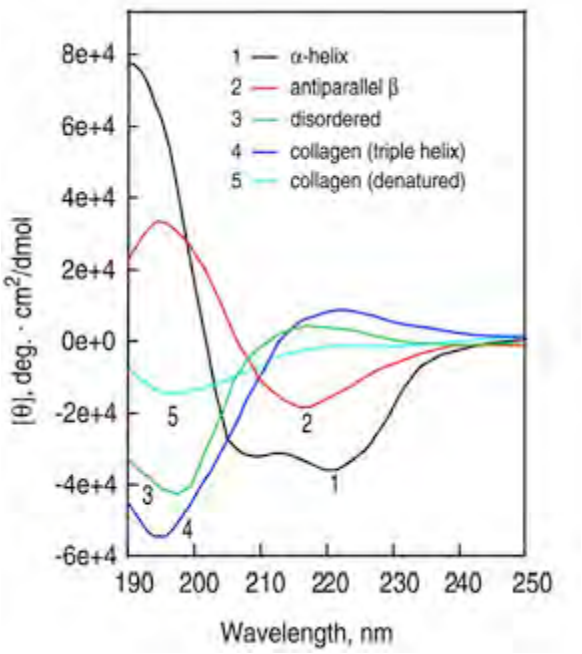

Figure 4.2 Secondary structures produce characteristic spectra. The excitation of various electrons on specific orbitals causes each secondary structure to produce a characteristic spectrum, thus making it possible to examine changes in secondary structure (Greenfield 2006c).

In addition to revealing the secondary structure of native protein, CD can be utilized to examine conformational changes of the protein in response to ligand

binding (Greenfield 2006a). Similarly, it is possible to examine changes within the spectra in response to the addition of ligands, and thereby explore the effect of small molecules on protein folding and the binding affinity of the small molecules. CD cannot, in most cases, provide specific molecular information regarding protein ligand binding at an atomic level, and it is therefore employed in conjunction with other techniques such as ITC, NMR or X-ray crystallography (Rogers & Hirst 2004). It does, however, provide an indication of structural change and makes it possible to obtain a preliminary disassociation constant (K_d). This, in turn, provides insight into the affinity of the ligand (or drug) for the protein (Kelly & Price 2006; Kelly et al. 2005).

In addition to CD as a measure of drug–protein interaction, we used ITC to measure the thermodynamics of the binding interactions between KpnB1 and INI-43. Successful interaction between a drug molecule and the target protein requires the formation of non-covalent bonds (Holdgate & Ward 2005a). Formation of these bonds is regulated by the affinity of the ligand for the respective protein, and the production of these bonds can be measured by using isothermal calorimetry (ITC). This thermodynamic technique is regarded as the gold standard in measurement of drug–protein interactions and generation of data on binding.

The ITC apparatus measures the changes in temperature or enthalpy (ΔH) that accompany molecular binding interactions (Holdgate & Ward 2005a), and the measurements obtained enable calculation of a thermodynamic profile of the binding interaction between the drug and the protein of interest.

The ITC apparatus is a closed system in which differential feedback is used to measure and determine the precise, minute temperature changes that indicate the occurrence of drug binding. The apparatus maintains a constant baseline temperature, and should the closed system temperature shift due to the energetics of drug binding the system immediately corrects itself via comparison with a reference cell. ITC's quantification of change from a baseline value provides valuable insight into the thermodynamics of drug binding when 3-D binding data is not available. The information provided by ITC includes the binding constant (K_a) and its dissociation constant (K_d), which together give key insight into the affinity of the ligand for its target (Equation 4.1) (Holdgate & Ward 2005a).

$$K_{d=}\frac{1}{K_a} \qquad \text{(Holdgate \& Ward 2005b)}$$

Equation 4.1: Dissociation constant K_d is determined experimentally. It can be calculated once the association constant is known.

ITC also provides thermodynamic data on the types of binding involved in drub–protein interaction.

In the closed system of constant temperature and pressure, the free energy (ΔG) can be calculated by:

$$\Delta G = -RTlnK_a = \Delta H° - T\Delta S° \qquad \text{(Holdgate \& Ward 2005b)}$$

Equation 4.2: Equation for Gibbs free energy constant, where R is the gas constant, T is temperature in Kelvin, and K_a is the binding constant.

The free energy represented by ΔG is a measure of how spontaneously a reaction takes place. The more negative this factor is, the more favourable the binding reaction. Further information regarding drug binding comes from the enthalpy value (ΔH). This parameter provides information on the energy content in the simultaneous breaking and creating of bonds during interaction with the drug. An increase in the formation of bonds results in a release of heat and thus in negative enthalpy. The more negative the value of ΔH, the more favourable the binding reaction (i.e. the more bonds formed). This value provides information relating to the possible formation of hydrogen bonds and van der Waals interactions. It must however be taken into account that solvents and buffers can affect this value; the ideal is therefore it is ideal to have 3D crystallographic data if a completely accurate measure of binding is required (Ladbury 2010; Holdgate & Ward 2005a).

Entropic information on the drug interaction is represented by the ΔS value (Holdgate & Ward 2005a). This value provides insight into the disorder within the system. As bonds form between the drug and protein, the amount of overall disorder within the system decreases, producing a more favourable, positive ΔS (Holdgate & Ward 2005b). The value of ΔS can be affected by the presence of water in the solvent, as hydrophobic interactions are involved in the release of water caused by drug binding (Liang 2008; Holdgate & Ward 2005a). The degree of hydrophobic binding can be determined from entropy change data using the equation:

$$-T\Delta S = \Delta G - \Delta H \qquad \text{(Holdgate \& Ward 2005b)}$$

Equation 4.3: Measurement of hydrophobic interactions is calculated experimentally. Once the parameters ΔG and ΔH have been calculated by experimentation they can be used to solve the equation for –TΔS.

This chapter describes our use of purified protein for biophysical analysis with CD and ITC, prompted by *in-vitro* data (Chapter 2), which suggests that INI-43 inhibits nuclear membrane transport of KpnB1. Biophysical techniques, were accordingly used to determine whether INI-43 interacts directly with KpnB1 to cause this effect.

4.2 Results

4.2.1 Circular Dichroism to investigate KpnB1–INI-43 interaction

Having established that GST purification methods enrich for GST-KpnB1, this purified protein was used in CD experiments. Using a final protein concentration of 0.2mg/mL for GST-KpnB1, a spectral analysis of KpnB1 was obtained in the absence of INI-43. Once a spectral range was established, purified GST-KpnB1 was measured in combination with increasing concentrations of INI-43. The INI-43 was titrated into the protein, using a Hamilton syringe, to measure the effects of increasing INI-43 concentration on protein folding (Figure 4.3).

Initial experiments were performed with INI-43 solubilised in DMSO. However we found, that DMSO absorbs strongly within the 280nm range, causing

anomalies in the data generated (data not shown). Subsequent experiments were therefore conducted with INI-43 solubilised DMF, which did not cause such anomalies.

Based on the spectra for purified KpnB1 only (black line Figure 4.3), the protein appears to be rich in alpha helices, evident from the positive band at 190nm value and negative bands at 233 and 240nm.

On addition of INI-43, there is a distinct rightward and upward shift in the spectra observed (Figure 4.3). This shift was strongly evident around the 233nm region. Spectral shifts within this wavelength have previously been attributed to possible interactions in a region of the protein containing numerous aromatic amino acids (Rogers & Hirst 2004; Greenfield 2006a).

There was a rapid saturation of binding, which was an indicator that lower concentrations of INI-43 were required for a better titration. INI-43 appeared to have quenched KpnB1 rapidly, thereafter dominating the reading. Our results provide evidence that INI-43 binds to a region rich in aromatic amino acids (present in the region where INI-43 was designed to bind) but because aromatic amino acids are distributed throughout KpnB1 we cannot definitely conclude that INI-43 binds within the region of HEAT repeats 5 and 6. Structural data would be required to verify this observation. Figure 4.4 shows where all of these aromatic amino acids are located within the protein highlighted by the purple squares, and in particular that some are present in the region of HEAT repeats 5 and 6, which is the location where INI-43 was postulated to bind.

The spectra generated in Figure 4.3 was analysed using online software CAPITO (Wiedemann et al. 2013) to examine the secondary structure of the purified protein (no drug added). The data collected is comparable to the published structures on the protein database (codes 1ibr, 2bku and 1qgk) (Rogers & Hirst 2004; Kelly et al. 2005; Greenfield 2004). Neural network software programs like CAPITO are not completely accurate. Such programs gather data, which is input by users over time. The program uses all this stored data to create outputs or results. The structural data obtained from the program is largely dependant on how much data other users have already loaded into the program and how similar it is to the current user's data. In addition, the absence of CD spectral data for KpnB1 with which we could compare our results means that the program as used in our study must be taken as a guide rather than as an absolute measure. Figure 4.5 A is the program estimate of how the CD spectra should look based on the amino acid sequence and loaded spectral data from Figure 4.3. Figure 4.5 B is the how the program interprets the secondary structure of the protein, red is alpha helix, green is beta sheet and black is irregular. This is based on the amino acid sequence and shows 99% alpha helix content where as the actual result is 30% according to the PDB (for the bound structure of KpnB1). As much as it is important to remember that the program itself is merely a guideline to the spectral and secondary structural information of the protein being examined, it is also important to remember that not only is there no data loaded for KpnB1 into the software creating error in the analysis, there is also not data on the PDB for the structure of unbound KpnB1. This limits us in giving us no accurate comparison for our structural and binding data. What

this data does show, is that the purified KpnB1 is rich in alpha helices, which suggests the structure of the protein is intact. Figure 4.5 C is proteins already in the database, which may resemble the protein being analysed. If the protein being analysed has been loaded by another user it should appear here.

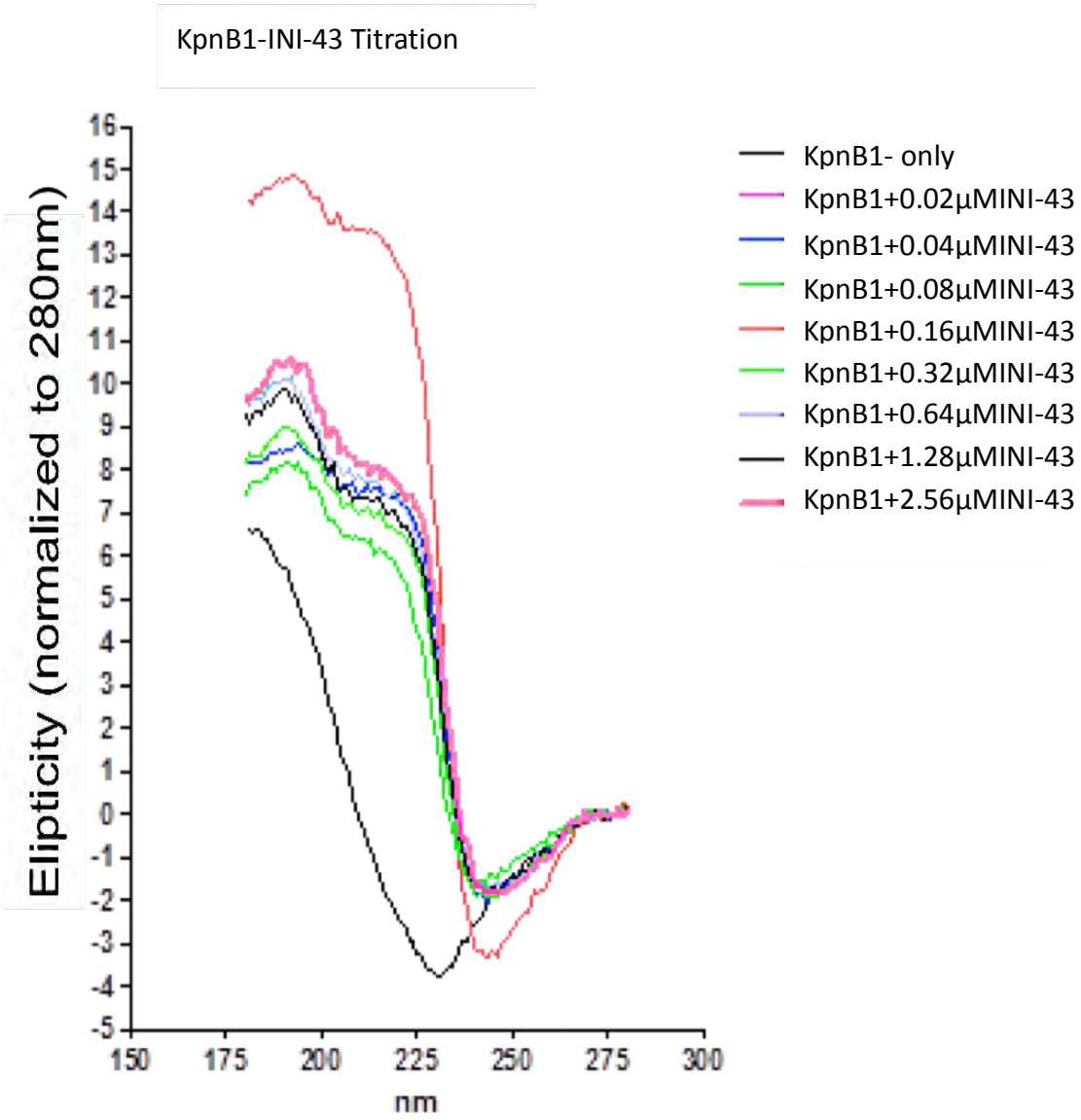

Figure 4.3 Spectral analysis of KpnB1 with INI-43 shows direct interaction of the drug with the protein. INI-43 was titrated into purified KpnB1 enabling the elliptical data to be examined over a range of wavelengths, scanning from 180nm to 280nm. The spectral pattern of the purified protein appears to closely resemble a protein rich in alpha helices.

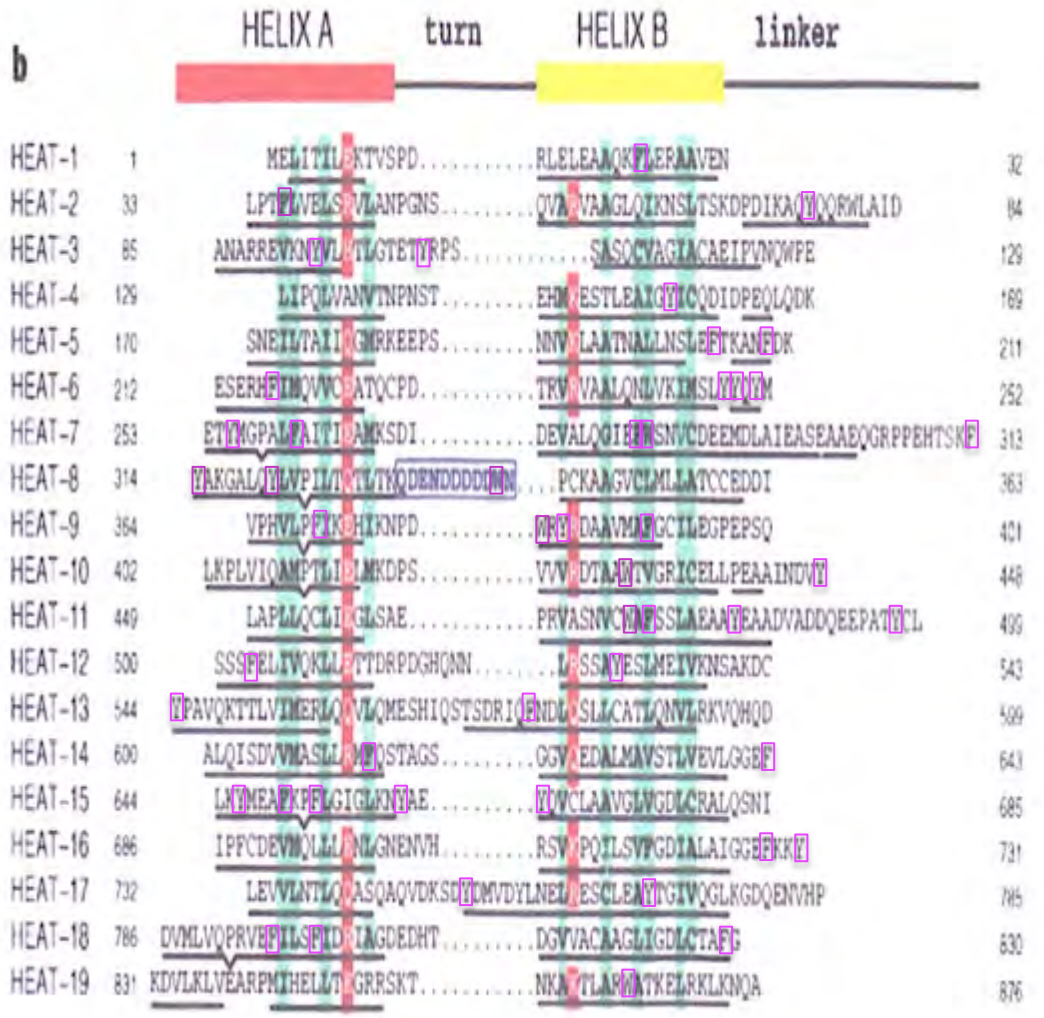

Figure 4.4: HEAT repeats 5 and 6 of KpnB1 contain aromatic amino acids. Amino acid sequence of KpnB1 showing HEAT repeats 1 to 19. The region of HEAT repeats 5 and 6 contains 7 aromatic amino acids. Conserved hydrophobic and polar residues highlighted in green and red respectively. Acidic loop outlined in blue and aromatic residues are highlighted by pink boxes (Figure from (Cingolani et al. 1999).

A.

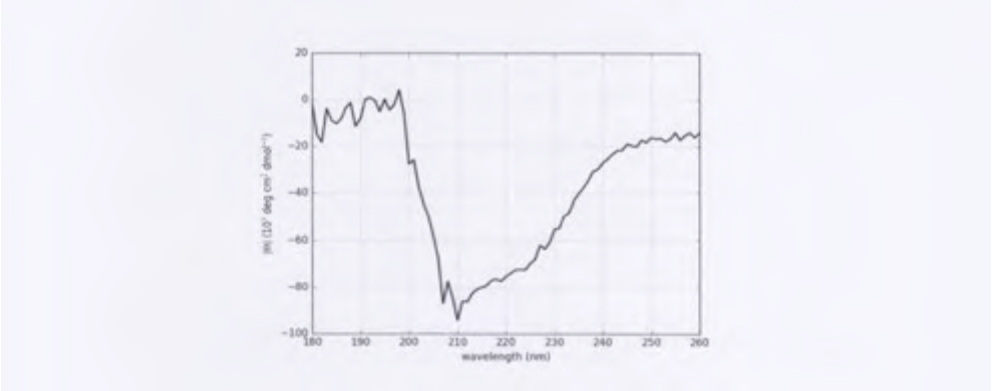

B.

Prediction via Chou-Fasman-algorithm (only based on provided amino acid sequence)

helix	β-strand	irregular
0.48	0.44	0.08

MELITILEKT VSPDRLELEA AQKFLERAAV ENLPTFLVEL SRVLANPGNS QVARVAAG
LQ IKNSLTSKDP DIKAQYQQRW LAIDANARRE VKNYVLQTLG TETYRPSSAS QCVA
GIACAE IPVNQWPELI PQLVANVTNP NSTEHMKEST LEAIGYICQD IDPEQLQDKS NE
ILTAIIQG MRKEEPSNNV KLAATNALLN SLEFTKANFD KESERHFIMQ VVCEATQCPD
TRVRVAALQN LVKIMSLYYQ YMETYMGPAL FAITIEAMKS DIDEVALQGI EFWSNV
CDEE MDLAIEASEA AEQGRPPEHT SKFYAKGALQ YLVPILTQTL TKQDENDDDD DW
NPCKAAGV CLMLLATCCE DDIVPHVLPF IKEHIKNPDW RYRDAAVMAF GCILEGPEPS
QLKPLVIQAM PTLIELMKDP SVVVRDTAAW TVGRICELLP EAAINDVYLA PLLQCLI
EGL SAEPRVASNV CWAFSSLAEA AYEAADVADD QEEPATYCLS SSFELIVQKL LETT
DRPDGH QNNLRSSAYE SLMEIVKNSA KDCYPAVQKT TLVIMERLQQ VLQMESHIQS
TSDRIQFNDL QSLLCATLQN VLRKVQHQDA LQISDVVMAS LLRMFQSTAG SGGVQED
ALM AVSTLVEVLG GEFLKYMEAF KPFLGIGLKN YAEYQVCLAA VGLVGDLCRA LQS
NIIPFCD EVMQLLLENL GNENVHRSVK PQILSVFGDI ALAIGGEFKK YLEVVLNTLQ Q
ASQAQVDKS DYDMVDYLNE LRESCLEAYT GIVQGLKGDQ ENVHPDVMLV QPRVEFIL
SF IDHIAGDEDH TDGVVACAAG LIGDLCTAFG KDVLKLVEAR PMIHELLTEG RRSKT
TKQKP LLHGQQKN

C.

Prediction via basis spectra

	helix	β-strand	irregular
▾ show predicted CD curve	0.99	0.01	0.59

Similarity hits based on nearest 25 neighbours

N	Name of protein	helix	β-strand	irregular
43	Subtilisin Carlsberg	0.29	0.20	0.51
40	Calmodulin	0.57	0.05	0.38
39	Human serum albumin	0.72	0.00	0.28

{ frequency of particular reference spectrum among the 25 nearest neighbours compared to your query in the range of 180-240 nm

Figure 4.5: Predicted secondary structural content of purified GST-KpnB1. Spectral data was loaded into a webserver-based analytical tool to analyse secondary structural content. In relation to differences from the predicted structure, allowance must be made for a degree of inaccuracy in the software. (Wiedemann, Bellstedt, & Gorlach, 2013) (A) Shows the predicted CD spectral curve of GST-KpnB1 based on the software. (B) Shows the percentage of secondary structural content based on the amino acid content as calculated by the software. (C) Shows the percentage of secondary structural content based on the spectral data input.

Once the CD data was collected, we corrected it to remove any effects due to the presence of the solvent. This was accomplished by scanning INI-43 alone and plotting standards at varying wavelengths (Figure 4.6 A). The data from the INI-43 titration was then used to develop a spectral analysis of KpnB1, and the effect of INI-43 on KpnB1 can be seen after subtracting the solvent effect (Figures 4.6 A–D). The maxima (190nm) (Figures 4.6 B) and minima (233nm) (Figure 4.6 C) were examined, and also the wavelength 210nm (Figure 4.6 D), as these provide insight into changes in secondary structures within KpnB1 when it binds to INI-43 (Rogers & Hirst 2004).

Spectral analysis of INI-43 in the absence of KpnB1 was performed to ensure the titrations performed were as accurate as possible (Figure 4.6 A). The figure shows that at the four selected wavelengths, there is an overall linear change in the spectra as the concentration of INI-43 is increased. This data was used to standerdise the raw data. Overall insight into the binding interactions of KpnB1 and INI-43 thus included examination of spectral changes across the varying concentrations of INI-43 at wavelengths 190nm, 210nm and 233nm. The INI-43 only titration can be subtracted from subsequent KpnB1 binding data.

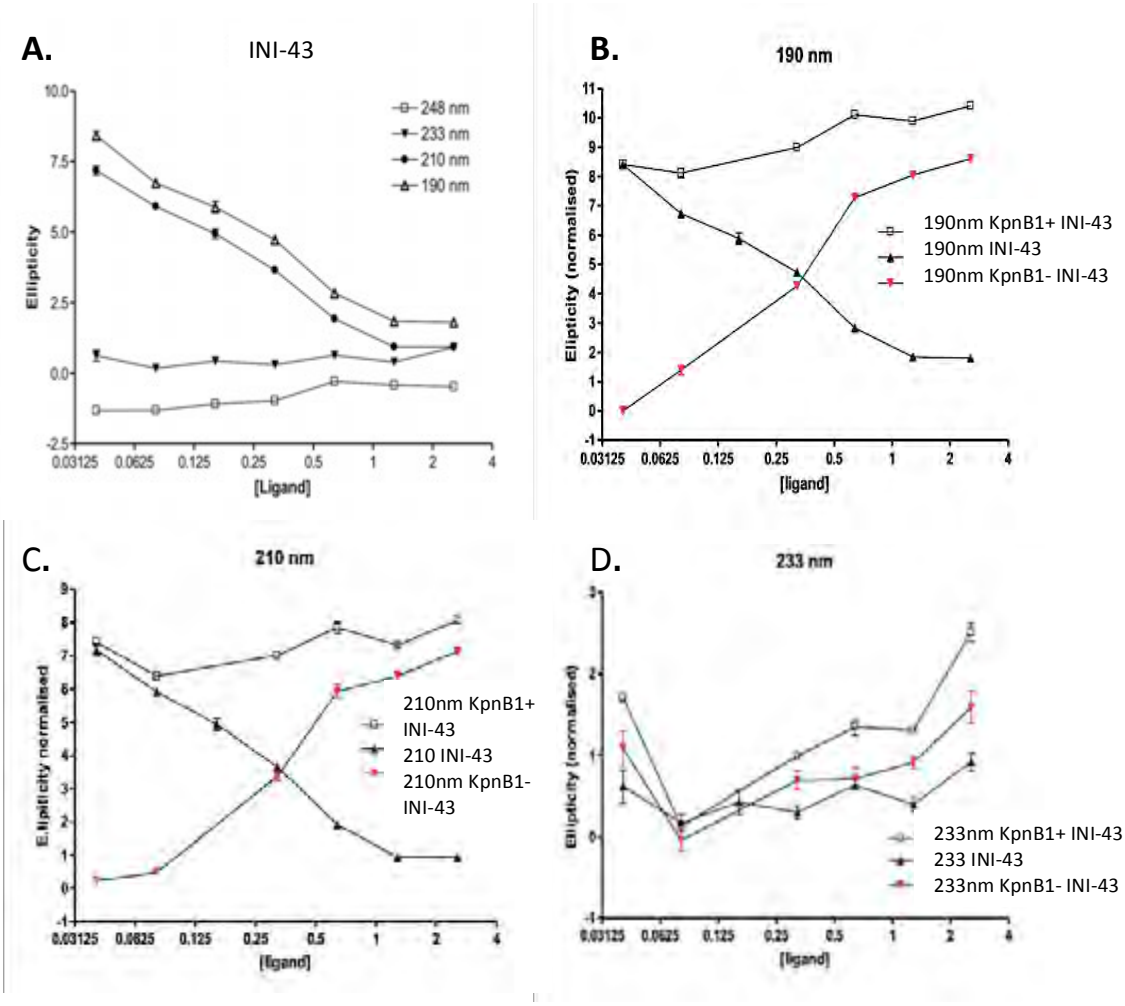

Figure 4.6: Spectral analysis of INI-43 titration shows possible secondary structural change of KpnB1 upon binding to INI-43: Graphs show ellipticity vs ligand concentration at predetermined wavelengths. (A) Spectral analysis of INI-43 at wavelengths of 190-233 nm. (B) Examination of KpnB1 and KpnB1 with INI-43 vs. INI-43 at the maxima 190nm shows change in secondary structure and interaction between INI-43 and KpnB1. (C) Examination of KpnB1 and KpnB1 with INI-43 vs. INI-43 210nm shows change in secondary structure and interaction between INI-43 and KpnB1. (D) Examination of KpnB1 and KpnB1 with INI-43 vs. INI-43 at the minima, 233nm shows possible interactions between aromatic amino acids and interaction between INI-43 and KpnB1.

At 190nm, an inverse relationship between the ellipticity of INI-43 and KpnB1 was observed as increasing concentrations of INI-43 was titrated into the purified protein solution (Figure 4.5 B). Based on this, INI-43 appeared to be interacting with KpnB1 causing a shift in the secondary structure. A similar result was visualised at 210nm where again inverse relationship between the ellipticity of INI-43 and KpnB1 was observed when increasing concentrations of INI-43 was titrated into the purified protein solution (Figure 4.6 C). At 233nm there was a shift in the spectra, indicative of possible interactions with aromatic amino acids as described previously.

To further visualise the possible INI-43-KpnB1 interaction, the original binding data (Figure 4.3) was used to generate binding isotherms using GraphPad Prism software. We examined three different wavelengths – 190nm, 208nm (another region where secondary structural changes are observed) and 210nm. From these binding isotherms we were able to obtain a Bmax and K_d to aid in the setup of the ITC experiments. Bmax is a measure of the maximum quantity of binding sites occupied, while K_d is the disassociation constant and measure of affinity. The isotherm data suggested that INI-43 binds to KpnB1 with an affinity in the range of 0.06-0.1µM. Figure 4.7 A, B, C are repeat saturation binding graphs performed at different wavelengths to attain K_d values with a close range. The graphs show saturation of binding as concentration of INI-43 increases. The scatchard plot is used to display the K_d and Bmax visually. Based on the K_d values in figure 4.7 it is suggested that KpnB1 binds to INI-43 in the µM range. For this reason future ITC experiment were carried out in the µM range.

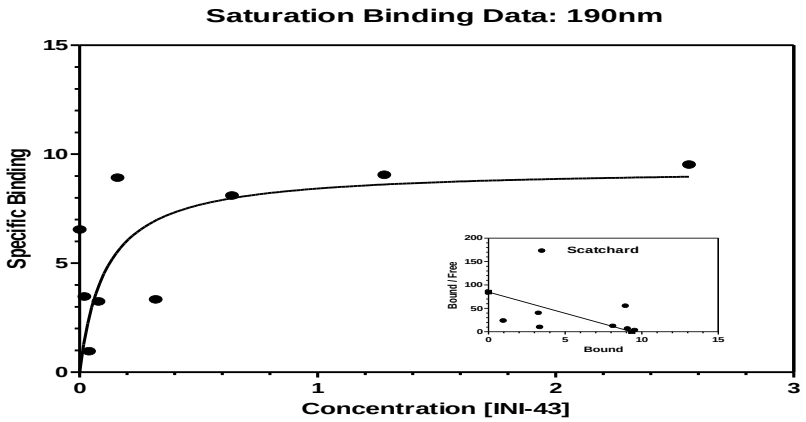

BMAX = 9.353µM
KD = 0.1102µM

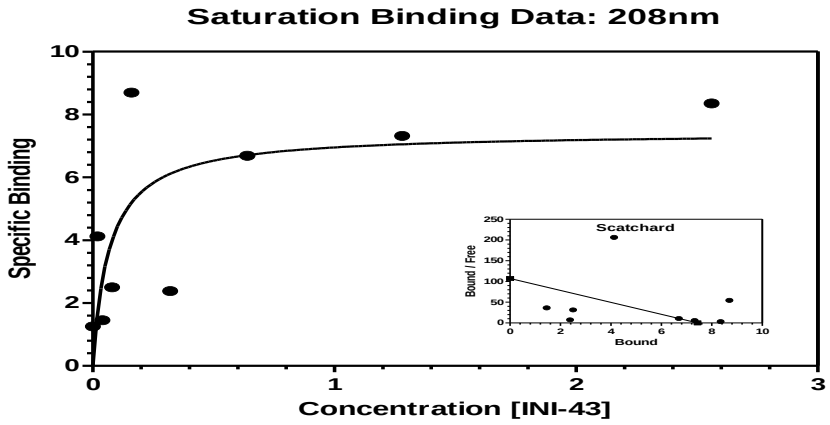

BMAX = 7.4434µM
KD = 0.06691µM

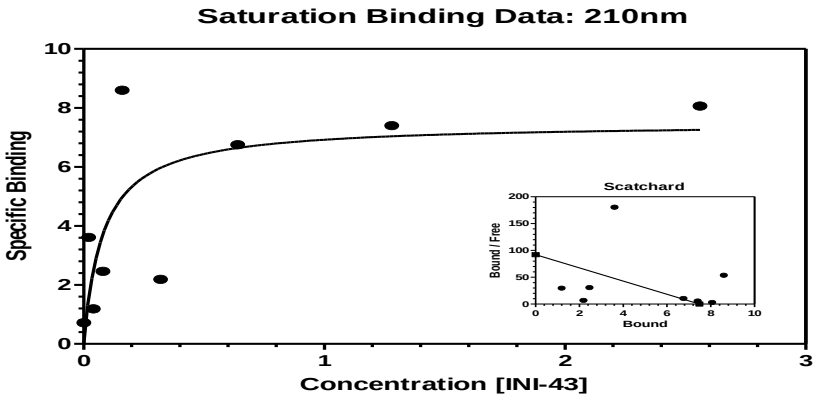

BMAX = 7.483µM
KD = 0.08124µM

Figure 4.7: Saturation binding and scatchard plots at three different wavelengths: 190nm, 208 and 210nm, show that INI-43 is binding to KpnB1 with a K_d raging from 0.06-0.1

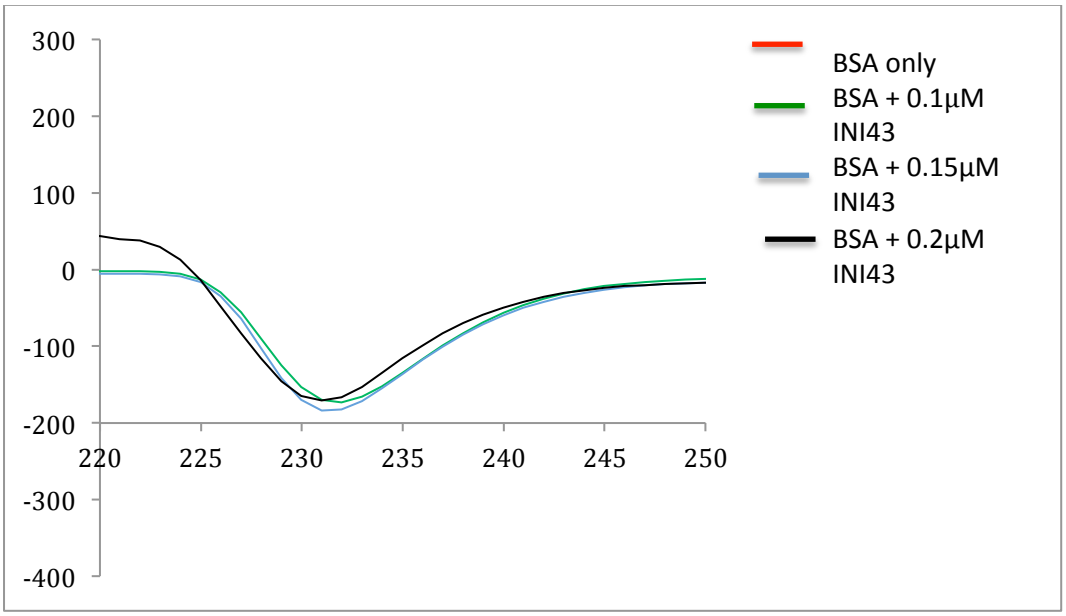

Figure 4.8: Spectral analysis of BSA with INI-43 shows direct interaction of the drug with the protein. INI-43 was titrated into BSA enabling the elliptical data to be examined over a range of wavelengths, scanning from 180nm to 280nm. The spectral pattern demonstrates some off target binding of INI-43 to BSA.

4.2.2 ITC to investigate KpnB1-INI43 interaction

ITC experiments were performed using a MicroCal™ iTC_{200} (GE Healthcare) at 24°C with purified GST- KpnB1 in 50mM Hepps buffer and 8.5% DMSO in the sample cell, and INI-43 in 50mM Hepps buffer and 8.5% DMSO was titrated into the chamber via the syringe with constant mixing. We used Hepps as it had a low heat of ionisation and allowed us to provide a pH of 8, and DMSO was used to balance out the solvent in the syringe. DMSO has a very high heat of ionisation, and if the cell and the syringe are not balanced, the heat of ionisation will mask any heat of binding. This experiment was repeated in triplicate and at three separate intervals. Data analysis was performed using Origin 7 software (MicroCal, USA).

From the ITC data that we collated we were able to observe binding between INI-43 and the purified KpnB1 protein; however, we were unable to optimise the binding data to further reveal a full differential binding isotherm. The solubility of INI-43 proved to be problematic when adding the drug to the buffer. For this reason, we were required to work at concentration 8.5% of DMSO. As the drug is injected into the cell containing KpnB1 the ITC apparatus measures the temperature. Heat released as the drug binds it visualised by the peaks in the raw data. The raw data is converted into a binding isotherm by the software, which then produces important binding data (Figures 4.8-4.10) as represented in figures, the protein saturates rapidly and only the top of the binding curve can be collected. During the course of the study and within our time frame we had difficulty improving the curves further.

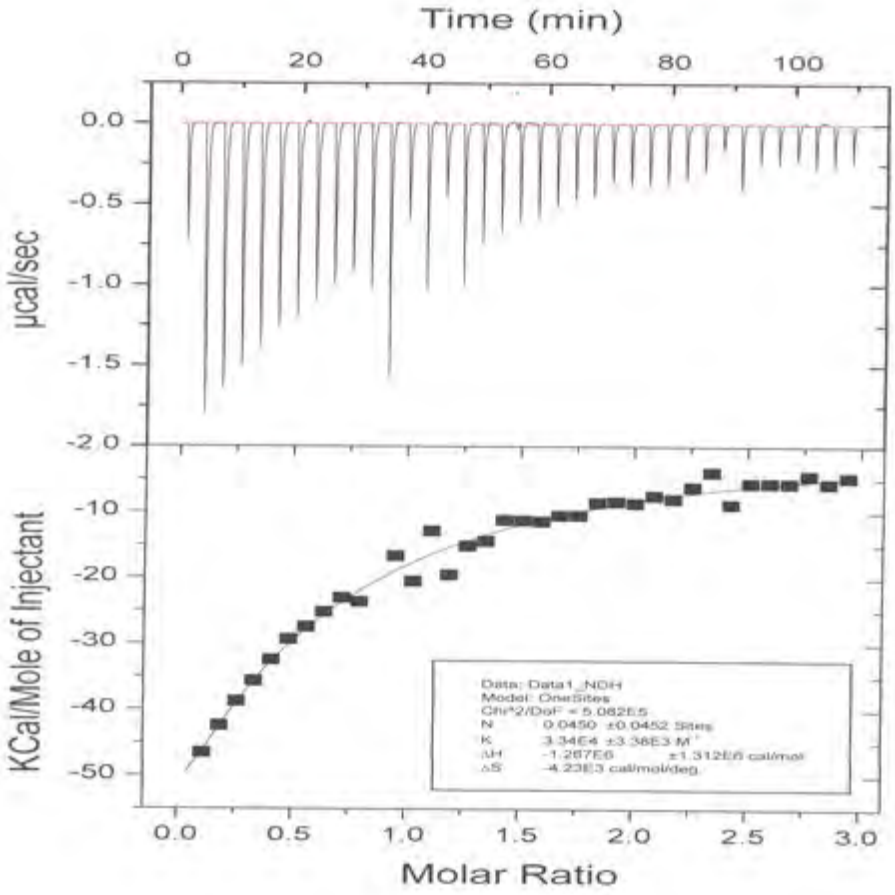

Figure 4.9: ITC data for INI-43 with KpnB1. Binding data generated using 750 µM INI-43 with 50 µM KpnB1 protein. Upper graph represents the raw ITC data in which the incremental heat changes are shown as microcalories per second plotted against time in minutes over the progression of the experiment. Lower graph shows the normalised integration data in terms of kcal.mol^{-1} of injectant plotted against the molar ratio of the added titrant with the curve fitted to single site model. The two axes are linked, allowing the interacted area for each peak to be positioned directly below the associated peak in the raw data. The negative peaks correspond to addition of an aliquot of ligand. The calorimetric output indicated that an exothermic process was occurring in the cell.

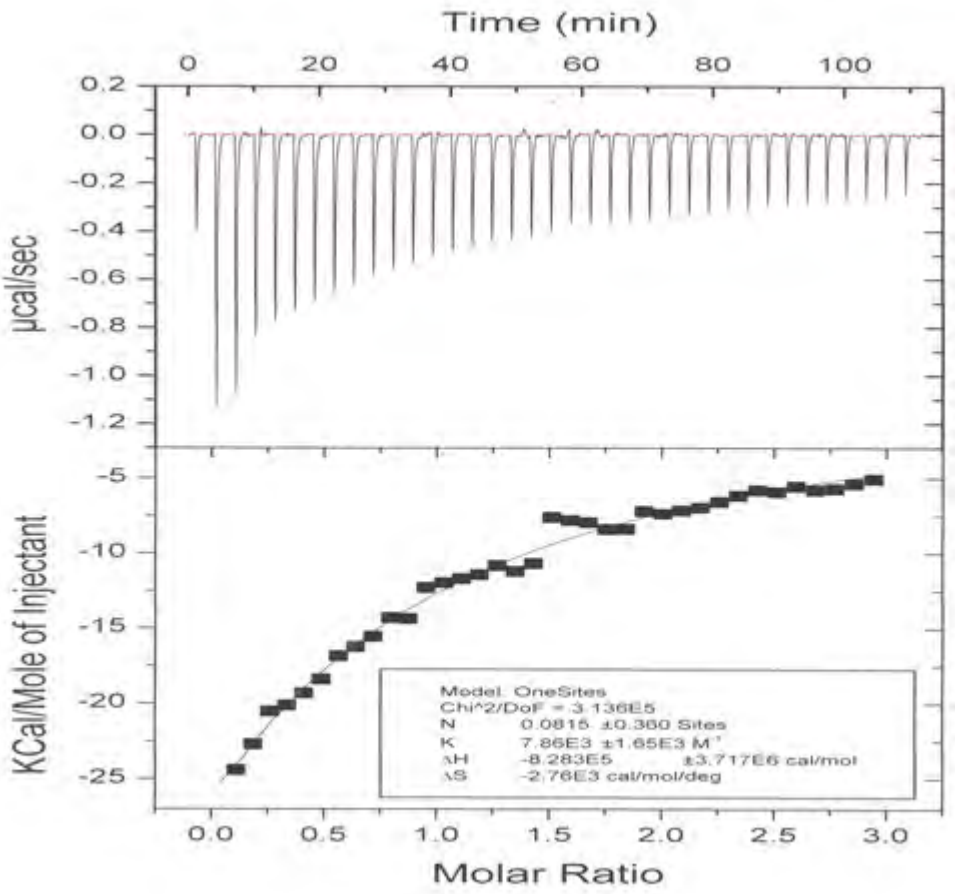

Figure 4.10: ITC data for INI-43 with KpnB1. Repeat of binding data generated 750 µM INI-43 with 50 µM KpnB1 protein. Upper graph represents the raw ITC data in which the incremental heat changes are shown as microcalories per second plotted against time in minutes over the progression of the experiment. Lower graph shows the normalised integration data in terms of kcal.mol^{-1} of injectant plotted against the molar ratio of the added titrant with the curve fitted to single site model. The two axes are linked, allowing the interacted area for each peak to be positioned directly below the associated peak in the raw data. The negative peaks correspond to addition of an aliquot of ligand. The calorimetric output indicated that an exothermic process was occurring in the cell. (Repeat to obtain smoother data)

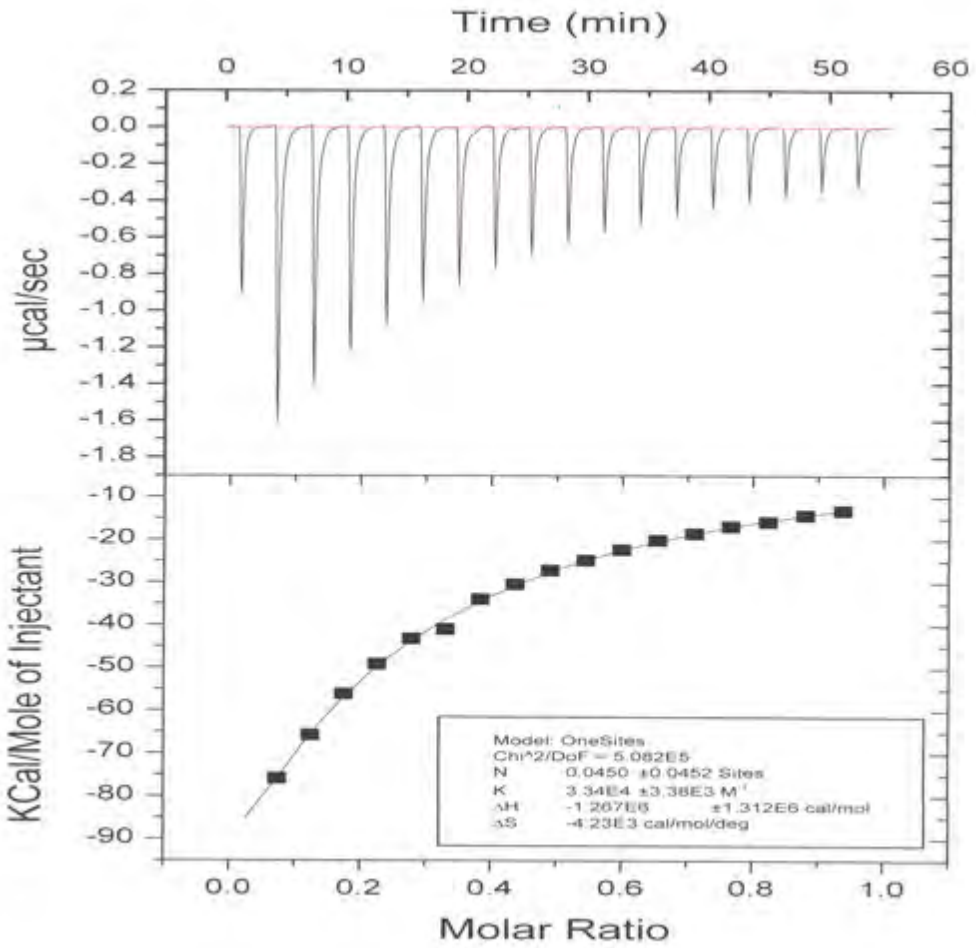

Figure 4.11: ITC data for INI-43 with KpnB1. Binding data shown for 250 µM INI-43 with 50 µM KpnB1 protein. Upper graph represents the raw ITC data in which the incremental heat changes are shown as microcalories per second plotted against time in minutes over the progression of the experiment. Lower graph shows the normalised integration data in terms of kcal.mol^{-1} of injectant plotted against the molar ratio of the added titrant with the curve fitted to single site model. The two axes are linked, allowing the interacted area for each peak to be positioned directly below the associated peak in the raw data. The negative peaks correspond to addition of an aliquot of ligand. The calorimetric output indicated that an exothermic process was occurring in the cell.

In the initial ITC experiments, we used a relatively high concentration of INI-43 (750 µM) and KpnB1 (50 µM) and saw the drug saturating the protein too quickly (Figures 4.8 & 4.9), preventing the generation of a complete binding curve. ITC experiments wee also performed using 250 µM INI-43 and 50 µM KpnB1 and binding curves shown in Figure 4.10 as with the higher drug concentrations, optimal binding data was not obtained. We did however use this data in an attempt to generate thermodynamic data.

Using the data collected from ITC (Figures 4.8-1.10) and the equations 4.1-4.3, Table 4.1 was constructed to summarise the results and important thermodynamic data. Based on the table it is clear that the results vary between the experiments as we were unable to acquire complete binding data for INI-43 with KpnB1. Of particular interest is the number of binding sites is less than 1, this being an indicator of INI-43 having a low affinity for KpnB1 and can result in incomplete binding data. The K_d values obtained from ITC were higher than those obtained using CD analysis which predicted a K_d value range of between 0.06-0.1 µM. The best K_d value obtained using, ITC was 2.99×10^{-5} (~0.3 µM). This value suggests that INI-43 binds to KpnB1 with weak affinity.

Table 4.1 summary of thermodynamic data collected from ITC experiments. Of particular interest is the K_d, number of binding sites and the free energy all of these factors give insights into INI-43 have an affinity for KpnB1 albeit a low one.

From the data we collected we derived the following constants:

[KpnB1]	[INI-43]	ΔH° (cal/mol)	ΔS° (cal/mol/deg)	ΔG°	-T ΔS°	N (Sites)	Kd (Mol $^{-1}$)
0.05mM	0.75mM	-1.267×10^{6}	-4.23×10^{3}	-2.573×10^{4}	1.267×10^{6}	0.045	0.299
0.05mM	0.75mM	-8.283×10^{5}	-2.76×10^{3}	-2.216×10^{4}	8.061×10^{5}	0.081	1.272×10^{-4}
0.05mM	0.25mM	-1.267×10^{6}	-4.23×10^{3}	-2.573×10^{4}	1.241×10^{6}	0.045	2.99×10^{-5}

4.2 Discussion

Initial analysis of INI-43 and KpnB1 interactions was performed using CD to measure drug–protein interactions. The advantage in adopting this technique was that it required minimal amounts of purified protein to potentially detect the effects of INI-43 on KpnB1. In performing this CD analysis we titrated INI-43 into the purified protein and determined the spectra. The purified KpnB1 on its own exhibited characteristic spectra in which there was a positive band at 190nm and a negative band between 210 and 220nm, indicative of a protein rich in alpha helices (Rogers & Hirst 2004). Although circular dichroism is not a completely accurate method of determining secondary structure and X-ray crystallography can provide precise measurements of key aspects of protein secondary structure within the protein, the data achieved here regarding protein structure is nonetheless in accordance with the structures in the PDB. After testing a range of varying INI-43 concentrations with the purified protein, it was clear that there was a binding interaction between KpnB1 and INI-43, possibly within the region rich in aromatic amino acids. This was concluded from the observed shift in the spectra, which occurred specifically in the 233nm region. It is also possible that INI-43 binding causes changes to the secondary structure of the protein. Energy transitions within a peptide chromaphore leads to an excitation of electron orbitals observed between the regions of 190nm and 222nm on the CD spectrum. This excitation can be negative or positive depending on the protein structure (Rogers & Hirst 2004). For this reason, the 210nm wavelength was chosen for closer examination as spectral changes at this

wavelength provide information on modifications in secondary structure in the protein under review (Rogers & Hirst 2004; Greenfield 2006c). Aromatic residues, can have a significant effect on the CD spectra in the 230nm region (Rogers & Hirst 2004); we therefore included this region in our observations.

The difficulty of using CD to measure the binding affinity of INI-43 with KpnB1 required us to employ a secondary method. And as such we chose to use ITC to measure drug–protein interactions. It was expected that the data thus generated would provide us with the required information to determine whether or not INI-43 was indeed directly binding to KpnB1, together with all corresponding kinetic data. The data gathered through this technique showed that although INI-43 was interacting directly with KpnB1 the affinity of the drug for the protein was low. It is possible that further chemical modification of INI-43 could improve its affinity for KpnB1. However, the incompleteness of binding data limited what we could deduce about the types of bonding interactions that are involved.

Another possible reason for INI-43 being unable to bind to KpnB1 is that the GST- is able to dimerise which could mask the binding site for INI-43 (Fabrini et al. 2009). GST is known to regulate apoptotic pathways in cells and have been shown experimentally to have Kd values within the nM range (Fabrini et al. 2009). Removing the tag or using alternative purification methods may be a better approach.

We were unable to collect complete binding data for INI-43 with KpnB1 when using ITC. Possible reasons for this may include INI-43 was identified using an in silico approach where the region of interest lies with a large concave surface of

KpnB1. As such, this suggests that it may be difficult for INI-43 to bind effectively, and remain bound, to KpnB1. INI-43 has to enter and become attached to the concave surface of KpnB1 in the correct orientation, and the fact that this surface plane is large in comparison to the drug molecule would in itself limit the potential for INI-43, applying appropriate energetics, to bind to the target region of specific interest within the protein. INI-43 must remain bound to the protein and any torsion or alteration of the protein structure could result in displacement of the drug if the bonding is not strong enough.

While the ITC data is no replacement for a 3-D crystallographic analysis of the integration between INI-43 and KpnB1, we can conclude that INI-43 is indeed binding to KpnB1, although the binding strength is low in terms of K_d and $\Delta G°$. The binding reaction could potentially be more favourable if modifications are made to the structure of INI-43. Low K_d values (in the μM range) were obtained with the data generated suggested a weak interaction between KpnB1 and INI-43. Successful small molecule inhibitors are described to have a K_d of approximately $1x10^{-9}$ and $1x10^{-12}$, (Kuriyan et al. 2009). The K_d we obtained was within the μM range. It is possible that further chemical modification of INI-43 could improve affinity for KpnB1.

Chapter 5

Conclusions

Identification of new drug therapies with low resistance and minimal side effects has been the focus of considerable interest in the past decade (Alifrangis & McDermott 2014). Literature reports and from our laboratory and others, reports that the upregulation of the nuclear transport family of proteins known as Karyopherins associates with cancer (van der Watt et al. 2009; Ward et al. 2011; Gerecitano 2014; Abdul Razak et al. 2016). This study focuses specifically on the import protein KpnB1, as we have previously shown that targeting this protein specifically, using siRNA, results in cervical cancer cell death (van der Watt et al. 2009; van der Watt et al. 2013). These observations lead to the hypothesis that the nuclear import protein KpnB1 is necessary for the proliferation of cancer cells and we therefore used a rational drug design approach to identify small molecule inhibitors with potential to bind to and inhibit KpnB1.

Using the known crystal structure of KpnB1, an *in silico* screen was performed against 12 662 570 compounds, searching for structures with the ability to bind KpnB1. Our laboratory tested forty-seven of the compounds identified with potential to bind KpnB1, using *in vitro* experiments with CaSki cervical cancer cells. These compounds were tested for their effects on cell death and proliferation, and their ability to inhibit nuclear transport. Of the compounds tested, a compound referred to as inhibitor of nuclear import 43 (INI-43) not only showed cytotoxic effects but also had the ability to block nuclear import, as

shown by immunofluorescence microscopy and cell fractionation studies (van der Watt et al. 2016). Aspects of our research presented in this thesis were included in the van der Watt *et al.,* (2016) manuscript.

This project was aimed at investigating the biological effects of small molecule INI-43 and examining its ability to interact with KpnB1 via drug-protein interactions. During *In vitro* analysis to investigate the effects of INI-43 on cervical cancer cells, INI-43 was found to be cytotoxic with an IC_{50} of approximately 10μM in both HeLa and CaSki cervical cancer cells. Further studies into the mode of cell death indicated that INI-43 treated cells were dying via apoptosis, as shown by PARP cleavage. INI-43 was also observed to inhibit nuclear import. This result was apparent by a dose-dependent reduction in the transcriptional activity of KpnB1 target proteins such as the transcription factor NFAT. We were able to observe a dose-dependent decrease in NFAT activity with increasing doses of INI-43, indicating inhibition of nuclear import of the transcription factor NFAT.

Using immunofluorescent analysis and confocal microscopy, we visualised both endogenous and exogenous expression of KpnB1 in cervical cancer cells in the absence and presence of INI-43. Endogenously expressed KpnB1 showed altered localisation from the nucleus to the cytoplasm and a concentration of KpnB1 in the peri-nuclear region in the presence of INI-43. This effect was likely due to inhibition of KpnB1 nuclear translocation on treatment with INI-43.

HeLa cells expressing exogenous levels of far-red fluorescently tagged KpnB1 (FRFP-KpnB1) displayed a similar relocation of FRFP-KpnB1 after INI-43

treatment. INI-43 was observed to be taken up by the cells within 20 minutes, and use of an FRFP-KpnB1 showed that treatment of HeLa cells with INI-43 resulted in a redistribution of the FRFP-KpnB1 from a mainly nuclear localisation to the peri-nuclear region of the cell, showing a peri-nuclear FRFP-KpnB1 was formed in treated cells. This provided further evidence that INI-43 interferes with the nuclear localisation of KpnB1.

Having achieved conclusive data that INI-43 was cytotoxic in nature, initiating cancer cell death via apoptosis, and that it was able to inhibit nuclear transport, we wanted to examine whether these effects were due to INI-43 interacting directly with KpnB1. Initial experiments using FRET photo bleaching to examine potential INI-43 and KpnB1 interactions were performed. FRFP-KpnB1 was used as the excitation and emission spectra of the fluorescent protein overlaps with that of INI-43, allowing for investigations using FRET photobleaching. Our initial results looked promising, as we observed both peri-nuclear localisation of KpnB1 (which co-localised with INI-43 fluorescent signals) and also presumed high FRET efficiency. However, negative controls displayed a colour shift in the FRFP-KpnB1 spectrum from a red to green signal in the absence of INI-43, making the interpretation of results obtained in the presence of INI-43 problematic. Similar observations have been made by others in the literature (Kremers et al. 2009).

As an alternative to FRET photobleach analysis, we proposed to use biophysical analysis to examine drug–protein interactions. After optimisation of protein purification employing a number of different clones and purification techniques, we were able to purify GST-KpnB1 using glutathione sepharose via batch binding

techniques. The purified protein was confirmed by mass spectrometry. We then used the purified protein in a circular dichroism spectral analysis of KpnB1. Titration of INI-43 into the purified KpnB1 protein showed a rightward and upward shift in the spectra at the 233nm region. This shift in the spectra was indicative of INI-43 binding, possibly in a region rich in aromatic amino acids. Spectral shifts in the 190nm and 210nm region suggested that there could be a possible secondary structural change in the KpnB1 on binding to INI-43. The binding dynamics of the spectra provided us with a preliminary K_d value.

To further investigate whether or not INI-43 was binding directly to KpnB1, ITC was performed to examine the thermodynamics involved in the possible interaction between KpnB1 and INI-43. The data achieved from this analysis suggested that INI-43 bound KpnB1 with low affinity. Thermodynamic data calculations yielded a best K_d value of 2.99×10^{-5}. Due to the low affinity of the compound for KpnB1, complete binding data could not be attained, making it difficult to obtain information on the types of interactions involved.

The reason for the low binding affinity that we observed is not clear. One possibility for the low binding affinity of INI-43 is that INI-43 was originally identified using *in silico* crystal structures of KpnB1, which may not necessarily entirely reflect what would happen when using purified protein in *in vitro* analyses. It is also possible that the binding of INI-43 to KpnB1 in live cells may differ from that observed using free purified protein. Crystallographic data of protein– INI-43 interaction would add significantly to a study of this nature.

Another possibility for the low binding affinity of INI-43 to KpnB1 is that INI-43 binds to a small select area on a large concave surface that encompasses the KpnB1–Ran–Kpna2 interaction area rather than a small binding pocket as with most other small molecule inhibitors. Small molecules ideally have a K_d of less than 1 x 10^{-9}M, meaning they have a high affinity for the receptor (Kuriyan et al. 2009). In the case of Imatinib, this is achieved by hydrogen bonding and having a small specific binding pocket (Druker 2002b); similarly SINE compounds achieve a high affinity by binding deep within the NES binding pocket (Fung & Chook 2014). It is possible that INI-43 does not fit into a small binding pocket as in the above examples, hence affinity of the drug for the protein is lower than what is considered ideal.

It is important to consider that we have limited knowledge on how this binding occurs in a cellular system when other factors such as RanGTP or KpnA2 are present. The presence of these proteins could enhance the affinity of INI-43, however confirmation of such an interaction would require X-ray crystallography. Significant amounts of purified protein is required (50mg/mL) for crystallisation (Cingolani et al. 1999) – quantities that were difficult for us to achieve during the course of this study.

While INI-43 has shown promise as an anti-cancer agent in that it displays cytotoxic effects and is able to block both nuclear import KpnB1-associated pathways and KpnB1 itself, we have only been able to show low binding affinities

despite the weak binding data. Should INI-43 be pursued further, optimisation of the structure to improve its binding affinity will be required. Crystallographic data would also substantially assist in the generation of more conclusive KpnB1–INI-43 binding data. Furthermore, at present there is very little/no in the literature describing the biophysical nature of KpnB1–small molecule interactions, and no crystal structures of KpnB1 bound to small molecules. To our knowledge this is the first time a biophysical analysis of a small molecule inhibitor targeted at the nuclear import pathway, specifically KpnB1, has been carried out.

Our key findings can be summarized as follows: Using cell culture systems we show that a small molecule, INI-43, kills cervical cancer cells by inducing cell death via apoptosis. We observed that INI-43 inhibits the proliferation of cancer cells and interferes with the nuclear import and activity of KpnB1 target protein NFAT. We were also able to show INI-43 interferes with the nuclear localisation of both endogenously and exogenously expressed KpnB1, and that INI-43 localises with KpnB1 after treatment of cells with the drug. Using biophysical analysis we were able to show that INI-43 binds purified KpnB1 with low affinity (within the μM range). Overall, this study has shown that there is promise for derivatives of INI-43 as future anti-cancer agents. Future work that is required includes modification of INI-43 that improves binding affinity and efficacy.

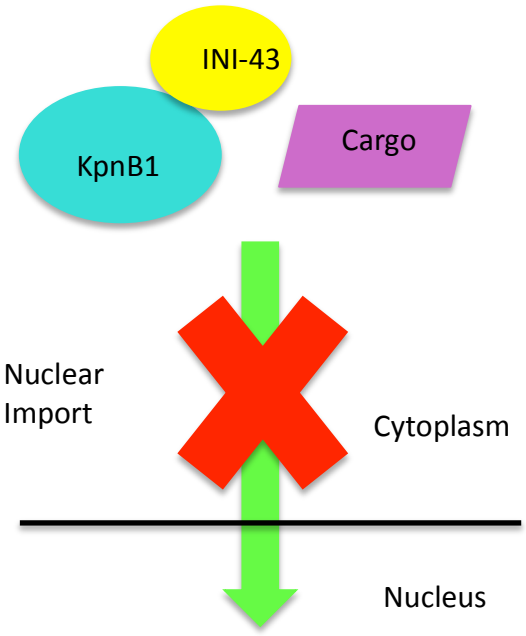

Figure 5.1: Schematic overview of inhibition of nuclear import caused via INI-43 interaction with KpnB1. Based on the evidence of this study, INI-43 binds to KpnB1 preventing nuclear import.

Chapter 6

Materials and Methods

6.1 Materials

6.1.1 Cell lines

The human cell lines were obtained from the American Type Culture Collection (ATCC) (Rockville, MD, USA): HeLa and CaSki cervical cancer cell lines HPV positive.

6.1.2 Cell line Growth conditions

Cells were grown in Dulbecco's Modified Eagle'sMedium (DMEM) (Gibco, Life Technologies, Carlsbad, CA, USA) with 10% heat inactivated Fetal Calf Serum (FCS) (Gibco, Life Technologies, Carlsbad, CA, USA), 100 U/ml penicillin and 100 µg/ml streptomycin maintained at 37°C in a 5% CO2 incubator and grown in tissue culture treated dishes Greiner (Lasec, Cape Town, South Africa).

6.1.2 Drugs

The compound INI-43 (Molport, Riga, Latvia) was solublised in DMSO (Sigma-Aldrich, Johannesburg, South Africa) to make stock solution. The drug was stored at room temperature and away from light.

6.1.3 Plasmids

GFP-NFAT plasmid (Addgene, Cambridge, Massachusetts, USA, plasmid # 24219)

NFAT-luciferase (Addgene, Cambridge, Massachusetts, USA, plasmid # 10959) was used to assess transcriptional activity of the NFAT gene of in cells for the dual luciferase assay. A plasmid encoding the Renilla luciferase reporter pRL-TK (Promega, Madison, WI, USA) was used as an internal control for the transfection efficiency of Dual luciferase assays. The pGEM-T Easy plasmid (Promega, Madison, WI, USA) was used to sub-clone the PCR products of the KpnB1 into final respective vectors.

The pGFP-KpnB1 plasmid (a kind gift from M. Ciciarello, University of Bologna, Bologna, Italy) was used to obtain the human from of KpnB1 for sub-cloning into appropriate vectors for protein purification.

The pmKate-2c plasmid (a kind gift from John O. Trent, University of Louisville, Kentucky, USA) was used to create red fluorescent protein (FRFP) of KpnB1 for use in FRET and confocal studies. Since the drug INI-43 has inherent fluorescence in the green channel it is important we used a corresponding label for KpnB1 in the red channel for confocal analysis. This also worked in our favour for FRET as the excitation emission spectra had an over lap with that of INI-43. Unfortunately negative controls displayed a colour-shift of the RFP-KpnB1 from red to green.

The pGEX-6P1 plasmid (a kind gift from Prof. J. Blackburn, University of Cape Town, Cape Town, South Africa) was used as a final vector into which KpnB1 was cloned allowing for the production of an N-ternminal GST-tagged protein for use in purification using glutathion sepharose.

The pET-28b plasmid (a kind gift from Prof. T. Sewell, University of Cape Town, Cape Town, South Africa) was used as a final vector into which KpnB1 was cloned, allowing for the production of an N- and C-terminal His-tagged protein for use in optimization of protein purification using nickle affinity resin and ion exchange.

6.1.4 Chromatography resins

For His-tag purification we used the HisTrap HP 5mL (GE life sciences, Pittsburgh, USA). These columns were pre-packed with Ni sepharose high performance resin, which has a binding capacity (40mg/mL). Column was run on AKTA Avant 25 chromatography equipment (GE life sciences, Pittsburgh, USA) along with Unicorn software (GE life sciences, Pittsburgh, USA) used for data collection. This setup belonged to Prof Sewel and Dr. Weber, University of Cape Town, Cape Town, South Africa, who collaborated with us this part of the project.

For anion exchange we used Hiprep 16/10 QFF column 20mL (GE life sciences, Pittsburgh, USA). Columns were pre-packed with 6% cross linked agarose (charged group $-N^{+}(CH_3)_3$, strong anion) used in conjunction with Waters Delta Prep 3000 preparative chromatography system, Gilson 321 pump, Gilson UV/vis – 155 spectrometer and Gilson FC 204 fraction collector (Gilson Inc. Middleton, Wisconsin, USA). The software used for data collection was Unipoint (Gilson Inc. Middleton, Wisconsin, USA). This setup belonged to Prof Sewel and Dr. Weber who collaborated with us this part of the project.

For Gel Filtration we used S-200 HR (GE life sciences, Pittsburgh, USA) column which was pre-packed with 120ml Allyl dextran and N, N'-methylenebisacrylamide Gilson 321 pump, Gilson UV/Vis – 157/159 spectrometer and Gilson FC 203B fraction collector (Gilson Inc. Middleton, Wisconsin, USA). This setup belonged to Prof Sewel and Dr Weber who collaborated with us this part of the project.

For GST-tag affinity chromatography we used glutathione sepharose (GE life sciences, Pittsburgh, USA) glutathione ligand is coupled via a 10-carbon linker to cross-linked 4% agarose producing a binding capacity of 4mg/ml.

6.1.5 Methods

6.1.5.1 Kpnβ1 primers (GST-tagged clone)	
pIBKpnβ1 primers	
Forward Primer	Reverse Primer
5'AGC CCG GGT CAA GCT TGG TTC3'	5'GAA CCA AGC TTG ACC CGG GCT3'
PGEM-T-EASY Sequencing primers	
T7 forward primer	Sp6 Reverse Primer
5'TAA TAC GAC TCA CTA TAG GG3'	5'TATTTAGGTGACACTATAG3'

pGEX Sequencing primer for pGEX-6-Kpnβ1	
pGEX 5' Forward primer	PGEX 3' Reverse Primer
5'GGG CTG GCA AGC CAC CTT TGG TG3'	5'CCG GGA GCT GCA TGT GTC CAG AGG3'
Walk Along Sequencing for pGex-6-Kpnβ1	
Forward Primer	Reverse Primer
5'CAC TTT ATT ATG CAG GTG GTC3'	5'GGA CTT ATG GTC CAA ACA AA3'
6.1.5.2 Kpnβ1 primers (His-tagged clones)	
Primers for N-terminal His tag clone	
Forward Primer	Reverse Primer
5’AG GGA TCC AGC TGA TCA CCA TTC TCG3’	5'AG GCG GCC GCA AGC TTG GTT CTT CAG3’
Primers for C-terminal His tag clone	
Forward primer	Reverse Primer
5'AG GGA ATG AGC TGA TCACCA TTC TCG3’	5'A GGC GCC GCA TTA AGC TTG GTT CTT CAG3’

PGEM-T-EASY Sequencing primers	
T7 forward primer	Sp6 Reverse Primer
5'TAA TAC GAC TCA CTA TAG GG3'	5'TATTTAGGTGACACTATAG3'
pGEX Sequencing primer for pGEX-6-Kpnβ1	
pGEX 5' Forward primer	PGEX 3' Reverse Primer
5'GGG CTG GCA AGC CAC CTT TGG TG3'	5'CCG GGA GCT GCA TGT GTC CAG AGG3'
Walk Along Sequencing for pGex-6-Kpnβ1	
Forward Primer	Reverse Primer
5'CAC TTT ATT ATG CAG GTG GTC3'	5'GGA CTT ATG GTC CAA ACA AA3'

6.2 Methods

6.2.1 Transformation by Heat Shock

1-2µl of reconstituted DNA was added to 30 µl of JM109 (Promega, Madison, WI, USA) competent cells in an eppendorf tube which then the contents of the tube was tapped to gently mix. The tube was incubated on ice for 20 minutes before being heat shocked at 42°C for 1 minute then promptly returned to ice for a further 2 minutes. Following the rest on ice 950 µl of LB (no antibiotics) was added to the bacteria/DNA mixture and the eppendorf tube was placed in the orbital shaker for 1.5 hours at 37°C at 150 rpm. Finally the mixture was plated on Luria agar plates made with the appropriate concentration of antibiotic depending on the plasmid. 100 µl was plated per plate and these were left to grow over night inverted in an incubator at 37°C.

6.2.2 Ligation Reaction

Restriction enzymes were used to excise the insert of interest or PCR was used to amplify the region of interest, which was electrophoresed, using a 1% agarose gel and the band of interest removed and cleaned up using the SV wizard Gel/PCR clean up kit (Promega, Madison, WI, USA). The excised insert was ligated into the linearized plasmid. Ligation of the insert into the vector was performed using the following equation:

(ng vector/kb vector) x Kb insert x 3/1 = ng insert

The insert and linearized vector DNA were then combined in a PCR tube and incubated at 45˚C for 5 minutes in a PCR machine followed by a 5 minute incubation on ice. This frees up the sticky ends and makes ligation more efficient. The vector and insert DNA was subsequently combined with 1 x T4 ligase buffer (Promega, Madison, WI, USA), 5% polyethylene glycol (PEG 4000) (Promega, Madison, WI, USA) and 3 units of T4 DNA ligase (Promega, Madison, WI, USA). The ligation was performed at 16 degrees overnight in a PCR machine and the following day, half of the ligation mix was transformed into *E. Coli* JM109 competent cells as described earlier. The transformation mixture was plated on agar plates containing the appropriate antibiotic. A negative control of linear vector was also simultaneously transformed to ensure that ligation was successful. Colonies were picked at random from the ligation plate and grown in 5mL of Luria broth containing appropriate antibiotics and mini-preps were performed.

6.2.3 A-Tailing

The PCR product required A-tailing to enable it to be inserted into the pGEM®-T Easy shuttle plasmid (Promega, Madison, WI, USA). The A-tailing reaction required 1 x Taq polymerase buffer, 2.5mM MgCl2 and 0.2mM dATP, 6 µl of the purified PCR product and 5 units of Taq polymerase (Thermo Fisher Scientifice, Massachusetts, USA). This reaction was performed in the PCR machine at 70˚C for 30 min and the resulting product ligated into pGEM®-T Easy. For the ligation reaction 100ng of purified, A-tailed PCR product was added to 50ng of pGEM®-T

Easy vector, 1 x rapid ligation buffer and 3 units of T4 DNA ligase (Promega, Madison, WI, USA). This ligation was performed at 4˚C overnight.

The following morning 5 µl of the ligation mix was transformed into 30 µl of highly competent JM109 cells.

6.2.4 DNA Isolation via Mini-Prep -Pureyield mini-prep system (Promega, Madison, WI, USA)

Several colonies were picked and placed into 5mL of LB containing appropriate antibiotics. These were grown overnight in an orbital shaker at 37˚C, 150 rpm and from them glycerol stocks were created. The 1.5mL of the remaining bacterial culture was centrifuged at 13000 rpm for 1 min in a bench top microfuge to pellet the cells. The supernatant was discarded and an additional 1.5mL was added centrifugation repeated. Once the supernatant had been discarded and the cells were suspended in 600 µl of TE buffer then lysed with 100 µl of cell lysis buffer. The tubes were inverted several times to ensure complete lysis. 350 µl of cold neutralization buffer was added to each tube and again the tubes were inverted until a yellow precipitate formed signalling complete neutralization. The tubes were centrifuged at max speed for 3 minutes to remove the debris allowing for purification of the genomic DNA. The DNA containing supernatant was transferred into a pureYeild minicolumn, which has a silica membrane to facilitate DNA binding and permit high quality DNA purification. The minicolumn was inserted into a collection tube so as to create the minicolumn assembly. The minicolumn assembly containing the supernatant was centrifuged at maximum speed for 15 seconds and the flow through was

discarded. The silica membrane in the minicolumn was washed with 400 µl of column was solution to remove contaminants from the DNA bound to the silica matrix, and the minicolumn was again centrifuged at maximum speed for 30 seconds. After transferring the minicolumn to a clean eppendorf the purified DNA was eluted from the column using 20 µl of nuclease free water. The minicolumn was again centrifuged as before. The final DNA product was nano-dropped so as to measure the DNA concentration.

1µg of the DNA from each of the purified clones was mapped using restriction digests to ensure that the plasmid was correct. The plasmid was mapped using the restriction Enzymes. This clone was further confirmed using DNA fingerprinting; the procedure was performed here at Sellenbosch University, Cape Town, South Africa. The sequencing reaction is given below and primers in table 2.1.1

6.2.5 DNA isolation by Maxi-prep – (Qiagen, Hilden, Germany)

After transformation a yellow tip was used to scrape off a single colony from the agar plate and dropped into a 10 ml starter culture of LB which was grown for 2-5 hours at 37°C degrees with agitation (200 rpm) in orbital shaker. The starter culture was added to 490 mL of fresh LB with the appropriate antibiotic in a 1L conical flask and grow over night at 37°C with agitation as above.

The following morning glycerol stocks were made by adding 800 µl bactaria 200 µl autoclaved glycerol. Next the bacterial culture was harvested by centrifugation at 6000 x G for 15 min at 4°C and the supernatant discarded. 10mL of buffer P1

was added to the pellet and the bacterial cells re-suspended. Once the pellet was completely re-suspended and no clumps were visible 10mL of P2 was added to lyse the cells and the solution gently mixed**.** Addition of 10mL P3 was used to neutralize lysis and upon addition and the solution was gently mixed to ensure complete neutralization. Next the mixture was allowed to rest on Ice for 20 min to enhance precipitation of cellular debris following which the solution was centrifuged at 16 000 x G for 30 min 4°C and the DNA containing supernatant was preserved. The quiagen tip 500 was equilibrated with 10mL buffer QBT and the DNA containing supernatant was added to the quiagen tip and allowed to flow through. Following the addition of the supernatant the quiagen tip was washed with 30mL of buffer QC to remove unwanted carbohydrates. The bound DNA was recovered with 15mL buffer QF and precipitated by the addition of 10.5mL room temp isopropanol to the corex tube with eluted DNA solution and centrifuge at 14 000 x G for 30 min 4°C. the DNA was washed with 5mL 70% ethanol and centrifuge again at 14 000 x G for 10 min 4°C. Finally the pellet was allowed to air dry overnight after which it was re dissolved in between 200-500 µl of TE buffer and quantified using the nano drop (Thermo Fisher Scientifice, Massachusetts, USA).

6.2.6 Drug IC_{50}

The IC_{50} value of INI-54 was determined in both HeLa and CaSki cell lines. Cells were grown in complete media (DMEM, 10%FCS, 1%P/S) and seeded at 1000 cells per well for HeLa, 3000 cells per well for CaSki plated in 96-well tissue culture treated plates. Cells were received a 48 hour treatment with varying

concentrations of INI-43 (0, 1, 5, 8, 10, 15, 20 and 40 μM). This was performed in triplicate. After drug treatment MTT (Sigma) was added and four hours later the crystals formed were solubilised by the addition of Solubilisation Solution Reagent (10 % SLS in 0.01 M HCl). Absorbance readings were measured at 595nm the following day using a BioTek microplate spectrophotometer (Winooski, Vermont, USA) and IC50 curves were generated using GraphPad Prism software (Graphpad Software Inc. California, USA).

6.2.7 Cell Proliferation

The proliferation assay was conducted over a period of 5 days. HeLa and CaSKi cells were seeded into 96-well tissue culture treated plates at 1000 and 3000 cells per well respectively. A pre-determined concentration range of INI-43 (0, 5 and 10 and 15μM) was selected and treated to each cell line for each day and performed in triplicate. On each day that the assay performed, 10μL of MTT was added to each of the treated wells, then, 4 hours later 100μL of solubilization solution was subsequently added. The following day the plate was read at 595nM.

6.2.8 Harvesting and quantitating protein from cultured cells

Cells were lysed on using ice-cold RIPA buffer (see solutions) containing 0.5 mM PMSF, 1X complete protease inhibitor cocktail (Roche, Basel, Switzerland) and 2 mM Na3VO4 to inhibit the action of phosphatases. Using a cell scraper cells were removed from dishes and transferred into pre-chilled eppendorf tubes. Cell lysates were briefly sonicated then centrifuged at 12000 rpm for 15 min at 4°C to

remove the cell debris. Protein samples were stored at -80°C before use. Protein concentrations were quantitated using the Bicinchoninic Acid (BCA) protein assay kit (Thermo Fisher Scientific, Massachusetts, USA). According to the manufacturer'sprotocol.

6.2.9 Western blot analysis

Protein was separated based using the Mini Protean II System (Bio-Rad, California, USA) for SDS-PAGE. 10-40 µg of protein was separated by 8% or 10% resolving 4% stacking gel. Samples were prepared by adding appropriate volumes of 5X Laemmli loading dye (see solutions) following which they were heated/denatured at 90°C for 1 min. A protein molecular weight markers was run concurrently with the samples to determine the size of separated proteins: all makers are listed in the appendix. Once electrophoresis was concluded, the proteins were transferred to a HybondTM-ECLTM nitrocellulose membrane (GE life sciences, Pittsburgh, USA) using the wet/tank transfer system (Bio-Rad, California, USA). The membrane was blocked in a solution of 5% low fat milk powder made up in Tris-buffered saline with 0.1% Tween (TBST). Blocking was performed for 1 hour at room-temperature on a shaker following which the membrane was incubated with the primary antibodies overnight with shaking. The following day, membrane received three washes in TBST, each for 10 min before the horseradish peroxidase-conjugated secondary antibodies were added for 1 hour at room temperature with shaking. Following this step the membrane was washed a further three times in TBST for 10 minutes each wash. The protein bands detected using the LumiGLO or LumiGLO reserve chemiluminescent

substrate system (KPL Inc. Whitesci, Cape Town, South Africa). To re-probe membranes for another protein, antibodies were stripped from the membrane with 10% acetic acid, shaking for 15 min, flipping the blot over half way. The acetic acid was neutralized by washing the membrane four times for 10mins for each wash with fresh TBST. Blocking and the addition of antibodies, was performed normally after striping. ImageJ software (ImageJ, NIH, USA) was used to quantitate protein expression levels, and bar graphs represent the expression of each protein relative to β-tubulin (or alternative loading control).

6.2.10 PARP-1 Cleavage Assay

300 000 HeLa cells and 400 000 CaSki cells were seeded per 60mm dish in 4 mL complete media (DMEM, 10%FCS, 1%P/S) and incubate overnight at 37°C; 5% CO_2. Drug treatments were performed 24 hours later with 5 or 10 µM INI-43 and 48 hours cells were harvested collecting both adherent and floating cells. First the media was removed and place in sterile 12mL tubes. These were centrifuged at 12 000 rpm to harvest the floating cells. The pellet was gently washed with 1 x PBS and then re-suspended and placed in sterile eppendorf tubes followed by another round of centrifugation at 12 000 rpm for 15 min at 4 °C. The PBS was removed and the eppendorf tubes were placed on ice. The remaining cells attached to the dishes were harvested using RIPA mix and a cell scraper as in section 6.2.3. Following sonication and centrifugation the supernatant was placed in a clean pre-chilled eppendorf tube and using BCA regent (Thermo Fisher Scientific, Massachusetts, USA). PARP-1 cleave was detected using western blot analysis using 1:1000 primary antibody (sc-7150, Santa Cruz

Biotechnology, California, USA) and goat anti-rabbit horseradish peroxidase conjugate secondary (170-6515, Bio-Rad, California, USA) detected with lumiglo chemoluminesent reagent (KPL Inc. Whitesci, Cape Town, South Africa). To ensure the loading was accurate the blot was stripped using 10% acetic acid, then re-probed for B-tubulin and detected with lumiglo chemoluminesent reagent. Densitometric analysis was performed using image J subtracting the loading control from the results to create a quantitate result.

6.2.11 Ability of INI-43 to inhibit Nuclear Import-NFAT assay

30 000 HeLa cells were plated per well in 24-well tissue culture treated plates, and transfected with 50 ng GFP-NFAT plasmid (Addgene, Cambridge, Massachusetts, USA, plasmid # 24219, gift of Jerry Crabtree (34)), 50 ng NFAT-luciferase (Addgene, Cambridge, Massachusetts, USA, plasmid # 10959, gift of Toren Finkel (35)), and 5 ng pRL-TK, using 0.4 µl Genecellin^{TM} Transfection Reagent (Celtic Molecular Diagnostics, Cape Town, South Africa). 24 hours after transfection cells were treated with the various concentrations of INI-43 (0, 5, 10 µM). The following morning the cells were stimulated with 100 nM PMA (Sigma-Aldrich, Johannesburg, South Africa) and 1.3 µM Ionomycin (Sigma-Aldrich, Johannesburg, South Africa) for 3 hours, following which luciferase activity was measured.

Luciferase activity was assayed using the Dual-Luciferase^{R} Reporter assay system (Promega), according to the manufacturers' instructions, and luciferase readings were measured using the Veritas^{TM} microplate luminometer (Promega,

Madison, WI, USA) and normalised to Renilla luciferase in the same extract.

6.2.12 Confocal microscopy-Effects of INI-43 on Endogenous Expression of Kpnβ1

HeLa cells were grown on glass coverslips in 1000 mm dishes seeded at a density of 600 000 cells per well in a 6 well tissue culture treated plate in complete media (DMEM, 10%FCS, 1%P/S). Once the cells had settled they were treated with 10 µM INI-43 for 1.5 or 3 hours. For controls, equivalent volumes of DMSO (Sigma-Aldrich, Johannesburg, South Africa) were used. Subsequent to treatment, media was removed and the cells washed with 1 x PBS then fixed with 4% paraformaldehyde followed by 3 x 5 minute washes in 1 x PBS. Following fixation the cells were permeabliized with 0.5% triton X 100 and subsequently washed in 1 x PBS for 5 mins. 50mM NH_4Cl in PBS was used to quench for 5 minutes then blocking was performed using 0.2% gelatin. Immunofluorescence analysis was performed using 1:100 Kpnβ1 antibody (sc-11367, Santa Cruz Biotechnology, California, USA) in 0.2% gelatine incubated for 45 minutes and 1:300 Cy3 goat anti-rabbit secondary antibody (Jackson ImmunoResearch, West Grove, Pennsylvania, USA) in 0.2% gelatine incubated for 45 minutes. Cell nuclei were stained with 0.5 µg/ml DAPI. Images were captured using a Zeiss inverted fluorescence microscope under 100 X oil immersion (Carl Zeiss, New York, USA).

6.2.13 Confocal microscopy-Effects of INI-43 on Overexpression of Kpnβ1

The plasmid pmKate-2c was kindly donated by J. O Trent, university of Louisville, Kentucky USA. The fragment of interest (KpnB1) was amplified using PCR from a pre-existing pGEX6-KpnB1 plasmid. Primers were designed so that the fragment of interest (KpnB1) could be amplified via PCR (see primer list). Restriction sites (Sac11 and BamH1) were incorporated onto the 5' ends of the primers so as to facilitate the cloning of the Kpnβ1 fragment into the final plasmid. These particular restriction enzymes were chosen as they do not cut the KpnB1 or the shuttle vector pGEM®-T Easy

The PCR was performed using the primers (10pmol of each) to amplify 10ng of template DNA (pIB-GFP), 1x Pfu buffer (without $MgSO_4$), 1.5mM $MgSO_4$, 0.2mM dNTPs and 2.5 units Pfu Taq (Thermo Fisher Scientific, Massachusetts, USA). The PCR Reaction was performed as mentioned in the conditions below:

KpnB1 fragment amplification PCR cycle conditions

Cycle 1	95˚C	5min	
Cycle 2	95˚C	30sec	35 cycles
	60˚C	30sec	
	72˚C	3 min	
Cycle 3	72˚C	7min	
Cycle 4	4˚C	∞	

The PCR product was electrophoresed on a 1% agarose gel and the band of interest excised, cleaned up and purified as previously mentioned. A-tailing was performed on the purified DNA following which it was inserted into the shuttle vector pGEM®-T Easy (see section). Once the DNA had been transformed into *E. Coli JM109* competent cells (Promega, Madison, WI, USA), a blue/white screen was performed and several white colonies picked and mapped using the restriction enzymes BamH1, Sac1 and Sca1.

Once the correct clone was identified, the insert KpnB1 was removed using the restriction enzymes BamH1 and Sac11. Similarly, the final vector pmKate-2C was linearized using the same restriction enzymes. The digested products were electrophoresed and the bands corresponding to the size of interest were excised from the agarose gel. The DNA contained within the gel was cleaned and purified using the wizard SV kit (Promega, Madison, WI, USA),.

The ligation of the vector and the insert was performed as described previously. The ligation mix was transformed into *E. Coli* JM109 competent cells as before and grown on agar plates containing 30µg/µl Kanamycin (Sigma-Aldrich, Johannesburg, South Africa). Several colonies where picked and grown as before in LB containing 30µg/µl Kanamycin (glycerol stocks were made each time from each new clone). Mini-preps (Promega, Madison, WI, USA), were performed on the bacteria and the purified plasmid DNA was mapped using Sac11 and BamH1. The final plasmid was confirmed using DNA fingerprinting conducted at Stellenbosch University.

The pmKate-KpnB1 was transfected into HeLa cells to test for transfection efficiency. 450 000 cells per dish in 100 mm cell culture dishes (Greiner, Lasec, Cape Town, South Africa). and grown in complete media (DMEM, 10%FCS, 1%P/S). Cells were left to settle overnight. 24 hours later, the cells were transfected with pmKate-Kpnβ1. 2.9µg of plasmid DNA was added to 200µL serum free media and 9.6µL GeneCellin™ transfection reagent. The HeLa cells were harvested using RIPA buffer and Western Blot analysis performed, using a rabbit anti- Kpnβ1 (sc-11367, Santa Cruz Biotechnology, California, USA) primary antibody 1:1000 and goat anti rabbit IgG Conjugate secondary antibody 1:5000 (170-6515 Bio-Rad, California, USA).

The process was repeated but this time glass cells were grown on glass cover slips, transfected with pmKate-KpnB1 and on day 3 treated for various time intervals with INI-43 then fixed using 4% paraformaldehyde and left in 1 x PBS until viewed with confocal microscopy. Images were captured using a Zeiss inverted fluorescence microscope under 100 X oil immersion.

6.2.14 FRET Photo Bleaching

450 000 cells per dish in 100 mm cell culture dishes cells were grown on glass cover slips and grown in complete media (DMEM, 10%FCS, 1%P/S). Cells were left to settle overnight. 24 hours later, the cells were transfected with pmKate-Kpnβ1. 2.9µg of plasmid DNA was added to 200µL serum free media and 9.6µL GeneCellin™ transfection reagent. 24 hours after transfection cells were treated with 10 µM INI-43 for 30 and 45 minutes then subsequently fixed using 2% paraformaldehyde and left in 1 x PBS until viewed with confocal microscopy.

Zeiss LSM 510 Meta confocal microscope. Regions of interest (ROIs) containing cells that both exhibited INI-43 fluorescence and expressed mKate2-KpnB1 were selected for bleaching. The 561 nm laser line was used to excite and bleach the far-red signal. Bleaching was achieved by 20 intterations of the laser over the region of interest to completely remove the red signal. FRET efficiency was calculated as follows: FRETeff (%) = (Donor post – Donor pre)/Donor post X 100, where Donor pre and Donor post represent donor fluorescence intensity before and after photobleaching, respectively. At least 4 different cells were examined for the presence of FRET signals and used to calculate average FRET efficiencies. Zen Blue software (Zeiss) was used to convert the confocal images into FRET images.

6.2.15 Sub cloning of KpnB1 into pET-28b

The human variant of KpnB1 as amplified out of the pGEX-6KpnB1 plasmid via PCR. Two sets of primers were constructed so as to allow for one clone with an N-terminal His-tag, and a second with a C-terminal His-tag. Once amplified, the fragments were run on a 1% agarose gel and excised for clean-up using the SV-wizard gel and PCR clean up kit (Promega, Madison, WI, USA). The separate fragments were A-tailed in preparation for insertion to the shuttle plasmid pGEM-T-EASY. Following the A-tailing process, the separate fragments were ligated into pGEM-T-EASY shuttle plasmids at 4°C over night and transformed into JM109 bacterial cells. Once in pGEM-T-EASY, a blue/white screen was performed and the white colonies were picked and screened for inserts using mini-prep DNA isolation methods. Upon isolation of the correct clones the

inserts were excised using BamH1 and SacII restriction enzymes (Fermentas Thermo Fisher Scientific, Massachusetts, USA) and the KpnB1 inserts were ligated into the pET-28b plasmid. Once again the ligations were transformed and mapped using restriction enzyme digest and finally DNA finger printing.

6.2.16 Sub cloning of KpnB1 into pGex6-P1

We were gifted with the plasmid pIB-GFP (Importin-Beta-GFP) kindly donated from M. Ciciarello et al (2004). Primers were designed so as to allow for amplification of the fragment of interest (KpnB1) via PCR. Restriction sites BamH1 and Xma1 were incorporated onto the 5' ends of the primers so as to facilitate the cloning of the KpnB1 fragment into the final plasmid. These particular restriction enzymes were chosen as they do not cut the KpnB1 or the shuttle vector pGEM®-T Easy (Promega, Madison, WI, USA). The stop codon had been mutated in the Importin-Beta-GFP plasmid so this to was incorporated in the reverse primer

The PCR was performed using the primers (10pmol of each) to amplify 10ng of template DNA (pIB-GFP), 1x Pfu buffer (without MgSO4), 1.5mM MgSO4, 0.2mM dNTPs and 2.5 units Pfu Taq (Fermentus Thermo Fisher Scientific, Massachusetts, USA). The PCR Reaction was run as follows

6.2.16.1 Kpnβ1 fragment amplification PCR cycle conditions

Cycle 1	95˚C	5min	
Cycle 2	95˚C	30sec	
	45˚C	30sec	35 cycles
	72˚C	3 min	
Cycle 3	72˚C	7min	
Cycle 4	4˚C	∞	

The PCR products were electrophoresed on a 1% agarose gel using the O'Gene ruler ladder mix marker (Fermentas Thermo Fisher Scientific, Massachusetts, USA) to specify the size of the bands present. PCR product was then excised from the gel and purified using the wizard SV PCR and Gel purification kit, (Promega, Madison, WI, USA).

PCR product of KpnB1 was A-tailed and ligated in to the shuttle plasmid pGEM-T-EASY where mini-prep DNA isolation was performed to isolate the correct clone via restriction enzyme digest followed by DNA finger printing. Once a clone with the correct insert was isolated this KpnB1 was existed using the restriction

enzyme BamHI (Fermentas Thermo Fisher Scientific, Thermo Fisher Scientific, Massachusetts, USA) and Xma I (NEB, Thermo Fisher Scientific, Massachusetts, USA) and re-ligated into the final plasmid pGEX-6P. Once again ligations were transformed and the DNA mapped via restriction digest and DNA fingerprinting.

6.2.17 Assessing GST-KpnB1 protein induction

A 10mL starter culture using TB 100µg/mL Ampicillin (Sigma-Aldrich, Johannesburg, South Africa) was grown for 2-5 hours before transferring to a 100 mL culture (TB 100µg/mL Ampicillin) which was grown over night in an orbital shaker at 37˚C 200 rpm. The following morning 50 mL was removed as un-induced cells and the bacteria collected by centrifugation at 6000 x G for 10 minutes at 4˚C. The remaining culture was every hour for 3 hours. The harvested bacteria was lysed by sonication and the crude lysate run on 10% SDS-PAGE then a western blot analysis was performed probing for KpnB1 to examine the amount of GST-KpnB1 induced over time.

6.2.18 KpnB1 protein purification - Nickel Affinity

A 10 mL starter culture was grown in TB (30µM Kanamycin) (Sigma-Aldrich, Johannesburg, South Africa) over night at 37˚C with shaking in a 100mL flask the following morning this starter culture was transferred to fresh TB with fresh 30µM (Kanamycin) and grown until OD600 is between 0.6. The culture was Induced with 1mM IPTG (final concentration 0.1mM) and continued to grow at 25˚C for a further 24 hours. Cells were harvested at 5000 rpm for 20 min and the supernatant discarded.

The bacteria cells were re-suspended in lysis buffer and sonication was carried out using 15-second pulses with 15 second rest periods repeated 30 times (total sonication time 8 mins) to lyse the cells.

The sonicated lysate was centrifuged ate 15 000 rpm for 30 min and the cleared lysate was filtered through a 0.45µM syringe filter, (if too viscous another round of sonication can be performed here then filtration) a sample of the filtered cleared lysate was maintained. The protein was purified using HisTrap HP1 ml column. The column was equilibrated by washing 5 x column volumes with wash buffer (see solutions). Protein was loaded on to the column and eluted at 0.5 mL/min with elution buffer (see solutions).

6.2.19 KpnB1 protein purification – Anion Exchange

A 10 mL starter culture was grown in TB (30µM Kanamycin) over night at 37˚C with shaking in a 100mL flask the following morning this starter culture was transferred to fresh TB with fresh 30µM (Kanamycin) and grown until OD600 is between 0.6. The culture was Induced with 1mM IPTG (final concentration 0.1mM) and continued to grow at 25˚C for a further 24 hours. Cells were harvested at 5000 rpm for 20 min and the supernatant discarded.

A lysate was prepared by dissolving Half an EDTA-free protease inhibitor tablet (Sigma-Aldrich, Johannesburg, South Africa) into 50 mL of buffer A (an anion exchange purification specific solution, see solutions appendix for recipe) into which the bacterial pellet was rigorously re-suspended in. The lysate suspension

was poured into a 50 mL glass beaker and stored within an ice, water and 70% ethanol bath, effectively ensuring a cold temperature was maintained. Sonication was carried out using 15 second pulses at 40W with 15 second rest periods, repeated 30 times (total sonication time 8 minutes). The sonicated lysate was centrifuged at 15 000 rpm for 30 minutes, and both the clear lysate as well as the pellet was kept.

The sonicated lysate was centrifuged ate 15 000 rpm for 30 min and the cleared lysate was filtered through a 0.45µM syringe filter (if too viscous another round of sonication can be performed here then filtration) a sample of the filtered cleared lysate was maintained. The pellet was homogenized with 40ml of buffer A then a sample taken. At this point it is important to run an SDS-PAGE gel to assess the induction and lysis.

High-resolution anion exchange column (QHP Seph 20mL) was equilibrated with 4 x column volume with buffer A (low salt) at a flow rate of 2.5 mL/min. The crude lysate was loaded onto the column 2.5 mL per minute and buffer A was run through until the A280 reading returned to baseline. The remainder of this purification program was run with buffer A added to a 50% gradient of buffer B released, producing a final step of 100% buffer B solution. This high-resolution ion exchange column made use of the Waters Delta prep 3000 chromatography system partnered to a Gilson 321 pump, aUV/Vis-155 spectrophotometer, as well as a Gilson FC 204 fraction collector. Fractions were electrophoresed and probed for KpnB1 using western blot analysis, then fractions of interest were pooled, de-salted using Ultracel® Ultrafiltration membrane (GE life sciences,

Pittsburgh, USA) and run once more through the anion exchange to remove contaminants before again being examine by SDS-PAGE and western blot. A polishing step was performed using Gel filtration was performed using Superdex 200 10/300 GL column equilibrated with 4 column volumes of 50mM Hepes in 150mM NaCl. The protein was loaded onto the column and eluted using a gradient o 30% buffer B from anion exchange. The fractions were collected and again examined by SDS-PAGE and western blot analysis before pooling those of interest for Mass spec analysis.

6.2.20 KpnB1 protein purification - Glutathione sepharose

E. Coli containing the plasmid pGex-6p-KpnB1 was grown up in a small volume of terrific broth overnight (200ml) while the remaining 800mL was placed in an incubator to keep it warm for the following morning. First thing in the morning the starter culture was mixed with the remaining warm broth and left to grow for 1 hr 30 minutes until the OD600 was approximately 1. The culture was induced with 1mL of 1mM IPTG (Promega, Madison, WI, USA).) and the temperature was dropped to 25˚C for further 24 hrs following which the cells were harvested via centrifugation at 6000 rpm for 10mins at 4˚C. The cell pellet was slowly frozen to -80·C in the freezer overnight then used in protein purification.

During the purification process, the bacterial cell pellet was first allowed to thaw at room temperature. Once thawed, the pellet was re-suspended in 1 x PBS pH7.5 (not autoclaved) for a 1L culture use 10mL 1 x PBS pH 7.5. It is important to note that from this point on, none of the solutions used were autoclaved if the

purification was being done for circular dichroism as this process effects the reading of the CD. Only glass or non-leaching plastics, such as those made by Eppendorf® (Eppendorf, Hamburg, Germany) were used. Ordinary plastic tips and eppendorfs were found to leach into the protein and cause errors in the results particularly circular dichroism. Similarly triton-x was not used either as it absorbs highly at the 280nm range throwing out the readings. For similar reasons we could not use DTT as this caused fluctuations in the ITC readings in the form of a baseline shift.

Once the bacterial cell pellet was completely re-suspended i.e. no solid cell clumps remaining, the bacterial mixture was sonicated while in an ice bath for 30 second intervals until lysis occurred. The next step was to collect the crude protein via centrifugation which was performed at 12 000 rpm for 10 min at 4˚C. The protein containing supernatant (crude lysate) was kept for further purification and the cell debris pellet was discarded.

The crude lysate collected as above was further purified using amicon ultra concentration device (GE life sciences, Pittsburgh, USA). The crude lysate was concentrated down to 2mL to maximise the capacity of the resin in the next stem. The concentrated crude lysate was the loaded onto 2mL of glutathione sepharose™ 4B affinity chromatography resin (GE life sciences, Pittsburgh, USA). The resin had been equilibrated prior to this step by washing twice with 10mL 1 x PBS pH7.5. Once the crude lysate was added to the resin, the system was placed on a rotator at room temperature for 4 hours, then moved to the cold room (4˚C) and continue to rotate overnight.

The following morning, collection of the flow through was carried out via centrifuging at 5000 rpm for 5min, removing the supernatant. A small amount was retained for analysis. The resin was then washed 2 times with 5mL cold 1 x PBS pH 7.5. To elute the protein form the resin a solutions of 50mM reduced glutathion (Sigma) in 1 x PBS pH 7.5 – 8 (always made fresh on the day) was used. Elution took place on the rotator for 1 hour at room temperature. Three eluents was seen to be sufficient at removing the bulk of the bound protein. The beads were then washed as before for the next round of purification.

The purified protein was electrophoresed using SDS-PAGE and stained with coomassie brilliant blue so as to examine the efficiency of the purification. Crude fractions, flow through, washes and all elutions were run the gel along with BSA standards. This enabled quantification of the amount of KpnB1 using image J densitometry software. The purified protein was then used for analysis such as circular dichroism, isothermal calorimetry and thermal shifts. These analyses were done in the presence and the absence of the test compound INI-43.

6.2.21 Circular Dichroism

Purified protein was concentrated and the reduced glutathione removed using amicon ultra 30K spin column (GE life sciences, Pittsburgh, USA). The final concentration of KpnB1 was quantified using BCA analysis and. Following this the protein was run through sephadex G10 resin to degas it in preparation for circular dichroism. This final protein solution was made up to a concentration of 0.2µg/mL with milliQ water. Circular Dichroism was performed using Chirascan CD Spectrometer and associated software (Applied Photophysics, Leatherhead,

United Kingdom). The setup used a 10mm pathlength and a 1nm bandwith step increment with 0.5s intervals per point. Each reading was repeated in triplicate.

The scans were performed with INI-43 in DMF solution as opposed to DMSO, as DMSO absorbs strongly within the 280nm range causing anomalies in the data generated. Initially a reading of the protein on its own was taken then subsequent readings of the protein with drug were taken slowly increasing the concentration of drug added to the protein so to create a titration effect. The raw data was normalized to 280nm and the effect of the solvent was subtracted form the data so that just the effect of the drug was visible. To do this scans of the various concentrations of drug used had to be taken and subtracted from the corresponding protein and drug scans.

Analysis of the results was performed by examining the effect of the various drug concentrations at specific wavelengths, and plotting these as individual graphs. Binding isotherms were also plotted individually for various wavelengths to gain insight into the affinity of INI-43 for KpnB1. This data analysis used both Microsoft Excel and Graph Pad Prism.

Raw CD data was captured and saved into Microsoft Excel. Solvent effect was subtracted from the raw data. Data points for a desired wavelength were chosen over increasing concentration of INI-43

Saturation binding curves were created using GraphPad Prism using single XY points graph and fitting the data to non-linear regression curve, one binding site (hyperbola).

To create the scatchard plot, the data was transformed to pharmacology and biochemistry settings selecting scatchard and a new graph was created.

The Bmax was divided by the Kd to create the line of best fit.

By selecting data tables and creating a new data table (Renamed Y and X intercepts), enter the following X= 0 ; Y= Bmax/Kd and X=Bmax; Y=0

Format the scatchard Line data connecting the two scatchard intercepts with a line and adding this scatchard plot to the binding isotherm.

6.2.22 ITC

The purified protein was used in further binding experiments in ITC using the MicroCal™ iTC200 System (GE life sciences, Pittsburgh, USA). The test cell was washed with buffer (See solutions) then protein was added at the desired concentration. Next the syringe was loaded with drug at the desired concentration and set to the closed position. The tip of the syringe was gently cleaned then inserted into the test cell and the program was setup to run 21 injections 2ul of drug was injected each time every 150 seconds while the temperature was set at 24°C and stirrer speed at 300 rpm. Appropriate controls were carried out including titrating buffer into buffer and checking the machine with a calcium, EDTA binding analysis.

6.2.23 Statistical analysis

All experiments were performed in triplicate and repeated at least two independent times. Results are presented as the mean value ± standard error of mean (SEM) unless stated otherwise. The Student's *t*-test (paired and unpaired) was applied to calculate statistically significant differences between samples. A two-tailed distribution was used. Statistical significance was defined using a type I error or p-value of 0.05 where the p-value is the probability of rejecting the null hypothesis when it is assumed to be true. Those p-values of less than 0.05 were considered statistically significant. P-values ≤ 0.05 were marked with a (*), while p-values ≤ 0.01 were marked with (**). All calculations were performed in Microsoft Excel for MAC 2011 and GraphPad Prism MAC compatible (GraphPad Prism 6.05 Software, La Jolla, CA, USA).

6.2.24 Creating Binding Isotherms and Scatchard plots

- Raw CD data was captured and saved into Microsoft Excel.
- Solvent effect was subtracted from the raw data.
- Data points for a desired wavelength were chosen over increasing concentration of INI-43
- Saturation binding curves were created using GraphPad Prism using single XY points graph and fitting the data to non-linear regression curve, one binding site (hyperbola).
- To create the scatchard plot, the data was transformed to pharmacology and biochemistry settings selecting scatchard and a new graph was created.
- The Bmax was divided by the Kd to create the line of best fit.
- By selecting data tables and creating a new data table (Renamed Y and X intercepts)

I enter the following X= 0 ; Y= Bmax/Kd

X=Bmax; Y=0

- Format the scatchard Line data connecting the two scatchard intercepts with a line and adding this scatchard plot to the binding isotherm.

6.3 Solutions

6.3.1 DNA Solutions

6.3.1.1 Agarose gel 1%

Agarose 1g, 1x TAE buffer 100mL, Microwave until completely melted and add 5ul of ethidium bromide

6.3.1.2 DNA Loading Buffer (6x)

250mM Tris (pH 6.8), 6% SDS, 0.005% bromophenol blue, 40% glycerol 10% B-mercapterethanol.

6.3.1.3 TAE Buffer 50x 1L

0.04M Tris acetate, 0.0001 EDTA pH 8. For each litre of solution: 242 g Tris Base (MW=121.1) 57.1 mL Glacial Acetic Acid 10 mL 0.5 M EDTA mix Tris with stir bar to dissolve in about 600 mL of ddH2O. add the EDTA and Acetic Acid, pH to 8.0. bring final volume to 1 L with ddH2O. store at room temperature

6.3.1.4 TE buffer 100mL

10mM Tris pH8, 1mM EDTA pH 8 (Autoclcave)

6.3.2 Tissue culture solutions

6.3.2.1 PBS

137 mM NaCl, 2.7 mM KCl, 4.3 mM Na2HPO4.7H20 (pH7.4), 1.4 mM KH2PO4

Autoclave the solution.

6.3.2.2 Trypsin-EDTA

0.05% trypsin, 137 mM NaCl, 2.7 mM KCl, 4.8 mM Na2HPO4.2H2O, 1.4 mM KH2PO4, 10mM EDTA (pH 8.0)

6.3.2.3 16% Paraformaldehyde (PFA)

Dissolve 16 g Paraformaldehyde in 80 ml dH20 by stirring at 60°C for 1 hour, ensuring the temperature does not exceed 60°C. Add drops of 10 M NaOH until the solution clears and pH to 7. Make the solution up to 100 ml and filter-sterilize using a 0.45µm filter. Store at -20°C.

6.3.2.4 Cell-freezing media

70% DMEM, 20% FCS, 10% DMSO

6.3.2.5 MTT Reagent (3-[4,5-dimethylthiazol-2-yl]-2,5-diphenyltetrazolium bromide) Sigma (M2128)

Dissolve 100 mg of MTT reagent in 20mL of 1xPBS by vortexing ad heating in 37˚C water bath. Filter sterilize using a 0.2uM syringe protect from light and

Store at 4˚C for up to 1 month.

6.3.2.6 MTT Solubilisation Solution 250mL

10% SDS in 0.01M HCl store at room temperature

6.3.3 WESTERN BLOT SOLUTIONS

6.3.3.1 RIPA Buffer 200mLs

150mM NaCl, 10mM Tris pH7, 1% triton X-100, 100% triton X-100, 0.1% SDS, 10% SDS. (Autoclave and store at 4°C)

6.3.3.2 RIPA mixture Solution

RIPA Buffer 45uL, 10 x PI 5uL, Na2VO3 0.05

6.3.3.3 10X Running Buffer

Dissolve 40 g Glycine, 63.2 g Tris and 10 g SDS in 1000 ml dH20.

6.3.3.4 10X Transfer Buffer

Dissolve 144 g Glycine and 38 g Tris in 1000 ml dH20.

6.3.3.5 1X Transfer Buffer

Dilute 100 ml 10X Transfer Buffer with 700 ml dH20 and add 200 ml methanol or Isopropanol.

6.3.3.6 Normal Coomassie Staining Solution

50% Methanol, 10% Acetic Acid, 0.05% Coomassie Brilliant Blue

6.3.3.7 Normal Destain

5% Methanol, 7% Acetic Acid

6.3.3.8 TBST

50 mM Tris (pH 7.5), 150 mM NaCl, 0.1 % Tween-20

6.3.4 Protein Purification Solutions

6.3.4.1 Luria Agar 1L

Tryptone 10g, yeast extract 5g, NaCl 10g, agar15g, autoclave. Cool to about 28 degrees calcium and add desired antibiotics and pour plates

*NB to make plates with IPTG and XGAL spread 100ul of 1M IPTG and 20uL 50mg/mL XGAL on to plates and let them soak in for at least an hour before plating

6.3.4.2 Ampicillin (100 mg/ml)

Dissolve 100 mg Ampicillin in 10 ml dH20. Filter-sterilize and store at -20°C.

6.3.4.1 X-gal (50 mg/ml)

Dissolve 50 mg X-gal in 1 ml DMSO. Protect from the light and store at -20°C.

6.3.4.2 IPTG (0.1 M)

Dissolve 72 mg IPTG in 3 ml dH20. Filter-sterilize and store at 4°C.

6.3.4.3 Luria Broth 1L

Tryptone 10g, yeast extract 5g, NaCl 10g, agar15g, autoclave. Add antibiotics when cool.

6.3.4.4 SOC Medium 50ml

0.5% yeast extract, 2% tryptone 10mM NaCl, 2.5mM KCl 20mM $MgSO_4$.

Autoclave. Once cool add 20% glucose solution.

6.3.4.5 Terrific Broth (TB) 1lL

Tryptone 12g, yeast extract 24g, glycerol 4mL, make up to 900ml with distilled H2O. Autoclave

6.3.4.6 10X Potassium butter for TB

0.72M K2HPO4, 0.169M KH2PO4 pH 7. Autoclave

Add 100mL of potassium buffer to TB broth just before use.

6.3.5 His tag purification solutions

6.3.5.1 Potassium Buffer

0.2M $NaH_2PO_4 2H_2O$, 0.2M Na_2HPO_4. Take the 0.2 Na_2HPO_4 and titrate in the 0.2M $NaH_2PO_4 2H_2O$ to make up to a pH of 8. This is the 0.2M potassium buffer pH 8

6.3.5.2 Binding buffer

50mM Potassium buffer, 300mM NaCl. pH 8

6.3.5.3 Wash Buffer

50mM Potassium buffer, 300mM NaCl, 200mM Imidazole. pH 8

6.3.5.4 Elution buffer

50mM potassium buffer, 300mM NaCl, 500mM imidazole. pH 8

6.3.6 Ion Exchange solutions

6.3.6.1 Buffer A: 50mM Tris pH8, 50mM NaCl

6.3.6.2 Buffer B: 50mM Tris pH 8, 1M NaCl

6.3.6.3 Lysis buffer

Add half an EDTA free protease inhibitor tablet to 50mL of buffer A

6.3.7 GST Tag Purification solutions

6.3.7.1 Lysis buffer

Add half an EDTA free protease inhibitor tablet to 50mL 1 x PBS

6.3.7.2 Wash Buffer

1 x PBS

6.3.7.3 Elution Buffer

50mM Reduced glutathione in PBS pH 7.5-8

Appendix

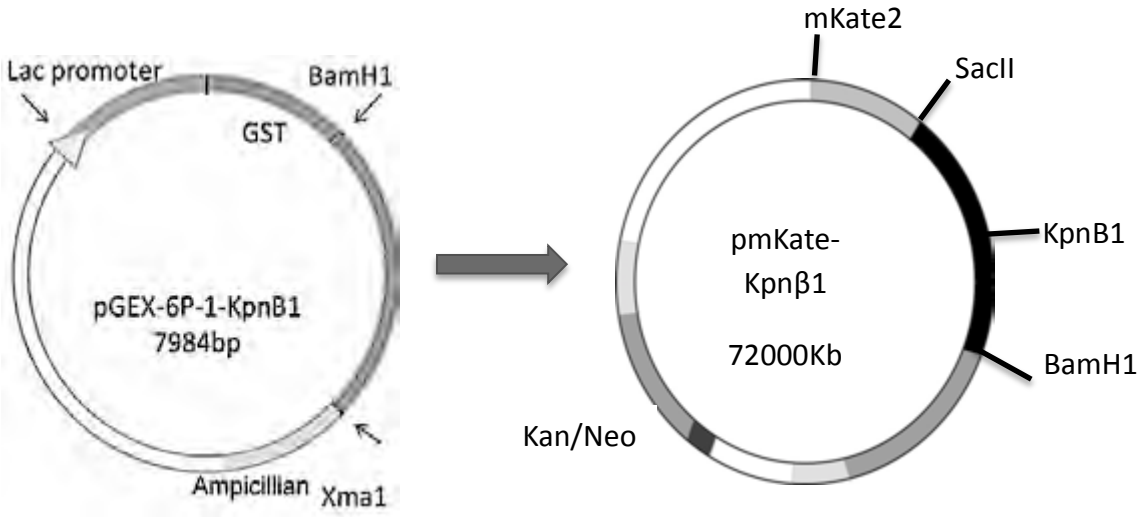

Figure 1: KpnB1 was cloned from pGEX-KpnB1 into pmKate-KpnB1. Schematic rendition of cloning process

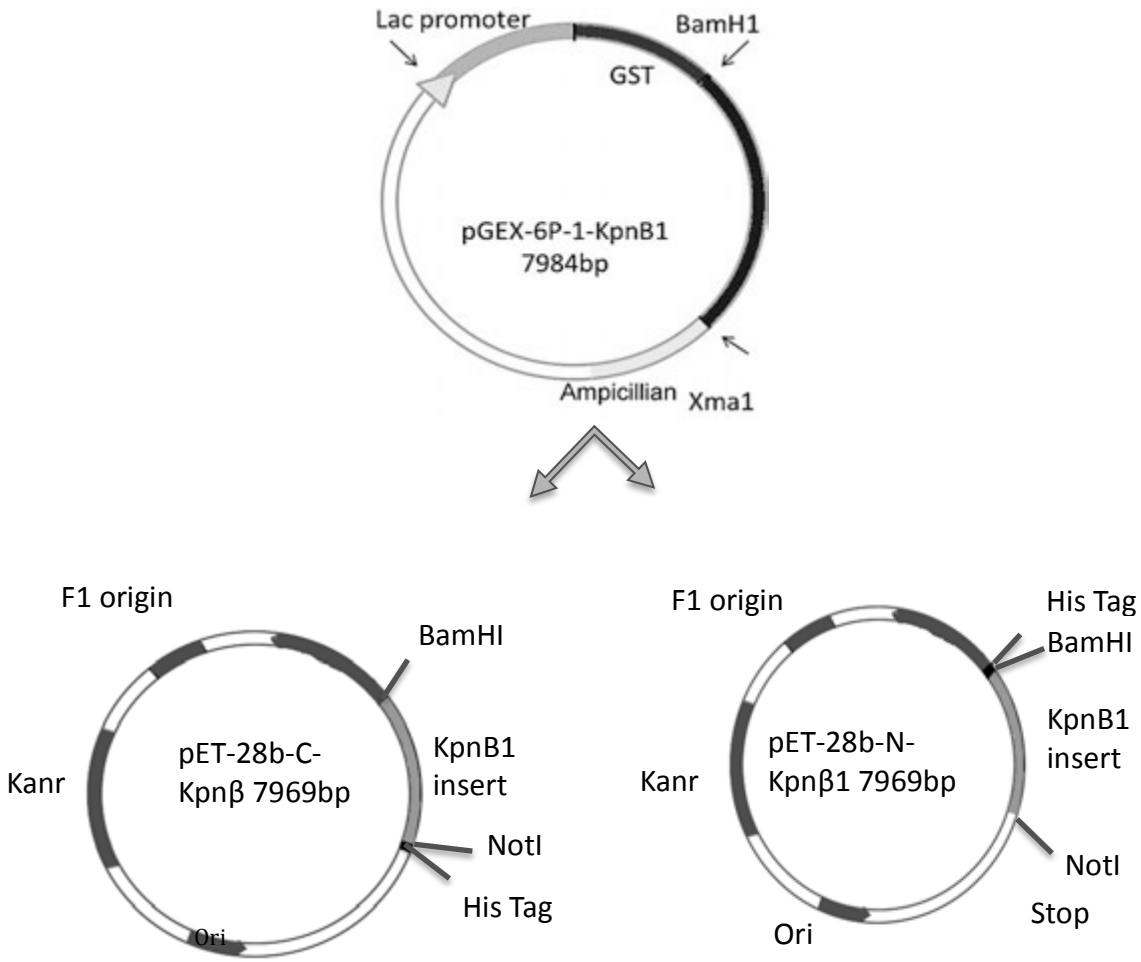

Figure 2: KpnB1 was cloned from pGEX- KpnB1 into pET-28b. Schematic rendition of cloning process to create C- and an N-His tagged clones.

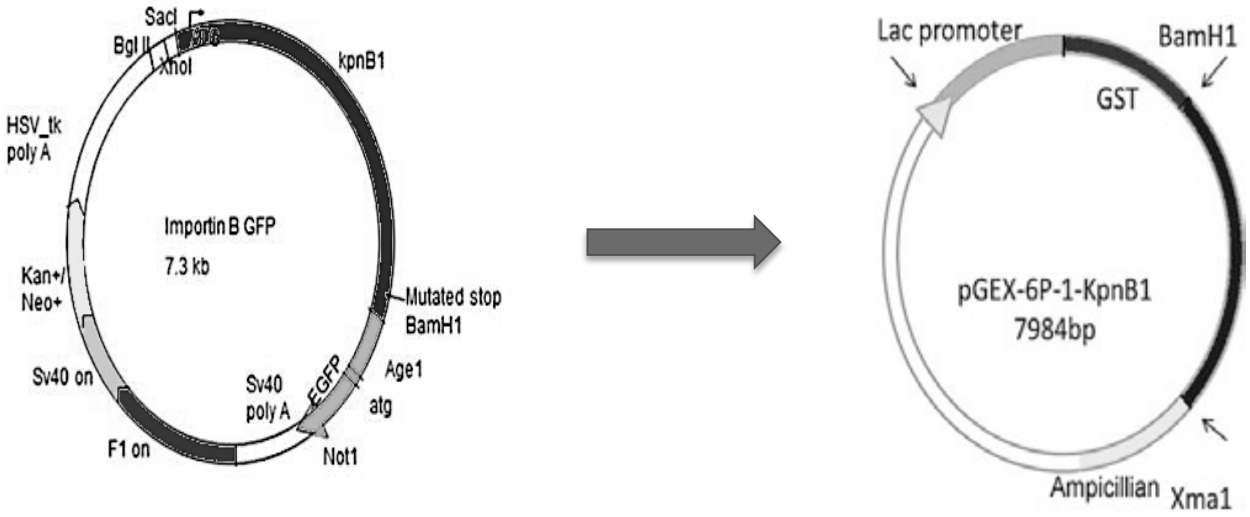

Figure 3: KpnB1 was cloned from Importin B GFP into pGEX-KpnB1. Schematic rendition of cloning process

References

Abdul Razak, A.R. et al., 2016. First-in-Class, First-in-Human Phase I Study of Selinexor, a Selective Inhibitor of Nuclear Export, in Patients With Advanced Solid Tumors. *Journal of Clinical Oncology*.

Adewole, I.F. et al., 2013. Consensus recommendations for the prevention of cervical cancer in sub-Saharan Africa. *Southern African Journal of Gynaecological Oncology*, 5, pp.47–57.

Akhtar, A. & Gasser, S.M., 2007. The nuclear envelope and transcriptional control. *Nature reviews. Genetics*, 8, pp.507–17.

Alifrangis, C.C. & McDermott, U., 2014. Reading between the lines; understanding drug response in the post genomic era. *Molecular oncology*, pp.1–8.

Angus, L., Van der Watt, P.J. & Leaner, V.D., 2014. Inhibition of the nuclear transporter, Kpnß1, results in prolonged mitotic arrest and activation of the intrinsic apoptotic pathway in cervical cancer cells. *Carcinogenesis*, 35, pp.1121–1131.

Arnau, J. et al., 2006. Current strategies for the use of affnity tags and tag removal for the purification of recombinant proteins. *Protein Expression and Purification*, 48, pp.1–13.

Ault, K.A., 2007. Human papillomavirus vaccines and the potential for cross-protection between related HPV types. *Gynecologic Oncology*, 107, pp.S31–

S33.

Beals, C.R. et al., 1997. Nuclear localization of NF-ATc by a calcineurin-dependent, cyclosporin- sensitive intramolecular interaction. *Genes and Development*, 11, pp.824–834.

Bird, G. et al., 2008. Possible role for cellular karyopherins in regulating polyomavirus and papillomavirus capsid assembly. *Journal of Virology*, 82, pp.9848–9857.

Bird, S.L., Heald, R. & Weis, K., 2013. RanGTP and CLASP1 Cooperate to Position the Mitotic Spindle. *Molecular biology of the cell*.

Blomberg, M. et al., 2015. Dose-related differences in effectiveness of human papillomavirus vaccination against genital warts: A nationwide study of 550 000 young girls. *Clinical Infectious Diseases*, 61, pp.676–682.

Bonanni, P. et al., 2015. Human papilloma virus vaccination: impact and recommendations across the world. *Therapeutic Advances in Vaccines*, 3, pp.3–12.

Botha, M. & Dochez, C., 2012. Introducing human papillomavirus vaccines into the health system in South Africa. *Vaccine*, 30 Suppl 3, pp.C28–C34.

Botha, M.H. & Richter, K.L., 2015. Cervical cancer prevention in South Africa: HPV vaccination and screening both essential to achieve and maintain a reduction in incidence. *South African Medical Journal*, 105, pp.33–34.

Cautain, B. et al., 2015. Components and regulation of nuclear transport

processes. *FEBS Journal*, 28, pp.445–462.

Cavazza, T. & Vernos, I., 2016. The RanGTP Pathway: From Nucleo-Cytoplasmic Transport to Spindle Assembly and Beyond. *Frontiers in Cell and Developmental Biology*, 3.

Chook, Y.M. & Süel, K.E., 2011. Nuclear import by karyopherin-βs: Recognition and inhibition. *Biochimica et Biophysica Acta - Molecular Cell Research*, 1813, pp.1593–1606.

Chook, Y.M. & Süel, K.E., 2011. Nuclear import by karyopherin-βs: recognition and inhibition. *Biochimica et Biophysica Acta*, 1813, pp.1593–1606.

Ciciarello, M. et al., 2004. Importin beta is transported to spindle poles during mitosis and regulates Ran-dependent spindle assembly factors in mammalian cells. *Journal of Cell Science*, 117, pp.6511–6522.

Cingolani, G. et al., 1999. Structure of importin-beta bound to the IBB domain of importin-alpha. *Nature*, 399, pp.221–9.

Clarke, P.R. & Zhang, C., 2004. Spatial and temporal control of nuclear envelope assembly by Ran GTPase. *Symposia of the Society for Experimental Biology*, 56, pp.193–204.

Clarke, P.R. & Zhang, C., 2008. Spatial and temporal coordination of mitosis by Ran GTPase. *Nature reviews. Molecular cell biology*, 9, pp.464–477.

Conti, E. et al., 1998. Crystallographic analysis of the recognition of a nuclear

localization signal by the nuclear import factor karyopherin α. *Cell*, 94(2), pp.193–204.

Conti, E., Müller, C.W. & Stewart, M., 2006. Karyopherin flexibility in nucleocytoplasmic transport. *Current Opinion in Structural Biology*, 16, pp.237–244.

Conway, M.J. & Meyers, C., 2009. Replication and assembly of human papillomaviruses. *Journal of dental research*, 88, pp.307–317.

D'Angelo, M.A. & Hetzer, M.W., 2008. Structure, dynamics and function of nuclear pore complexes. *Trends in Cell Biology*, 18, pp.456–466.

Druker, B.J., 2002a. Perspectives on the development of a molecularly targeted agent. *Cancer Cell*, 1, pp.31–36.

Druker, B.J., 2002b. STI571 (Gleevec) as a paradigm for cancer therapy. *Trends in Molecular Medicine*, 8, pp.14–18.

Durrant, J.D. & McCammon, J.A., 2011. Molecular dynamics simulations and drug discovery. *BMC Biology*, 9, p.71.

Dyson, N., 1998. The regulation of E2F by pRB-family proteins. *Genes & Development*, 12, pp.2245–2262.

Fabrini, R. et al., 2009. Monomer-dimer equilibrium in glutathione transferases: A critical re-examination. *Biochemistry*, 48, pp.10473–10482.

Ferenczy, G.G. & Keserũ, G.M., 2010. Thermodynamics guided lead discovery

and optimization. *Drug Discovery Today*, 15, pp.919–932.

Ferlay, J. et al., 2015. Cancer incidence and mortality worldwide: Sources, methods and major patterns in GLOBOCAN 2012. *International Journal of Cancer*, 136, pp.E359–E386.

Ferlay, J. et al., 2013. GLOBOCAN 2012 v1.0, Cancer Incidence and Mortality Worldwide: IARC CancerBase. No. 11 [Internet]. *Lyon, France: International Agency for Research on Cancer.*, 11, p.http://globocan.iarc.f.

Feske, S., Rao, A. & Hogan, P.G., 2007. The Ca2+-calcineurin-NFAT signalling pathway. *New Comprehensive Biochemistry*, 41, pp.365–401.

Fiander, a N., 2011. The prevention of cervical cancer in Africa. *Women's health (London, England)*, 7, pp.121–132.

Francis, S. a. et al., 2010. Examining attitudes and knowledge about HPV and cervical cancer risk among female clinic attendees in Johannesburg, South Africa. *Vaccine*, 28, pp.8026–8032.

Fung, H.Y.J. & Chook, Y.M., 2014. Atomic basis of CRM1-cargo recognition, release and inhibition. *Seminars in Cancer Biology*, 27, pp.52–61.

Gerecitano, J., 2014. SINE (selective inhibitor of nuclear export)--translational science in a new class of anti-cancer agents. *J Hematol Oncol*, 7, p.67.

Giuliano, A.R., 2007. Human papillomavirus vaccination in males. *Gynecologic Oncology*, 107(2 SUPPL.), pp.25–27.

Greenfield, N.J., 2004. Analysis of circular dichroism data. *Methods in enzymology*, 383, pp.282–317.

Greenfield, N.J., 2006a. Determination of the folding of proteins as a function of denaturants, osmolytes or ligands using circular dichroism. *Nature Protocols*, 1, pp.2733–2741.

Greenfield, N.J., 2006b. Using circular dichroism collected as a function of temperature to determine the thermodynamics of protein unfolding and binding interactions. *Nature Protocols*, 1, pp.2527–35.

Greenfield, N.J., 2006c. Using circular dichroism spectra to estimate protein secondary structure. *Nature Protocols*, 1, pp.2876–2890.

Gwack, Y. et al., 2007. Signalling to transcription: Store-operated Ca2+ entry and NFAT activation in lymphocytes. *Cell Calcium*, 42, pp.145–156.

zur Hausen, H., 2002. Papillomaviruses and cancer: from basic studies to clinical application. *Nature reviews. Cancer*, 2, pp.342–350.

Hebner, C.M. & Laimins, L. a., 2006. Human papillomaviruses: Basic mechanisms of pathogenesis and oncogenicity. *Reviews in Medical Virology*, 16, pp.83–97.

Hetzer, M.W., Walther, T.C. & Mattaj, I.W., 2005. Pushing the envelope: structure, function, and dynamics of the nuclear periphery. *Annual Review of Cell and Developmental Biology*, 21, pp.347–380.

Hetzer, M.W. & Wente, S.R., 2009. Border control at the nucleus: biogenesis

and organization of the nuclear membrane and pore complexes. *Dev Cell*, 17, pp.606–616.

Hintersteiner, M. et al., 2010. Identification of a small molecule inhibitor of importin β mediated nuclear import by confocal on-bead screening of tagged one-bead one-compound libraries. *ACS Chemical Biology*, 5, pp.967–979.

Hoelz, A., Debler, E.W. & Blobel, G., 2011. The structure of the nuclear pore complex. *Annual review of biochemistry*, 80, pp.613–43.

Hoffman, M. et al., 2003. Limited Pap screening associated with reduced risk of cervical cancer in South Africa. *International journal of epidemiology*, 32, pp.573–577.

Holdgate, G.A. & Ward, W.H.J., 2005a. Measurements of binding thermodynamics in drug discovery. *Drug Discovery Today*, 10, pp.1543–1550.

Holdgate, G.A. & Ward, W.H.J., 2005b. Measurements of binding thermodynamics in drug discovery. *Drug Discovery Today*, 10, pp.1543–1550.

Holt, P. a et al., 2009. Discovery of novel triple helical DNA intercalators by an integrated virtual and actual screening platform. *Nucleic acids research*, 37, pp.1280–1287.

Huggins, D.J., Sherman, W. & Tidor, B., 2012. Rational Approaches to

Improving Selectivity in Drug Design. *Journal of Medicinal Chemistry*, 55(4), pp.1424–1444.

Imai, K. & Takaoka, A., 2006. Comparing antibody and small-molecule therapies for cancer. *Nature reviews. Cancer*, 6, pp.714–727.

Irwin, J.J. & Shoichet, B.K., 2005. ZINC - A free database of commercially available compounds for virtual screening. *Journal of Chemical Information and Modeling*, 45, pp.177–182.

Jans, D.A., Chook, Y.M. & Süel, K.E., 2011. Nuclear import by karyopherin-βs: Recognition and inhibition. *Biochimica et Biophysica Acta (BBA) - Molecular Cell Research*, 1813, pp.1593–1606.

Jemal, A., Bray, F. & Ferlay, J., 2011. Global Cancer Statistics. , 61, pp.69–90.

Kalderon, D. et al., 1984. Sequence requirements for nuclear location of simian virus 40 large-T antigen. *Nature*, 311, pp.33–38.

Kau, T.R., Way, J.C. & Silver, P. a, 2004. Nuclear transport and cancer: from mechanism to intervention. *Nature reviews. Cancer*, 4, pp.106–117.

Kelly, S.M., Jess, T.J. & Price, N.C., 2005. How to study proteins by circular dichroism. *Biochimica et Biophysica Acta*, 1751, pp.119–139.

Kelly, S.M. & Price, N.C., 2006. Circular dichroism to study protein interactions. *Current protocols in protein science editorial board John E Coligan et al*, Chapter 20, p.Unit 20.10.

Kobayashi, J. & Matsuura, Y., 2013. Structural basis for cell-cycle dependent nuclear import mediated by the karyopherin Kap121p. *Journal of molecular biology*, 425, pp.1852–1868.

Koh, J. & Blobel, G., 2015. Allosteric Regulation in Gating the Central Channel of the Nuclear Pore Complex. *Cell*, 161, pp.1361–1373.

Kremers, G.-J. et al., 2009. Photoconversion in orange and red fluorescent proteins. *Nature methods*, 6, pp.355–358.

Kuriyan, Konforti & Wemmer, 2009. Molecular Recognition : The Thermodynamics of Binding. *The Molecules of Life*, pp.1–58.

Ladbury, J.E., 2010. Calorimetry as a tool for understanding biomolecular interactions and an aid to drug design. *Biochemical Society Transactions*, 38, pp.888–893.

Ladner, J. et al., 2012. Assessment of eight HPV vaccination programs implemented in lowest income countries. *BMC Public Health*, 12, p.370.

Lee, S.J. et al., 2005. Structural basis for nuclear import complex dissociation by RanGTP. *Nature*, 435, pp.693–6.

Lee, S.J. et al., 2000. The adoption of a twisted structure of importin-beta is essential for the protein-protein interaction required for nuclear transport. *Journal of Molecular Biology*, 302, pp.251–264.

Liang, Y., 2008. Applications of isothermal titration calorimetry in protein science. *Acta Biochimica et Biophysica Sinica*, 40, pp.565–576.

Lim, R.Y.H., 2007. Gate-crashing the nuclear pore complex. *Structure London England 1993*, 15, pp.889–891.

Liu, J. & York, N., 2001. Nuclear Envelope: Organization and Dynamics. *Life Sciences*,pp.1–8.

Lott, K. & Cingolani, G., 2011. The importin β binding domain as a master regulator of nucleocytoplasmic transport. *Biochimica et biophysica acta*, 1813, pp.1578–1592.

Ma, J. & Yang, W., 2010. Three-dimensional distribution of transient interactions in the nuclear pore complex obtained from single-molecule snapshots. *Proceedings of the National Academy of Sciences of the United States of America*, 107, pp.7305–10.

Marty, R. et al., 2013. Estimating the clinical benefits of vaccinating boys and girls against HPV-related diseases in Europe. *BMC cancer*, 13, p.10.

Mbulawa, Z.Z.A., Coetzee, D. & Williamson, A.-L., 2015. Human papillomavirus prevalence in South African women and men according to age and human immunodeficiency virus status. *BMC infectious diseases*, 15, p.459.

Van Montfort, R.L.M. & Workman, P., 2009. Structure-based design of molecular cancer therapeutics. *Trends in biotechnology*, 27, pp.315–328.

Moroianu, J., Blobel, G. & Radu, A., 1996a. Nuclear protein import: Ran-GTP dissociates the karyopherin alphabeta heterodimer by displacing alpha from

an overlapping binding site on beta. *Proceedings of the National Academy of Sciences of the United States of America*, 93, pp.7059–7062.

Moroianu, J., Blobel, G. & Radu, A., 1996b. The binding site of karyopherin alpha for karyopherin beta overlaps with a nuclear localization sequence. *Proceedings of the National Academy of Sciences of the United States of America*, 93, pp.6572–6576.

Pereira, J. a et al., 2014. Quinoxaline, its derivatives and applications: A State of the Art review. *European journal of medicinal chemistry*, pp.2–10.

Pihan, E. et al., 2015. Computational and biophysical approaches to protein-protein interaction inhibition of Plasmodium falciparum AMA1/RON2 complex. *Journal of Computer-Aided Molecular Design*, 29, pp.525–539.

Rogers, D.M. & Hirst, J.D., 2004. Calculations of protein circular dichroism from first principles. *Chirality*, 16, pp.234–243.

Rosano, G.L. & Ceccarelli, E.A., 2014. Recombinant protein expression in Escherichia coli: Advances and challenges. *Frontiers in Microbiology*, 5.

Soderholm, J.F. et al., 2011. Importazole, a small molecule inhibitor of the transport receptor importin-β. *ACS Chemical Biology*, 6, pp.700–708.

Soderholm, J.F. et al., 2011. Importazole, a small molecule inhibitor of the transport receptor importin-β. *ACS Chemical Biology*, 6, pp.700–708.

Stanley, M., 2015. Immunology of HPV Infection. *Current Obstetrics and Gynecology Reports*, 4, pp.195–200.

Sun, Q. et al., 2013. Nuclear export inhibition through covalent conjugation and hydrolysis of Leptomycin B by CRM1. *Proceedings of the National Academy of Sciences of the United States of America*, 110, pp.1303–8.

Timinszky, G. et al., 2002. The importin-beta P446L dominant-negative mutant protein loses RanGTP binding ability and blocks the formation of intact nuclear envelope. *Journal of Cell Science*, 115, pp.1675–1687.

Vetter, I.R. et al., 1999. Structural view of the Ran-importin beta interaction at 2.3 angstrom resolution. *Cell*, 97, pp.635–646.

Vetter, I.R. et al., 1999. Structural View of the Ran–Importin β Interaction at 2.3 Å Resolution. *Cell*, 97, pp.635–646.

Villa, L.L. et al., 2005. Prophylactic quadrivalent human papillomavirus (types 6, 11, 16, and 18) L1 virus-like particle vaccine in young women: A randomised double-blind placebo-controlled multicentre phase II efficacy trial. *Lancet Oncology*, 6, pp.271–278.

Ward, M.C. et al., 2011. Deregulated LAP2?? expression in cervical cancer associates with aberrant E2F and p53 activities. *IUBMB Life*, 63, pp.1018–1026.

van der Watt, P.J. et al., 2016. Targeting the nuclear import receptor, Kpnβ1 as an anti-cancer therapeutic. *Molecular Cancer Therapeutics*, 15, pp 560-573.

van der Watt, P.J. et al., 2009. The Karyopherin proteins, Crm1 and

Karyopherin beta1, are overexpressed in cervical cancer and are critical for cancer cell survival and proliferation. *International journal of cancer. Journal international du cancer*, 124, pp.1829–40.

van der Watt, P.J., Ngarande, E. & Leaner, V.D., 2011. Overexpression of Kpn??1 and Kpn??2 importin proteins in cancer derives from deregulated E2F activity. *PLoS ONE*, 6, pp.1–10.

van der Watt, P.J., Stowell, C.L. & Leaner, V.D., 2013. The nuclear import receptor Kpnβ1 and its potential as an anticancer therapeutic target. *Critical reviews in eukaryotic gene expression*, 23, pp.1–10.

Weisner, J. et al., 2015. Covalent-Allosteric Kinase Inhibitors. *Angewandte Chemie (International ed. in English)*, 54, pp.10313–6.

Wiedemann, C., Bellstedt, P. & Gorlach, M., 2013. CAPITO - A web server-based analysis and plotting tool for circular dichroism data. *Bioinformatics*, 29, pp.1750–1757.

Yoneda, Y. et al., 1999. Nucleocytoplasmic protein transport and recycling of Ran. *Cell Structure and Function*, 24, pp.425–433.

Young, C.L., Britton, Z.T. & Robinson, A.S., 2012. Recombinant protein expression and purification: A comprehensive review of affinity tags and microbial applications. *Biotechnology Journal*, 7, pp.620–634.

Yuh, M.C. & Blobel, G., 2001. Karyopherins and nuclear import. *Current Opinion in Structural Biology*, 11, pp.703–715.

Zhang, J., Yang, P.L. & Gray, N.S., 2009. Targeting cancer with small molecule kinase inhibitors. *Nature reviews. Cancer*, 9, pp.28–39.

Zhou, J. et al., 1994. Interaction of human papillomavirus (HPV) type 16 capsid proteins with HPV DNA requires an intact L2 N-terminal sequence. *Journal of virology*, 68, pp.619–25.